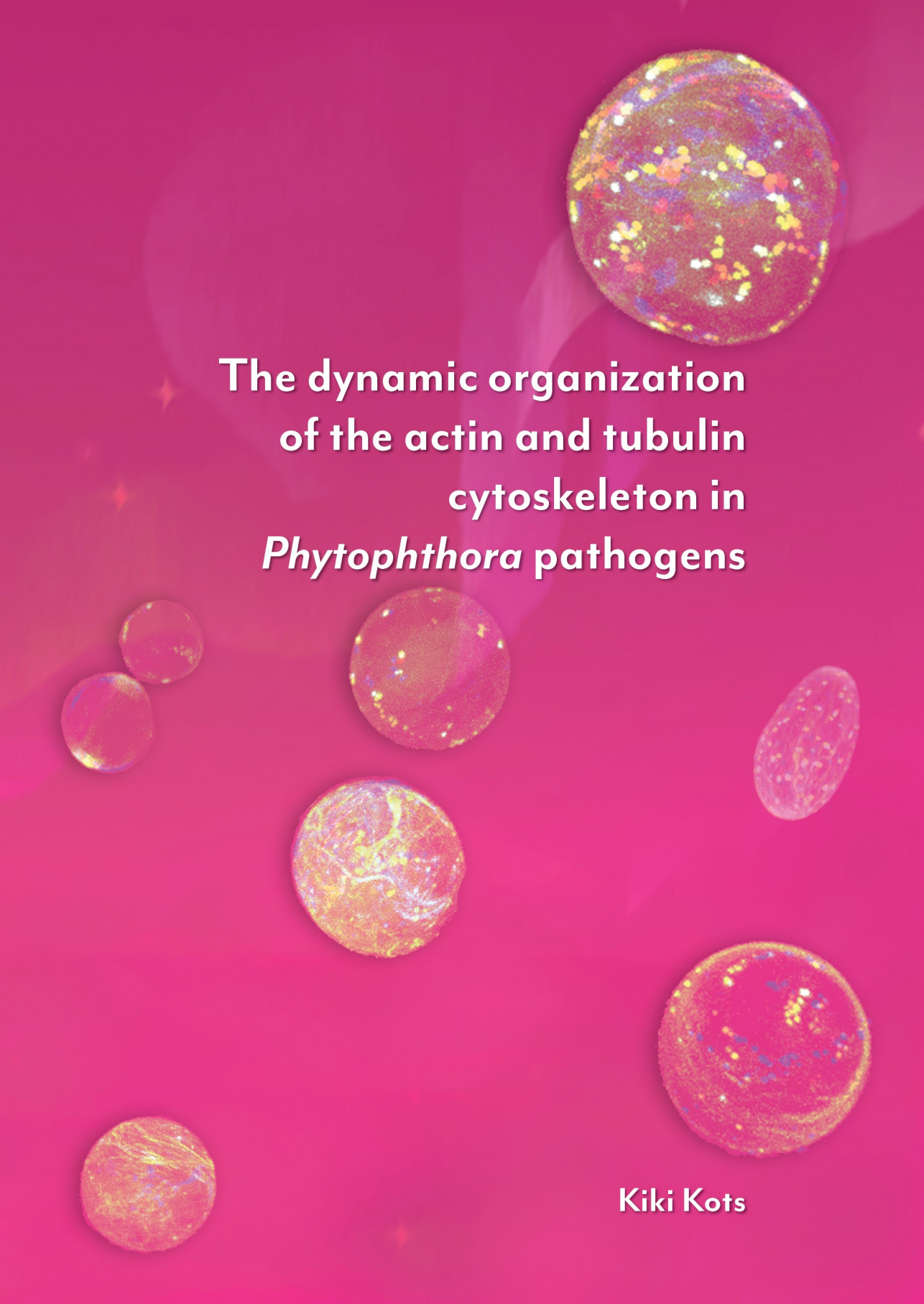

The dynamic organization of the actin and tubulin cytoskeleton in *Phytophthora* pathogens

Kiki Kots

Propositions

1. The discovery of unique actin configurations in *Phytophthora* opens new avenues for combatting these notorious plant pathogens. (this thesis)

2. Defining *Phytophthora* infection structures as appressoria is misleading. (this thesis)

3. When studying organisms with highly flexible genomes model organisms are useless.

4. The giant bacterium Thiomargarita namibiensis (*Volland et al., 2022, Science 376-6000: 1453-1458*) is a prokaryotic coenocyte.

5. Changing consumers standards towards fresh produce appearance will diminish the amount of waste in the food supply chain.

6. Regular knitting activity enhances one's ability to recognise patterns in imaging data.

Propositions belonging to the thesis, entitled

'The dynamic organization of the actin and tubulin cytoskeleton in *Phytophthora* pathogens'

Kiki Kots

Wageningen, 28 October 2022

The dynamic organization of the actin and tubulin cytoskeleton in *Phytophthora* pathogens

Kiki Kots

Thesis committee

Promotor
Prof. Dr Francine Govers
Personal chair at the Laboratory of Phytopathology
Wageningen University & Research

Co-promotor
Dr Tijs Ketelaar
Assistant Professor at the Laboratory of Cell Biology
Wageningen University & Research

Other members
Prof. Dr Richard G.H. Immink, Wageningen University & Research
Dr Sebastian Schornack, Sainsbury Laboratory, UK
Dr Vivianne G.A.A. Vleeshouwers, Wageningen University & Research
Dr Nicole N. van der Wel, Amsterdam UMC

This research was conducted under the auspices of the Graduate School for Experimental Plant Sciences (EPS)

The dynamic organization of the actin and tubulin cytoskeleton in *Phytophthora* pathogens

Kiki Kots

Thesis

submitted in fulfilment of the requirements for the degree of doctor
at Wageningen University
by the authority of the Rector Magnificus,
Prof. Dr A.P.J. Mol,
In the presence of the
Thesis Committee appointed by the Academic Board
to be defended in public
on Friday October 28, 2022
at 11 a.m. in the Omnia Auditorium.

Kiki Kots
The dynamic organization of the actin and tubulin cytoskeleton in *Phytophthora* pathogens
142 Pages
PhD thesis, Wageningen University, Wageningen, the Netherlands (2022)
With references, with summary in English

ISBN: 978-94-6447-299-8
DOI: 10.18174/572969

Contents

Chapter 1

Introduction

In biology, most attention is focused on evolutionary supergroups composed of multicellular organisms that have a clear importance to us, humans. In particular the supergroups Opisthokonta, harbouring animals and fungi, and Archaeplastida, harbouring the land plants, red algae and green algae, have been studied heavily. Besides these two supergroups, there are other supergroups that are less known. One of these is the TSAR supergroup, harbouring the Telonemia, Stramenopiles, Alveolata and Rhizaria (Burki et al 2020). Although this supergroup has received relatively little attention, numerous TSAR species are economically and ecologically important. Amongst them are oomycota or oomycetes, close relatives of the brown algae and diatoms, and as such three main lineages in the Stramenopiles. Commonly called water moulds, oomycetes comprise saprophytes, feeding on dead organic material, and pathogens, both of animals as well as plants (Thines & Kamoun 2010).

1.1 Oomycetes are not fungi

Oomycetes are filamentous organisms that morphologically resemble fungi and until the 1990's they were indeed formally classified as fungi, albeit that some features, such as cell wall composition and mitochondria (Paquin et al 1995) were recognized as unusual. With the onset of modern-day molecular biology and DNA based identification methods, it was demonstrated that from an evolutionary point of view the oomycetes, as heterokonts, are more closely related to brown algae and diatoms than to the unikont fungi (Keeling & Burki 2019). Although oomycetes are now widely accepted as evolutionary distinct from fungi, they are still often referred to as fungi, even in scientific literature. The similarities in lifestyle of these two groups adds to the confusion, as they both grow as filamentous hyphae, produce mycelia and disperse by means of spores. These similarities are considered to be a result of convergent evolution (Latijnhouwers et al 2003), likely in part facilitated by horizontal gene transfer (Richards Thomas et al 2011).

Why is it so important to keep hammering on the fact that oomycetes are not fungi? Many oomycetes cause economically costly diseases and treating them with fungicides, i.e., chemicals developed to control fungal diseases, does not necessary lead to the desired effect in oomycete borne diseases. Often oomycetes appear to be insensitive to these chemicals or the efficacy is lower, either because the fungicide target is absent in oomycetes, or because the response pathways are not conserved between fungi and oomycetes. An example of this is the reduced efficacy of the fungicide benomyl in oomycetes (Cai et al 2015). To indicate chemical agents specifically targeting oomycetes, it was suggested to name these agents 'oomicides' rather than 'fungicides' (Govers 2001). Oomycetes differ from true fungi in many aspects, such as cell wall composition, genome ploidy and biochemical and metabolic pathways (Judelson & Blanco 2005). For example, targeting the cell wall is a popular and effective way to inhibit growth of a pathogen; however, the main cell wall component in

fungi is chitin, while in oomycetes this is cellulose combined with β-glucans (Melida et al 2013). Therefore, a better understanding of oomycetes can open new avenues to combat oomycete borne diseases.

1.2 Phytophthora species

Many oomycetes are notorious pathogens. For example, the large variety of downy mildews causes severe problems in agriculture. *Pythium* species are also mainly plant pathogens causing seedling damping-off, although some are known to be parasitic on animals. Additionally, *Saprolegnia* species, also known as cotton moulds, are well known pathogens on fish in aquaculture. One genus of oomycetes particularly known for harbouring many notorious plant pathogens, is *Phytophthora*. The direct translation of *Phytophthora* from Greek is 'plant destroyer.' The most widely known species is *Phytophthora infestans,* the causal agent of potato late blight. In the mid-nineteenth century this disease led to the Irish potato famine; mass migration of poor Irish peasants to America and starvation of countless others (Boddy 2016). Even today, nearly 170 years later, potato late blight is still a common and costly disease in potato and tomato crop cultivation worldwide with yearly outbreaks. Next to *P. infestans*, many other *Phytophthora* species have become known as annoying pathogens in agriculture and natural ecosystems. For example, *Phytophthora cinnamomi* is a threat to many plants indigenous in Australia as well as being a problem in avocado plantations (Engelbrecht & van den Berg, 2013). *Phytophthora palmivora* is an example of a tropical species with a broad host range. First described on palm trees in the early 1900's, it has since been described on numerous other hosts such as coconut, papaya, and cacao (Ochoa et al 2019, Perrine-Walker 2020). Like other *Phytophthora* spp., it thrives in humid conditions, and it can spread quickly through asexual spores (**box 1.1**). Other species causing substantial damage in many different hosts include *Phytophthora ramorum, Phytophthora sojae, Phytophthora capsici* and *Phytophthora parasitica* (Kamoun et al 2015).

Box 1.1 *Phytophthora* asexual life stages studied in this thesis

Phytophthora diseases have the reputation of spreading quickly through a crop. For example, a potato field can be destroyed by *P. infestans* in a matter of weeks. One of the reasons *Phytophthora* spp. can spread so quickly is the production of countless asexual sporangia that can be carried by the wind across large distances (Judelson & Blanco 2005). Other methods of dispersal are also known, such as splashing of rain on infected material and in *P. palmivora* it was reported that sporangia can be carried across large distances by beetles (Konam & Guest 2004). The sporangia can either germinate directly or indirectly. During indirect germination sporangia can produce motile biflagellate zoospores. The process of zoosporogenesis is induced in different ways in the various species and is influenced by factors such as temperature, moisture, light, and starvation (Erwin et al 1983). When the zoospores touch a plant surface they encyst, forming a thick cell wall enclosing the former zoospore. The cyst then germinates and forms a germ tube, that can invade the host. Previously, it was taken for granted that plant cell infection via cyst germination takes place through the formation of an appressorium, but more recently we reported that *P. infestans* uses a different mechanism, coined as 'naifu' invasion; hyphae slice through the plant surface at an oblique angle and the pointiness of the hyphal tip is important for efficient for plant cell invasion (Bronkhorst et al 2021, Bronkhorst et al 2022).

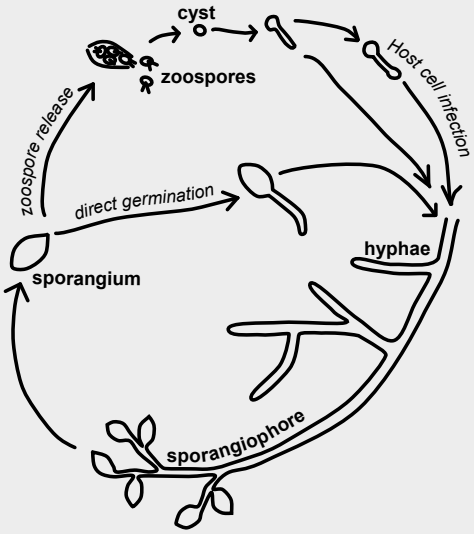

1.3 Why study the cytoskeleton in oomycetes?

To control plant diseases, farmers around the world heavily rely on chemical control agents. In the past decades awareness was raised that many of these chemicals might have an adverse effect on more than just the plant pathogen. The negative impact of agriculture on the environment and the ecosystem is high on the political agenda and upcoming

regulations force farmers to adapt their disease management practices and lower the input of chemical control agents. Studying oomycetes in more depth at the molecular and cellular level will bring us closer to understanding their infection strategies and might lead to novel ways to specifically target oomycetes. In this thesis I focus on understanding the oomycete cytoskeleton and cell. As true coenocytes, the oomycete cell consists of one continuous cytoplasm, stretching over a large distance and containing many nuclei (**figure 1.1**). Many well-known and frequently used pesticides target the cytoskeleton and have proven to be very useful in pest control. For example, benomyl is used as a fungicide and oryzalin is used as a weed killer. Both these drugs work specifically on the microtubule cytoskeleton. Benomyl is widely used in agriculture and on ornamental plants to prevent fungal mycelium from growing by disrupting their microtubule organization. Although benomyl does not seem to harm plants, there are reports of negative effects on animal cells (Kara et al 2020). Oryzalin can disrupt the microtubule cytoskeleton in plants while causing no measurable effects in animals. However, a single point mutation in the β-tubulin gene can cause resistance against this drug in plants (Anthony et al 1998, Hugdahl & Morejohn 1993). As these examples show us, cytoskeleton targeting pesticides can be valuable tools in disease control, providing they are species specific, and their target sites are conserved and essential to prevent loss of efficacy. The cytoskeleton is essential for all eukaryotes and although a large part of the machinery is highly conserved, upstream and downstream processes can differ greatly between organisms in different evolutionary groups. Because the cytoskeleton plays such a central role in growth and differentiation of so many organisms, if forms an excellent focus for the discovery of next generation drug targets.

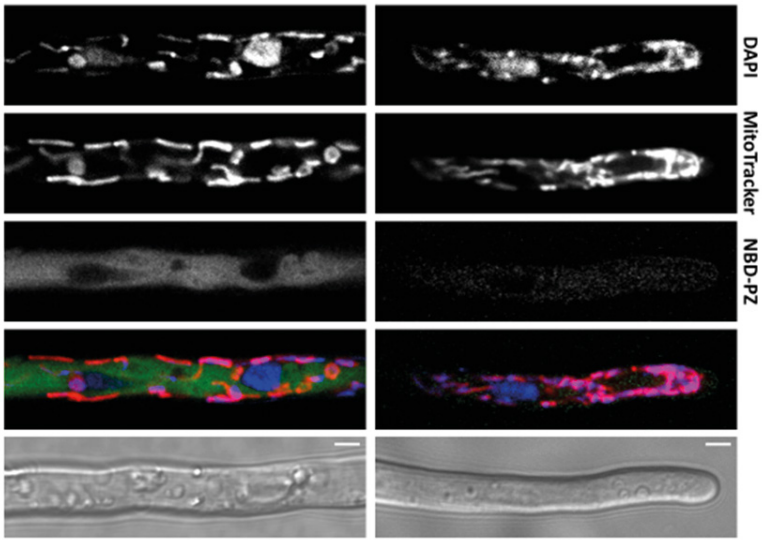

FIGURE 1.1 | *Phytophthora infestans* hyphae from wild type strain 88069 stained with DAPI to label the nuclei (blue), with MitoTrackerRed to label mitochondria (red) and with the pH indicator NBD-PZ to label vacuoles (green). The left panels show a distal area of the hypha and the right panels the tip region. The bottom panels are bright field images. Scales are 5 µm.

1.4 The actin cytoskeleton

The actin cytoskeleton is conserved amongst eukaryotes. It forms a highly dynamic intracellular network of filamentous actin (F-actin) and many other proteins interacting with the actin, collectively called actin binding proteins (ABPs). It is essential for proper functioning of a wide variety of cellular processes. For example, in animal cells the actin network is involved in force generation for cellular movement, muscle contraction and cytokinesis by means of a contractile ring (Qin & Yang 2011), in filamentous fungi it contributes to cell expansion and polarized growth and in plant cells it is essential for tip growth and cytoplasmic streaming (Berepiki et al 2011, Fischer et al 2008, Koestler et al 2009, Pollard & Borisy 2003). Although the functions of the actin cytoskeleton differ between supergroups and various species, similarities in organization are frequently observed.

At a first glance the actin cytoskeleton organization in oomycetes is similar to that found in fungi. In both groups F-actin cables, consisting of an unknown number of actin filaments, as well as cortical F-actin foci can be observed (Bachewich & Heath 1998, Deora et al 2008a, Harold & Harold 1992, Heath et al 2000, Jackson & Hardham 1998, Ketelaar et al 2012). In fungi, these foci are named patches and in oomycetes plaques (Chitcholtan et al 2012, Ketelaar et al 2012). However, a close examination of these foci revealed remarkable differences. Fungal patches are motile structures with a short lifespan that persist for approximately 15 seconds in yeast (*Saccharomyces cerevisiae*) and filamentous ascomycete fungi (Berepiki et al 2011, Moseley & Goode 2006, Pelham & Chang 2001, Sirotkin et al 2010, Taheri-Talesh et al 2008, Upadhyay & Shaw 2008). The actin polymerization in the patches drives the internalization of endocytic vesicles (Kaksonen et al 2003). In contrast, Meijer et al (2014), who performed live cell imaging to study the dynamic behaviour of the *P. infestans* actin cytoskeleton, found that oomycete plaques have an extremely long lifetime of sometimes over one hour and no inward moment was ever observed.

Additionally, a screening of the *P. infestans* genome for ABP encoding genes revealed differences between the ABP repertoire in yeast and in *P. infestans* (Meijer et al 2014). One ABP missing in *P. infestans* is Sla2p, a protein that operates at the centre of patch mediated yeast endocytosis (Kaksonen et al 2003). The combination of the lack of any Sla2 homologue in *P. infestans* and the different dynamic behaviour of plaques makes it unlikely that actin plaques function in the same way as actin patches. But if they are not involved in endocytosis, what is their function? It has been suggested that the plaques could serve as actin organizing centres (Bachewich & Heath 1998, Deora et al 2008a). An interesting observation made by Meijer et al (2014) is the correlation between hyphal growth velocity and distance between the extreme tip and the first occurring plaque; the faster a hypha grows, the further away plaques are from the apex. In non-growing hyphae plaques appear in the extreme tip. Another group of ABPs that seems peculiar

in oomycetes are myosins. *Phytophthora* has a large and diverse array of myosins. They all contain a myosin domain that is combined with various other protein domains. The diversity of domain combinations in *Phytophthora* myosins is larger than in myosins in any other studied organism, with some of these combinations being unique and not found in other taxa (Richards & Cavalier-Smith 2005). None of these myosins has been submitted to functional studies so far, so their role and functions are not known.

In filamentous fungi another actin configuration, namely a filamentous actin cap, was reported to be present in hyphal tips (Tanabe & Kamada 1994). Such an actin cap was also reported in the oomycetes *Saprolegnia ferax*, *Achlya bisexualis* and *Aphanomyces cochlioides* (Bachewich & Heath 1998, Deora et al 2008a, Walker et al 2006, Yu et al 2004), but as was recently suggested this is likely an artefact of the fixation procedure (Bronkhorst et al 2022). All F-actin structures observed in oomycetes locate to the cell cortex, close to the plasma membrane (Meijer et al 2014). Application of the actin depolymerizing drug latrunculin B (LatB) leads to a variety of concentration dependent effects, like disturbance of hyphal growth with irregular hyphal diameters, more branching and sometimes even ballooning of the hyphal tip (Ketelaar et al 2012).

Nearly all studies on actin structures in oomycetes are based on observations, made in fixed tissue, using either phalloidin staining or immunolabelling (**table 1.1**). From fixed material, information about actin organization can be obtained, but information on dynamics lacks. In two studies, approaches have been employed that provide information on actin dynamics, one being the injection of rhodamine-phalloidin into living sporangia to observe actin during zoosporogenesis (Jackson & Hardham 1998). However, a drawback of this approach is that phalloidin has a stabilizing effect on actin, which is particularly an issue when high concentrations are required for microscopic observations. The other is a study by Meijer et al (2014), who made use of a Lifeact-GFP expressing *P. infestans* strain and showed the added value of in vivo life cell imaging. Lifeact is a peptide based on an actin binding domain from yeast ABP140. In vivo expression of Lifeact linked to a fluorescent protein has been employed successfully to visualize the dynamics of actin organization in a wide variety of organisms (Riedl et al 2010, Vidali et al 2009). **Figure 1.2A** shows a hypha of *P. infestans* expressing Lifeact-GFP. Expression of Lifeact-GFP in *P. infestans* did not cause any obvious growth defects (Meijer et al 2014), showing that the effect of Lifeact-GFP expression on cell functioning is limited. Without continuous monitoring the in vivo dynamics of the actin cytoskeleton in a timeseries, it would not have been possible to distinguish the differences between the fungal actin patches and the oomycete actin plaques.

TABLE 1.1 | Actin visualization studies performed in oomycetes.

Species	Material	Labelling	Reference
Achlya bisexualis	Hyphae, sporangia, cleaving sporangia, zoospores, cysts	Phalloidin	Harold & Harold 1992
	Hyphae	Phalloidin	Yu et al 2004
	Hyphae	Phalloidin	Chitcholtan & Garrill 2005
	Hyphae	Phalloidin	Walker et al 2006
	Hyphae, plasmolysed hyphae	Phalloidin	Chitcholtan et al 2012
Aphanomyces cochlioides	Hyphae, zoospores, cysts	Phalloidin	Islam 2008
	Hyphae, zoospores, (germinating) cysts, sporangia	Phalloidin	Deora et al 2008a
	Hyphae	Phalloidin	Deora et al 2010
	Hyphae	Phalloidin	Islam & Fukushi 2010
Eurychasma dicksonii	Infection hyphae	Phalloidin	Tsirigoti et al 2013
Phytophthora cinnamomi	Zoospores, (cleaving) sporangia	Phalloidin	Jackson & Hardham 1998
	Hyphae	Phalloidin	Walker et al 2006
Phytophthora infestans	Hyphae and germinating cysts	Antibody against actin	Temperli 1990
	Hyphae	Phalloidin	Ketelaar et al 2012
	Hyphae	Lifeact-GFP	*Meijer et al 2014
Phytophthora megasperma	Hyphae	Antibody against actin	Porschewski et al 2001
Phytophthora melonis	Germinating cysts and hyphae	Phalloidin	Zhu et al 2007
Plasmopara viticola	Cysts, germinating cysts	Phalloidin	Riemann et al 2002
Pythium aphanidermatum	Hyphae	Phalloidin	Deora et al 2008b
	Hyphae	Phalloidin	Deora et al 2010
Saprolegnia ferax	Hyphae	Phalloidin	Kaminskyj & Heath 1994
	Hyphae	Phalloidin	Gupta & Heath 1997
	Hyphae, germinating cysts	Phalloidin	Bachewich & Heath 1998
	Hyphae, developing sporangia	Phalloidin	Levina et al 2000
	Hyphae, (germinating) protoplasts	Antibody against actin	Heath et al 2000

*Live cell imaging study

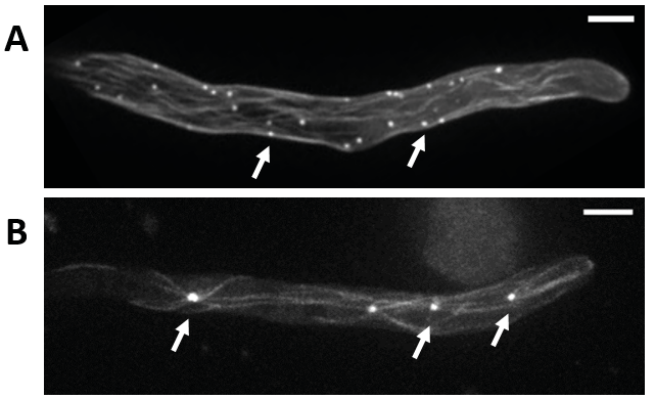

FIGURE 1.2 | A) *Phytophthora infestans* hypha expressing Lifeact-GFP and showing actin cables and plaques (arrows). B) *Phytophthora palmivora* hypha expressing GFP-α-tubulin and showing microtubules radiating from MTOCs (arrows). Scales are 5 μm.

1.5 The microtubule cytoskeleton

Like actin, microtubules are conserved amongst diverse eukaryotic supergroups. Microtubules are hollow tubes with a diameter of 24 nm, assembled from α-β-tubulin heterodimers. Microtubules are polarized structures with a plus and a minus end with distinct behaviour. They play a role in various cellular processes such as mitosis, cell motility, intracellular transport, cell shape regulation and flagellar movement (Wickstead & Gull 2011). The role of microtubules in some of these processes, like mitosis and flagellar movement, are conserved in evolution (Wickstead & Gull 2011). The roles of microtubules in other processes are more specific for certain evolutionary groups, such as their involvement in guiding the cellulose microfibril synthesizing machinery during cell wall depositions in plant cells (Paredez et al 2008). Microtubules are highly dynamic. The plus end of a microtubule alternates periods of growth (polymerization) and shrinkage (depolymerization), which is referred to as dynamic instability (Horio & Murata 2014). During microtubule polymerization, the plus end contains GTP-bound heterodimers composed of α- and β-tubulin, referred to as the GTP-cap. GTP bound to heterodimers within the microtubule lattice is rapidly hydrolysed; a GTP-cap is only maintained when a constant flow of GTP-bound dimers is added. When hydrolysis of GTP occurs faster than incorporation of GTP-bound heterodimers, GDP-bound heterodimers are exposed at the plus end of a microtubule. This causes a switch from polymerization to depolymerization, which is referred to as a catastrophe. Microtubule depolymerization continues until incorporation of GTP-heterodimers outcompetes GTP-hydrolysis and a new GTP-tubulin cap is formed. This swich between depolymerization and polymerization is referred to as a rescue. The process of dynamic instability mainly occurs at the plus end of the microtubule. The minus end of the microtubule is often capped by γ-tubulin, which serves as a microtubule nucleator (Tovey & Conduit 2018). Exposed minus ends undergo depolymerization under physiological conditions (Akhmanova & Steinmetz 2015). As with the actin filaments, numerous proteins interact with the microtubule cytoskeleton, collectively referred to as the Microtubule Associated Proteins (MAPs). Different classes of MAPs harbour a plethora of different functions. For example, the motor proteins, kinesin and dynein exhibit directional movement over the microtubules. Besides roles in transport, these motors also function in organizational processes (Mitchison & Salmon 2001, Vicente & Wordeman 2015). Some MAPs are specifically associated with the microtubule plus end, such as EB1 and CLASP. Other MAPs specifically function in processes that contribute to microtubule organization and perform scaffolding functions such as katanin, that severs microtubules (Qiang et al 2006), or MAP65/PRC1/AseI that acts as an antiparallel microtubule bundler (Lucas et al 2011, She et al 2019). For more information about MAP diversity and functions, see e.g., Bodakuntla et al (2019) or Gardiner (2013).

The microtubule cytoskeleton in oomycete species has received limited attention. So far, all visualization studies (listed in **table 1.2**) make use of immunolabelling, using fixed, dead material. The number of microtubules that ramify in the cytoplasm is less compared to the

number of actin cables visible after actin labelling (Kaminskyj & Heath 1994, Temperli et al 1991, **figure 1.2B**). Heath and Greenwood (1968) were the first to show that in oomycetes, in this case in mycelium of *Saprolegnia ferax,* all microtubules are linked to Microtubule Organizing Centres (MTOCs) that are embedded in the nuclear membrane, one MTOC per nucleus. Each MTOC contains two centrioles (Heath & Greenwood 1970). Before nuclear division, the MTOC duplicates and a spindle is formed that is contained within the nuclear membrane (Heath & Greenwood 1970). Such a nuclear division during which no nuclear envelope breakdown occurs, is referred to as a closed mitosis (Heath 1980). Although a closed mitosis is not observed in land plants and animals, its occurrence is not restricted to oomycetes, but might be linked to a coenocytic lifestyle (De Souza & Osmani 2007). A similar microtubule organization was observed in other oomycetes listed in **table 1.2**. In an attempt to gain insight in the functions of microtubules in oomycetes, Heath at al. (2000) applied the microtubule depolymerizing drugs nocodazole and methyl benzimidazole-2-yl carbamate (MBC). Exposure to the drugs for 24h resulted in a reduction in growth and a disruption of nuclear positioning (Heath et al 2000). Other studies focus on the role of microtubules during zoospore formation and functioning (Hardham 1987, Hyde & Hardham 1993). As heterokonts, oomycetes have zoospores with two flagella, one whiplash and on tinsel. Both flagella contain an axoneme, a structure conserved in eukaryotes, consisting of nine sets of radially arranged doublet microtubules and two central microtubules that drives flagellar motility (Ishikawa-Ankerhold & Muller-Taubenberger 2019). Flagella originate from a basal body. The basal bodies resemble centrioles in organization, both consisting of nine sets of microtubules (Preble et al 1999). During zoosporogenesis, the MTOCs in the cleaving sporangia mature into the basal bodies to provide templates for flagellar assembly (Hyde & Hardham 1992). Treatment of sporangia with the microtubule depolymerizing drugs cytochalasin D and oryzalin, revealed that cytochalasin D, despite causing abnormal cleavage, had no effect on the microtubule arrays and nuclear positioning during sporangial cleavage. The oryzalin treatment, additionally to causing abnormal cleavage, led to a disruption of the asymmetric positioning of microtubule arrays and nuclei during sporangial cleavage. In this study the authors hypothesize that this asymmetric disposition is essential to zoospore polarities (Hyde & Hardham 1993). To summarize, microtubule-based processes such as flagellar motility and mitosis are conserved in oomycetes, but little is known about the precise functions of interphase microtubules in mycelium.

TABLE 1.2 | Tubulin visualization studies performed in oomycetes.

Species	Material	Labelling	Reference
Eurychasma dicksonii	Infection hyphae	Antibody against tubulin	Tsirigoti et al 2013
Phytophthora cinnamomi	Sporangia, cleaving sporangia, zoospores	Antibody against tubulin	Hardham 1987; Hyde & Hardham 1993
Phytophthora infestans	Hyphae and germinating cysts	Antibody against tubulin	Temperli 1990
	Hyphae	Antibody against tubulin	Temperli et al 1991
Plasmopara viticola	Cysts, germinating cysts	Antibody against α-tubulin	Riemann et al 2002
Saprolegnia ferax	Hyphae, (germinating) protoplasts	Antibody against α-tubulin	Heath et al 2000
	Hyphae, germinating cysts	Antibody against α-tubulin	Bachewich & Heath 1998
	Hyphae	Antibody against α-tubulin	Kaminskyj & Heath 1994

1.6 Outline of this thesis

The research presented in this thesis focusses on the cytoskeleton in oomycete plant pathogens and makes use of live cell imaging to visualize the dynamics of the actin and tubulin cytoskeleton in *Phytophthora* spp. In **chapters 2**, **3** and **4** we make use of the Lifeact-GFP transformants of *P. infestans* generated by Meijer et al (2014), and for **chapter 5** we extended the toolbox by generating Lifeact-GFP and GFP-tubulin transformants of *P. palmivora*. The experimental set-up for live cell imaging and details with respect to the biological material are described in **box 1.1.**

The first live cell imaging study of Lifeact transformants of *P. infestans* by Meijer et al (2014) showed the dynamics of two cortically located actin configurations in hyphae, namely cables and plaques. In **chapter 2**, we studied the *P. infestans* Lifeact-GFP transformants in more depth, focussing on the life cell stages important for successful plant cell infection. This led to the discovery of two new actin configurations, namely (1) an actin accumulation associated with a cell wall plug deposition in germ tubes emerging from cysts and (2) an actin aster, present in the tip of hyphae attempting to invade glass coverslips.

In **chapter 3** we addressed the question whether the formation of actin asters is triggered by physical disturbance, a condition encountered by a plant pathogen when a hyphal tip touches the plant surface. To this end we mimicked physical disturbance of hyphae by laser ablation and monitored the response of the actin cytoskeleton over time.

The role of actin plaques in oomycetes remains elusive. While actin patches in fungi move inwards and likely facilitate endocytosis, actin plaques reside at the cortex. In **chapter 3** we tested the hypothesis that actin plaques have a role in anchoring the actin cytoskeleton to the cell wall plasma membrane continuum. To this end we generated protoplasts from young Lifeact-GFP expressing hyphae from *P. infestans* and studied the dynamics of the actin cytoskeleton in these wall-less cells and during cell wall recovery.

For many crop protection agents the precise mode of action is obscure and will often not be examined in depth until the product is on the market. The fungicide flumorph was reported to have a negative effect on actin organization in oomycetes (Zhu et al 2007), but the evidence was thin. In **chapter 4** we exploited a Lifeact-GFP expressing *P. infestans* transformant to refute the claim that flumorph targets the actin cytoskeleton. This study demonstrates the added value of live cell imaging of plant pathogens expressing fluorescent markers tagging subcellular compartments and structures, as it allows to gain more detailed insight in the mode of action of crop protection agents.

In **chapter 5**, we studied the microtubule cytoskeleton dynamics in *P. palmivora*. This is the first study of its kind in any oomycete. We generated GFP-tubulin labelled *P. palmivora* transformants, which enabled us to visualize the microtubule cytoskeleton during nuclear division, verify microtubule depolymerization in the presence of oryzalin and track microtubule dynamics during hyphal growth. Additionally, we provide a list of MAPs present in *P. infestans*.

In the general discussion, **chapter 6**, the main findings presented in this thesis are integrated and discussed in a broader perspective. I provide an overview of actin and microtubule interacting drugs that we and others have used to study the cytoskeleton in oomycetes and elaborate on the feasibility of the cytoskeleton as primary target for controlling plant diseases caused by oomycetes.

Box 1.2 Life cell imaging of *Phytophthora* spp.

When working with biological material, one should always strive for optimal conditions of the cells and tissues for experiments to be repeatable and reliable. Dying or distressed cells can show all kinds of artefacts and even autofluorescence. Optimal conditions can be species specific. For example, *P. infestans* is perfectly happy for two days or even longer in a biofoil slide (Meijer et al 2014), while *P. palmivora* growth is stunted and development of chlamydospores starts within hours of enclosure of the material in the biofoil slide. Both *P. infestans* and *P. palmivora* grow well in a glass bottom dish. Healthy growing hyphae usually have a slightly pointed tip, filled with cytoplasm. Vacuoles can be found in more distal areas of the hyphae. The appearance of vacuoles in the extreme tip is usually a sign of disrupted growth. This happens, for example after exposure of *P. infestans* hyphae to the actin depolymerizing drug latrunculin B (Meijer et al 2014). In old distal areas, cell wall plugs can be observed that completely seal off any cytoplasm depleted areas. Cysts, that are often used as starting material for life cell imaging, are readily obtained by triggering encystment of zoospores. After zoospores have been harvested, they can be encysted by vigorous shaking of the zoospore suspension. Notably, *P. palmivora* zoospores will also encyst when placed on ice. When cysts of *P. infestans* are placed on a surface, such as glass or plastic, they will form a hyphal swelling in the tip pushing against the surface, as though to invade the surface (Grenville-Briggs et al 2008). In the figure below most of the critical steps for life cell imaging are depicted.

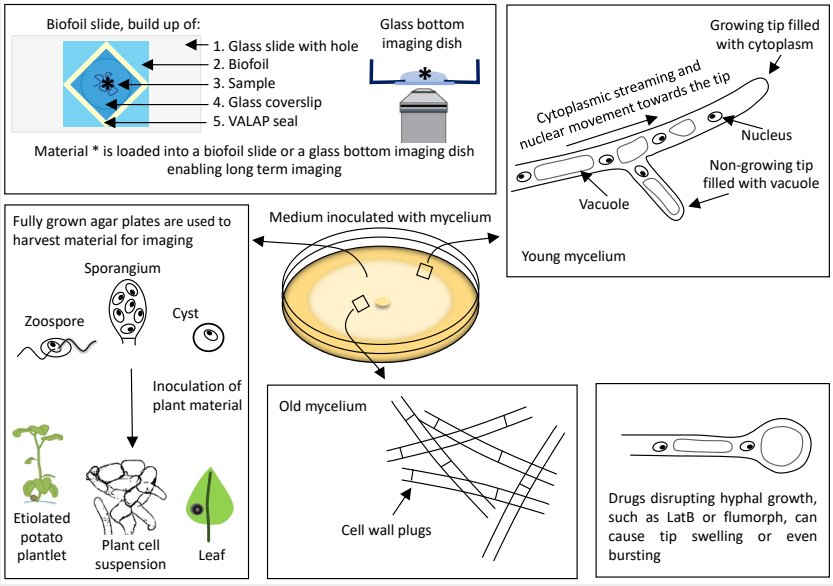

Chapter 2

Filamentous actin accumulates during plant cell penetration and cell wall plug formation in *Phytophthora infestans*

Kiki Kots*
Harold J. G. Meijer*
Klaas Bouwmeester
Francine Govers
Tijs Ketelaar

* Equal contribution

This chapter is published in 2017 in *Cellular and Molecular Life Sciences* 74(5): 909-920

2.1 Abstract

The oomycete *Phytophthora infestans* is the cause of late blight in potato and tomato. It is a devastating pathogen and there is an urgent need to design alternative strategies to control the disease. To find novel potential drug targets we study the actin cytoskeleton, using Lifeact-GFP expressing *P. infestans* for high resolution live cell imaging of the actin cytoskeleton during development. Previously, we identified actin plaques as structures that are unique for oomycetes. Here we describe two additional novel actin configurations; one associated with plug deposition in germ tubes and the other with appressoria, infection structures formed prior to host cell penetration. Plugs are composed of cell wall material that is deposited in hyphae emerging from cysts to seal off the cytoplasm-depleted base after cytoplasm retraction towards the growing tip. Preceding plug formation there was a typical local actin accumulation and during plug deposition actin remained associated with the leading edge. In appressoria, formed either on an artificial surface or upon contact with plant cells, we observed a novel aster-like actin configuration that was localized at the contact point with the surface. Our findings strongly suggest a role for the actin cytoskeleton in plug formation and plant cell penetration.

2.2 Introduction

Phytophthora infestans is a plant pathogen in the class oomycetes, filamentous organisms that resemble fungi in lifestyle and morphology but without evolutionary relationship with fungi. Oomycetes belong to the Stramenopile lineage together with the brown algae and diatoms (Bouwmeester et al 2009) and are well-known as pathogens mainly of plants but also of animals and other organisms. The genus *Phytophthora* comprises over 120 species, many of which are devastating plant pathogens (Kroon et al 2012). *Phytophthora infestans*, the causal agent of potato late blight, is the most notorious one and famous since the Great Irish Famine in the mid-nineteenth century. Today, *P. infestans* is still a major problem for potato production worldwide. For controlling late blight farmers spray crop protection agents every 5-7 days and up to 17 times per growing season. Similar intensive chemical treatments are needed to control other oomycete pathogens, not only in crops but also in aquaculture where saprolegniasis, a disease caused by *Saprolegnia parasitica*, is a major problem in salmon farming (van den Berg et al 2013).

Oomycetes grow as mycelium and reproduce and disperse by means of spores. The vegetative propagules of *P. infestans* are sporangia that germinate directly or indirectly, depending on the ambient temperature. At temperatures lower than 15 °C the sporangia cleave and release motile zoospores, while at higher temperatures the sporangia can germinate directly (Judelson & Blanco 2005, Schoina & Govers 2015). When encountering a suitable environment, like a leaf surface, the hyphal germlings emerging from sporangia

or from encysted zoospores develop an appressorium at the tip, and subsequently a penetration peg is formed that pierces the plant epidermis. After the pathogen has gained access to the plant, the hyphae grow intercellular in the mesophyll occasionally forming digit-like structures called haustoria that penetrate plant cells (Judelson & Blanco 2005, Schoina & Govers 2015). Contrary to fungal hyphae, the hyphae of oomycetes lack septa or cross walls and are therefore referred to as aseptate or coenocytic. However, under certain circumstances septa, in some cases referred to as cross walls, have been observed in oomycetes, for example at the basis of the sporangium, at the hyphal tip, in old mycelium or in response to wounding (Hardham 2009, Kortekamp 2005, Levina et al 2000). Interestingly, in *P. infestans* septa-like structures have also been described to form in the germ tube, separating the cyst form the appressorium (Kramer et al 1997).

Actin is an essential structural component in eukaryotic cells (Schmidt & Hall 1998). The actin cytoskeleton that consists of a highly dynamic network of filamentous actin polymers (F-actin) is involved in many cellular processes, including muscle contraction, cell motility, cytokinesis, and vesicle and organelle transport (Moseley & Goode 2006, Roman et al 2013, Van der Honing et al 2007). The precise function of the actin cytoskeleton differs among organisms and between tissues. For example, in tip-growing organisms such as fungi and oomycetes, and also in pollen tubes and root hairs, the actin cytoskeleton is indispensable for establishing and maintaining tip growth (Bachewich & Heath 1998, Gibbon et al 1999, Ketelaar 2013). In oomycetes, F-actin is organized in two prominent higher order structures, namely actin cables and dot-like actin structures, called actin plaques . Additionally, a few oomycete species, i.e. *Saprolegnia ferax, Achlya bisexualis* and *Phytophthora cinnamomi*, were shown to have hyphae with an apical cap of F-actin (Bachewich & Heath 1998, Temperli 1990, Walker et al 2006). Actin plaques seem to occur at higher frequencies in non-growing parts of the hyphae and in resting structures, while actin cables are more abundant during germination and in growing hyphae (Deora et al 2008, Ketelaar et al 2012, Meijer et al 2014). Moreover, as was found in *P. infestans,* plaques are more resilient to the actin depolymerizing drug latrunculin B than cables (Ketelaar et al 2012, Meijer et al 2014). The function of the different actin structures in oomycetes remains elusive. Previously it was hypothesized that actin plaques in oomycetes are similar to actin patches in fungi, with the latter functioning as force generators for vesicle internalization during endocytosis (Aghamohammadzadeh & Ayscough 2010, Delgado-Alvarez et al 2010, Kaksonen et al 2003, Lichius et al 2011, Moseley & Goode 2006). However, our recent study in which we used fluorescently tagged Lifeact for live cell imaging of the actin cytoskeleton in *P. infestans* showed that actin plaques in *P. infestans* have a far longer lifetime and are much less mobile than actin patches in fungi (Meijer et al 2014). We also showed that, in contrast to patches, plaques are not internalised and therefore it is unlikely that plaques have a function in endocytosis.

Prior to host cell invasion many (hemi-)biotrophic filamentous plant pathogens, including *P. infestans,* form a specialized rigid infection structure known as appressorium that facilitates penetration of the host. Microscopic imaging of the actin cytoskeleton in a Lifeact-

RFP expressing line of the rice blast fungus *Magnaporthe oryzae,* revealed that during plant cell invasion a toroidal F-actin network, scaffolded by septins, is assembled in appressoria (Dagdas et al 2012). Septins are small guanosine triphosphatases (GTPases) that are involved in reorientation and reorganization of the cytoskeleton. In this study we exploited the previously described *P. infestans* Lifeact-GFP strains (Meijer et al 2014) to investigate the organization and dynamics of the actin cytoskeleton in *P. infestans* in germ tubes emerging from sporangia or cysts, and during appressorium formation and plant cell infection. For this purpose we used two culture conditions. On the one hand we allowed sporangia or cysts to germinate on a hydrophobic surface that triggers the formation of appressoria in the absence of the host plant and, on the other hand we used a so-called *in vitro* infection system that makes use of tomato MsK8 cells grown in suspension. In this system we can mimic leaf infection and take advantage of the fact that the infection process is more synchronized and more suitable for microscopic imaging. In addition to the cortically localized actin cables and actin plaques that we described previously (Hua et al 2015, Meijer et al 2014), we identified two novel actin configurations. The first one is an actin accumulation in appressoria, at the site of contact with the hydrophobic surface or, in the case of the *in vitro* infection system, at the site where the penetration peg emerges from the appressorium to enter the host cell. The second one is associated with a structure that divides the germ tube into two compartments, one towards the tip that is full of cytoplasm and a basal part that seemingly lacks cytoplasm. We show here that this basal part is sealed off by cell wall plugs that are deposited centripetally and that this plug formation is preceded by a localized accumulation of actin filaments that remains present until a plug has been deposited. These observations provide further insights into the organisation of the actin cytoskeleton in *P. infestans*, in particular during cyst germination and in appressoria, the structures that play an important role in pathogenesis.

2.3 Materials and methods

Strains and cultures

Phytophthora infestans strain 88069 and a Lifeact-GFP (previously described in Meijer et al 2014) expressing strain were maintained on Rye Sucrose Agar plates (RSA; Caten & Jinks 1968), with appropriate selective antibiotics as described in Meijer et al (2014). Cultures were maintained by transferring mycelial plugs from fully grown plates to fresh plates every 2 to 3 weeks. The tomato MsK8 cell suspension culture was grown as described by Koornneef et al (1987).

Sample preparation

Zoospores were released by flooding sporulating cultures with Milli-Q water (4 °C) and subsequent incubation at 4 °C for 3 hours. The zoospore suspension was filtered through Miracloth (Calbiochem, Germany) and the zoospores were encysted by vortexing the filtrate for 5 minutes. Sporangia were collected as described previously (Meijer et al 2014). The cysts or sporangia were then transferred to biofoil-slides (Meijer et al 2014) containing water or liquid RS medium and incubated for 5 hours at 18 °C to allow cyst germination (Meijer et al 2014). For plant cell infection assays, 2 ml of zoospore suspension ($4*10^6$ zoospores per ml) was added to 2 ml of a 5 days old tomato MsK8 cell suspension culture (C. Schoina, personal communication). This mixture was incubated overnight at room temperature on a rotary shaker (80 rpm) in the dark. Alternatively, a small fraction of the plant cell and zoospore mixture was enclosed in a biofoil-slide and incubated stationary overnight at room temperature in the dark.

Microscopy

To visualize F-actin dynamics a Roper Spinning Disc Confocal System (Evry, France) consisting of a CSU-X1 spinning disk head (Yokogawa, Japan) mounted on a Nikon Eclipse Ti microscope (Tokyo, Japan) with Perfect Focus system was used. For imaging we used a 100× Plan Apochromat 1.4 N.A. oil immersion objective. Fluorescence imaging was performed using a 491 nm laser line combined with band pass emission filtering (530/50 nm; Chroma Technology). Images were acquired with an Evolve electron-multiplying (EM) charge-coupled device camera (Photometrics) at an EM gain of 200, controlled by Metamorph software (Molecular Devices, California). Z-stacks were collected using a 0.5 µm step size.

For cell wall staining, solutions with calcofluor white (Sigma-Aldrich, Missouri) or aniline blue (Sigma-Aldrich, Missouri) were added to germinated cysts shortly before imaging to the final concentrations of 0.0017% w/v and 0.2% w/v, respectively. Fluorescence imaging was performed using a Zeiss LSM 510 Meta confocal microscope equipped with a 63x Plan-Apochromat 1.4 N.A. oil immersion objective. Calcofluor white and aniline blue were imaged using the 405 nm laser line combined with a 420-480 nm band pass emission filter and a 420 nm long pass filter, respectively.

Image processing

All image processing was carried out using the software package ImageJ (rsbweb.nih.gov/ij/). Collected images were enhanced by contrast stretching and maximal intensity Z-projections were made. Orthogonal views were constructed by scaling the Z-axis to the size of x,y pixel dimensions (Scale plugin) and making kymographs (Multiple kymograph plugin) of scaled z-stacks.

2.4 Results

Germ tubes emerging from cysts have plugs containing cellulose and callose

When a zoospore touches a solid surface it immediately encysts and starts to germinate. In this early stage the cyst and germ tube are filled with cytoplasm. However, we noticed that upon germ tube elongation, the majority of the cytoplasm relocates to the tip of germ tube, a phenomenon that has been described before (Kramer et al 1997). After this retraction of cytoplasm from the cyst and basal part of the germ tube, we observed the formation of a wall-like structure that separated the basal part depleted of cytoplasm from the cytoplasmic rich apical part of the hypha (**figure 2.1**). This wall-like structure is reminiscent of structures observed in pollen tubes that are referred to as callose plugs. Callose plugs in pollen tubes, like the wall-like structure in *P. infestans,* separate the cytoplasm filled tip from the empty basal part (Raudaskoski et al 2001). In oomycete literature the term plug has been used to describe the cell wall material that is deposited in response to impalement with a glass electrode (Levina et al 2000), the term cross wall has been used to describe the wall-like structure that separates a sporangium from a hypha (Levina et al 2000) and the term septum has been used to describe cross walls in hyphae (Kortekamp 2005). Since the structures that we observe in the germ tubes are not associated with cytokinesis but appear to seal off a compartment that is depleted of cytoplasm, we hereafter use the term cell wall plug or simply plug.

To determine the influence of nutrients on cyst germination rates and plug formation we compared nutrient poor (water) with nutrient rich (rye sucrose medium; RSM) growth conditions. During overnight incubation of cysts of strain 88069 the germination rate in water and RSM was comparable and in most hyphae multiple plugs were deposited (up to 6 per hyphae; **figure 2.2a**) with no significant difference between water and RSM ($p=0.44$, unpaired t-test ($n=46$)). The distance between the first deposited plug and the base of the cyst was on average 38.1 µm and the distance between plugs 33.7 µm with no significant differences between water and RSM (**figure 2.2b** and **2.2c**; $p=0.12$, unpaired t-test ($n=46$) and $p=0.21$, unpaired t-test ($n=32$), respectively). We also tested whether the expression of the Lifeact-GFP caused differences in plug formation and positioning by comparing the previously described Lifeact-GFP expressing line (Meijer et al 2014) with its recipient strain 88069. No significant differences were found between strains in the distance between plugs or the distance between the first plug and the cyst (**figure 2.2**; unpaired t-tests, $n>20$ and $p>0.11$ for all tests).

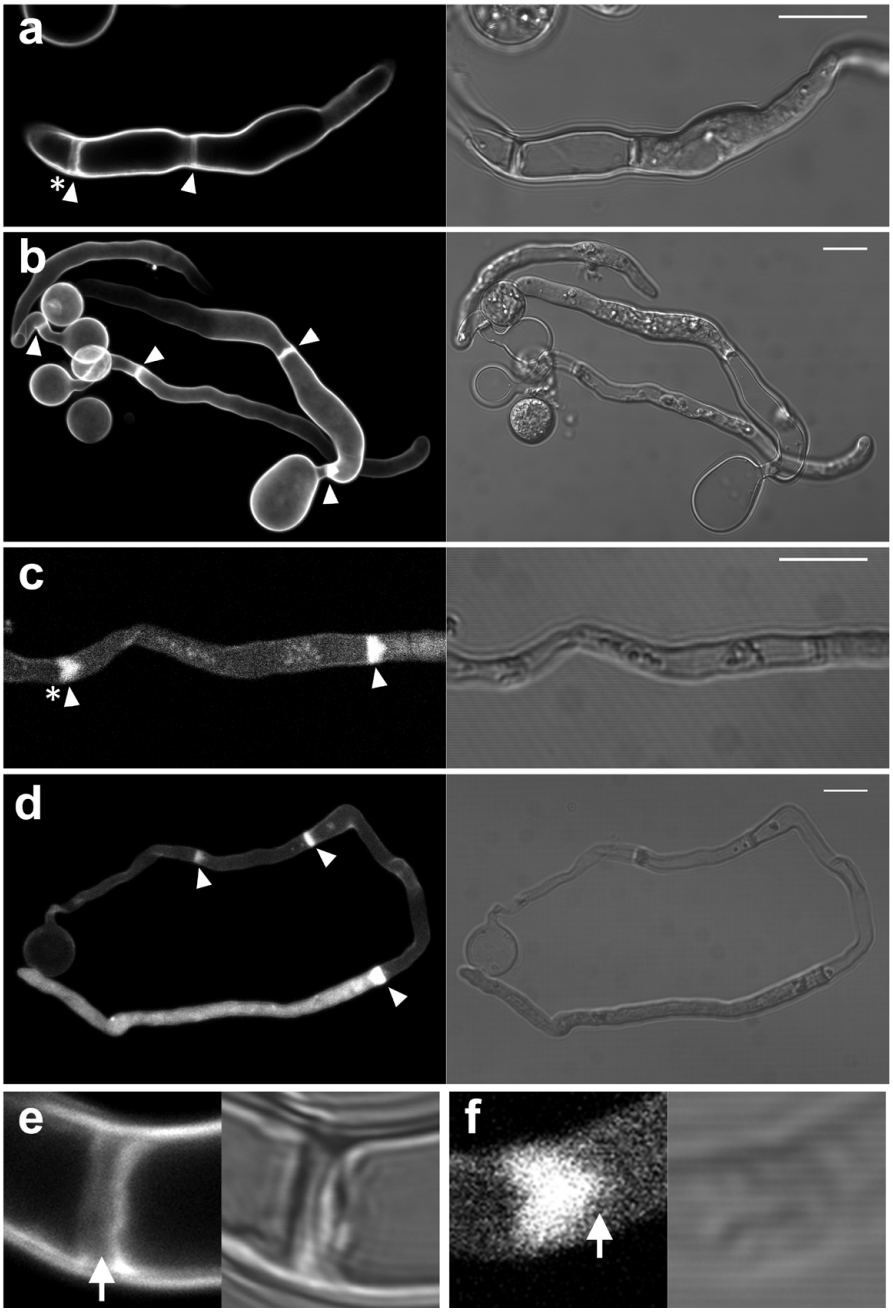

FIGURE 2.1 | Plugs in germ tubes emerging from *P. infestans* cysts contain cellulose and callose. Plugs (arrowheads) are visualized by staining with calcofluor white (a, b, e) and aniline blue (c, d, f) that reveal cellulose and callose, respectively. The plugs indicated with the asterisk in (a) and (c) are shown in more detail in (e) and (f), respectively. In (e) the arrow indicates the middle lamellae of the plug, which is not stained by calcofluor white. The arrow in (f) indicates the protruding side of the plug pointing towards the tip. The images represent single confocal planes (a, c, e, f) or z-projections (b, d). On the right are the bright field images and on the left the fluorescent channel images. Bar = 10 µm.

To learn more about the composition of the plugs, we stained hyphae with calcofluor white, which emits fluorescence when bound to chitin and cellulose (Harrington & Hageage 2003) and aniline blue, which has a high specificity for callose (Evans et al 1984, Nowicki et al 2012). Since oomycetes have hardly any chitin in their cell walls (<1% of the cell wall carbohydrates; Grenville-Briggs et al 2005, Meijer et al 2006, Melida et al 2013), the calcofluor white fluorescence most likely represents cellulose. **Figure 2.1** shows that staining with either calcofluor white or aniline blue resulted in a strong fluorescent signal, but the localization of the fluorescence differed. In 50% (n=24) of the plugs that were studied by confocal microscopy, calcofluor white staining revealed two lamellae with a high fluorescence intensity that surrounded a lamella with a much lower fluorescence intensity (detail shown in **figure 2.1e**). No such layering was observed in plugs in the aniline blue stained hyphae (detail shown in **figure 2.1f**; n=24). Instead, the aniline blue stained plugs were often (50%) triangularly shaped, with the protruding side of the plug pointing towards the hyphal tip (**figure 2.1f**). Occasionally, in the calcofluor white stained plugs a similar small protrusion pointing towards the hyphal tip could be observed. The layering that was often observed in the calcofluor white stained plugs and never in the aniline blue stained plugs, suggests that unlike callose, cellulose is not evenly distributed in plugs.

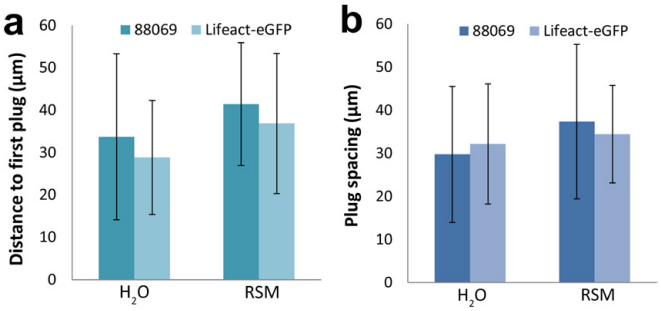

FIGURE 2.2 | The distance of the hyphal tip to the first deposited plug (a) and the spacing between plugs (b) in hyphae emerging from cysts from *P. infestans* strain 88069 and the Lifeact-GFP expressing derivative. Per data point 9 to 26 hyphae were measured. Error bars indicate standard deviations.

A ring-shaped actin filament assembly correlates with plug formation

Next, we studied the actin configuration during plug formation. Although most Lifeact-GFP is bound to filamentous actin, a limited amount of fluorescence does not appear to co-localise with actin filaments. This is recognisable as a faint staining of the cytoplasm and nucleus. We used this fluorescence to study the cytoplasmic organisation during plug formation by confocal microscopy. This revealed that plug formation is preceded by a rapid depletion of the cytoplasm from the basal part of the hypha (**video S2.1**). During cytoplasmic depletion, most of the Lifeact signal disappeared together with the retracting cytoplasm. Notably, the actin plaques frequently started to migrate into the apical part of the hypha and subsequently,

F-actin started to accumulate at the ultimate site of septum formation, resulting in a ring-like assembly (**figure 2.3a**). At the site of the actin accumulation, plug formation was initiated by centripetal ingression of the Lifeact fluorescence while cell wall material was deposited. During the centripetal expansion of the plug, the F-actin remained associated with its leading edge. Plug deposition took on average 11.5 minutes (± 1.9; n=10). A kymograph displaying the kinetics of plug formation revealed a uniform extension velocity during plug deposition (**figure 2.3i**). After completion of the plug, a small amount of cytoplasm was left basal of the plug in which a limited number of actin cables and plaques were observed. This remnant of cytoplasm basal of the plug lacked a nucleus, but a limited number of actin cables were maintained; this is in contrast to plaques that rapidly disappeared upon plug completion (**figure 2.3a-g**). In ~50% of the hyphae, the plaques in the cytoplasm remnant displayed a specific, rapid increase in intensity before fluorescence diminished and the plaques disappeared (**figure 2.3a-g** and **2.3j**) After disappearance of the plaques, hardly any or no cytoplasmic streaming was observed (**video S2.2**). To investigate if there is a continuum between the cytoplasm apical and basal of the plug, the Lifeact-GFP in the compartment basal of the plug was photobleached and the recovery was monitored. In contrast to the controls, i.e. in hyphae lacking plugs, where we could observe recovery, there was hardly any recovery visible in compartments basal of the plug and it is therefore unlikely that there is cytoplasm streaming from the apical to the basal part of the plug or *vice versa* (**figure 2.4**).

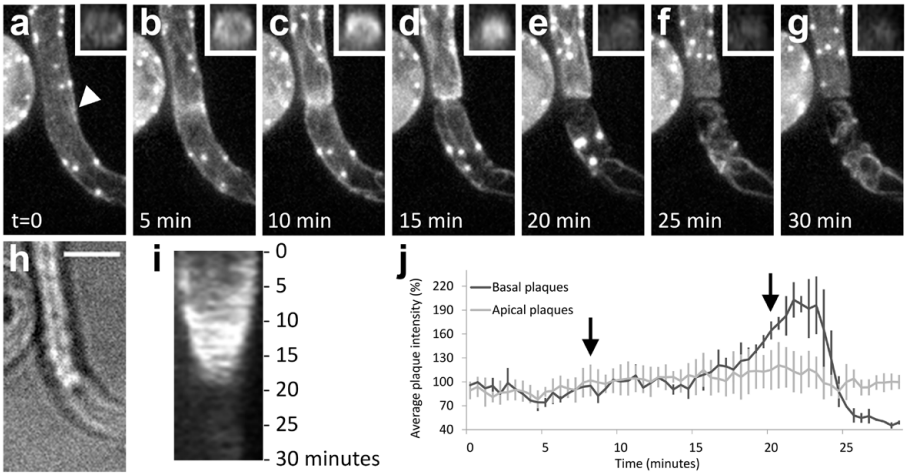

FIGURE 2.3 | A local accumulation of actin filaments precedes plug formation and is associated with the expanding plug during plug deposition. Plug formation over time (a-g) visualized by maximum intensity projections of Z-stacks of a hypha of a Lifeact-GFP expressing *P. infestans* strain with the hyphal tip (not visible) pointing upwards. The arrowhead in (a) indicates the plug deposition site. The insets in (a) to (g) are orthogonal views of the Z-stacks at the site where the plug is deposited. h is a bright field image of (d). i Kymograph of the plug deposition. j Average fluorescence intensity in percentage (Y-axis) over time of the plaques that remain in the basal part of the hypha after plug formation (n =3, dark grey line) with the average intensity over time of randomly picked plaques in the apical part of the hypha (n = 7, light grey line) set to 100%. At t=8 (first arrow) plug deposition is first visible and at t=20 plug formation is completed (second arrow). Error bars indicate standard deviations. Bar = 5 µm.

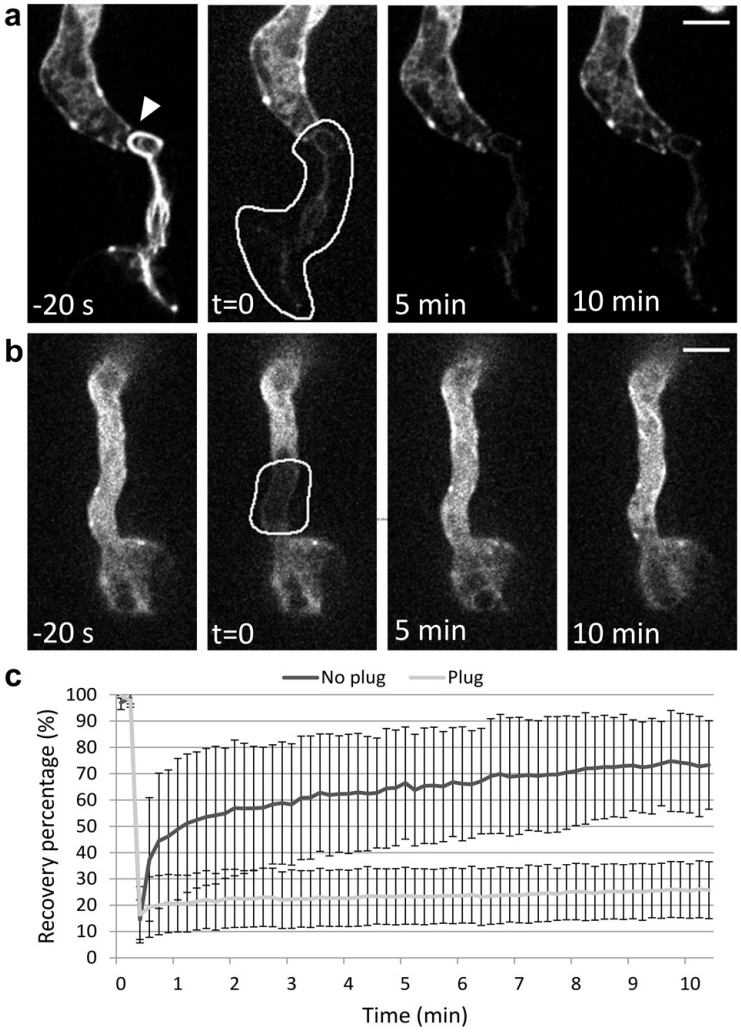

FIGURE 2.4 | Plugs in a *P. infestans* hypha block the cytoplasmic streaming between the apical and basal part of the hypha. A compartment of the hypha that was sealed off by a plug (a; indicated by the arrowhead) and a part of the hypha that was in contact with the rest of the hypha (b) was photobleached and recovery of Lifeact-GFP was recorded over 10 minutes. In (a) and (b) panels marked with -20 s show the fluorescence before photobleaching and t=0 shows the area selected for photobleaching (white line). Recovery was monitored immediately after photobleaching (t=0) and after 5 and 10 minutes. Bar = 5 µm. c The average fluorescence recovery after photobleaching (Y-axis) over time (X-axis) for hyphae with plug (n=7) and hyphae without plug (n=8).

A novel aster-like actin configuration in appressoria

When a cyst germinates and encounters a plant surface, the tip of the germ tube swells to form an appressorium (Judelson & Blanco 2005). Appressorium formation can also be induced on artificial surfaces in the absence of the plant (*in vitro*) for example on polypropylene foil or in Petri dishes (Grenville-Briggs et al 2008, Kramer et al 1997). We found that also glass coverslips are suitable as artificial surface for appressorium formation. This enables high resolution imaging of any actin configuration present in the appressoria. First we focused on the early stages of appressorium formation, and more specifically when the expanding hyphae grew against the coverslip. In these hyphae we consistently (n=15) observed an aster-like actin cable configuration while contact with the coverslip was established (**figure 2.5**). As clearly shown in a side view (**figure 2.5c**), this burst of F-actin is visible at the point where the hypha touches the coverslip. The fluorescence intensity of the aster-like structures is relatively high and at the contact point it is in the same range as the fluorescence of actin filament plaques (**figure 2.5d**). When followed over time, we observed centrifugally propagating waves of higher intensity of Lifeact-GFP fluorescence that originated from the centre of the aster-like structure (**video S2.3**). We have observed similar propagating waves of fluorescence in the tip of growing hyphae that we interpreted as waves of polymerization (Meijer et al 2014). Upon contact with the coverslip, the tips of the hyphae swelled slightly, although the swelling in young appressoria was less prominent than in fully grown appressoria (**figure 2.6**). In fully grown appressoria the aster-like structure disappeared and the actin organization resembled that of non-growing hyphae, consisting of actin filament cables and actin plaques that were evenly distributed along the cell cortex (Meijer et al 2014). In addition, as in non-growing hyphae, a nucleus frequently resided in the vicinity of the hyphal tip (n=10). Orthogonal projections of the z-stacks (**figure 2.6c**) revealed that all of fully grown appressoria were in direct contact with the coverslip, confirming that physical contact is required for appressorium formation. When we monitored the appressoria over time, we could indeed confirm that they had stopped growing (**video S2.4**). Occasionally we observed a new outgrowth emerging from fully grown appressoria that had the actin organization of a regular growing hypha in which actin plaques were absent from the apex (**video S2.5**).

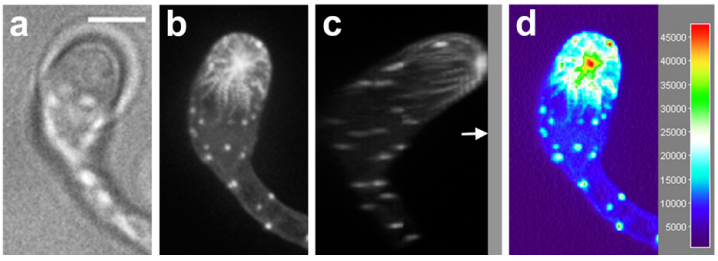

FIGURE 2.5 | An *in vitro*-formed appressorium of *P. infestans* with an aster-like actin structure at the contact point with the cover slip. Bright field image (a) and Z-projection showing the fluorescence of Lifeact-GFP (b). (c) is a side view of (b). The arrow points to a gray shaded bar that represents the cover slip. d Surface plot showing the fluorescence intensity of (b). Bar = 5 µm.

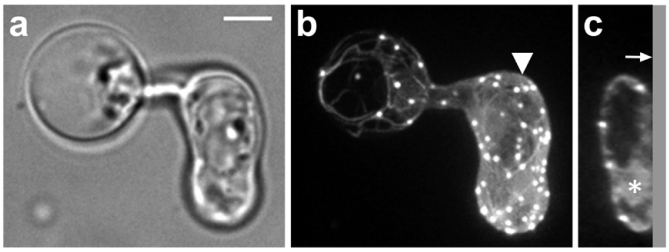

FIGURE 2.6 | Localization of actin in an *in vitro* appressorium formed by swelling of the tip of a germ tube that is emerging from a *P. infestans* cyst and adheres to a solid surface. Bright field image (a) and maximum intensity Z-projection (b) showing the fluorescence of Lifeact-GFP. The arrowhead in (b) indicates the position of the orthogonal projection shown in (c). In (c) the arrow points to a gray shaded bar that represents the cover slip and the asterisk marks the nucleus. Bar = 5 µm.

Transient actin accumulation in *P. infestans* during host cell penetration

In general it is challenging to study the dynamics of an infection process at the microscopic level. In the case of *P. infestans*, zoospores and plant tissue have to be brought together on a microscope slide and have be kept in optimal conditions for at least several hours. Moreover, actual penetration of the host has to occur close to the coverslip to allow high resolution imaging, and in addition, the host tissue has to be as thin as possible to be able to follow the infection process. We developed an experimental set-up that enabled us to visualize the interaction between *P. infestans* and its host at the microscopic level over time. This set-up makes use of gas-permeable bio-foil slides in which plant cells grown in suspension are co-cultivated with *P. infestans.* In this study we made use of two plant cell lines, namely the tomato MsK8 suspension cells (Koornneef et al 1987) and the tobacco BY-2 suspension cells (Nagata et al 1992). The tomato MsK8-*P. infestans* pathosystem has been developed and optimized in our laboratory, and MsK8 cells turned out to be a very suitable host for *P. infestans*. On the other hand, BY-2 cells display less autofluorescence and are therefore more suitable for imaging than MsK8 cells. However, the infection rates that we obtained with BY-2 cells were extremely low and thus we only used MsK8 cells.

We first focused on the moment of penetration of a MsK8 cell by a *P. infestans* hypha (**figure 2.7a-f**). Zoospores of *P. infestans* were added to MsK8 cells in a bio-foil slide, so that infection could be followed over time. It was challenging to predict when a hypha was about to penetrate a cell and to have this event in focus at the right time. Also, the image quality was reduced when compared to images of hyphae that grow against the coverslip. The large distance between most infection events and the coverslip caused an increased scattering of photons thus resulting in less clear images. Nevertheless, we were able to detect a transient accumulation of F-actin precisely at the penetration point. We examined several penetration events and in all cases we observed this transient accumulation (**figure 2.7b**; **video S2.6**; n=4).

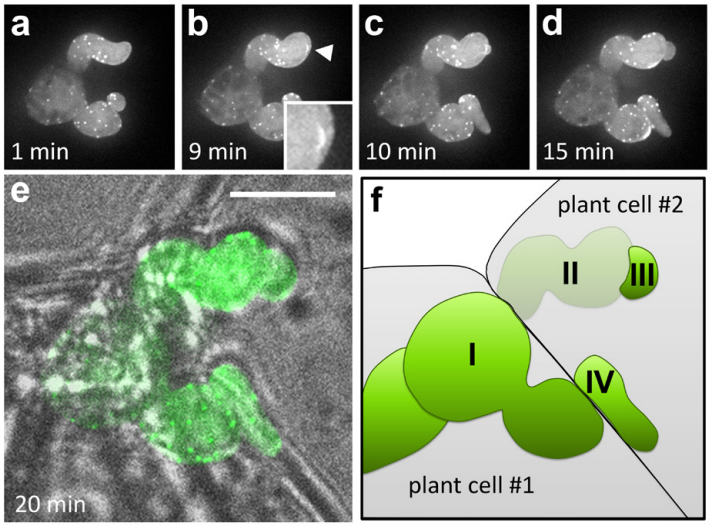

FIGURE 2.7 | Localization of actin in a *P. infestans* hypha penetrating a MsK8 tomato cell. Maximum intensity Z-projections of Lifeact-GFP fluorescence over time at 1 (a), 9 (b), 10 (c), 15 (d) and 20 minutes (e) from the start of the imaging. At t=9 (b) penetration takes place. A transient accumulation of F-actin, enlarged in the inset and indicated by an arrowhead, marks the moment of plant cell penetration. e shows the overlay of the bright field and the Lifeact-GFP fluorescence at 20 min. f Schematic overview of (e). (I) Hypha growing in plant cell #1. (II) Hypha exiting plant cell #1 and growing outside the plant cells before entering (III) plant cell #2. (IV) New outgrowth of hypha (I) crossing the cell wall between plant cell #1 and #2. Bar = 10 µm.

The actin organization in invasive hyphae is indistinguishable from that in hyphae grown in medium

When MsK8 cells were exposed to *P. infestans* zoospores in a bio-foil slide, two types of infections were observed: (1) *P. infestans* hyphae that directly penetrate MsK8 cells, and that exit the cell to continue further growth in the medium (**figure 2.8a-b**); and (2), *P. infestans* hyphae that penetrate MsK8 cells only after hyphal branching (in the medium) outside cells (**figure 2.8c-d**). Both infection types were observed frequently. Also in this set-up, cell wall plugs were detected in the germinated cysts similar to those described above when cysts were germinating in the absence of plant cells. However, cell wall plugs were only formed before plant cell penetration and were never observed in hyphae growing inside or emerging from a plant cell (**figure 2.8b-d**). Hyphae growing outside MsK8 cells had a similar actin organization as hyphae cultured *in vitro* (previously described in Meijer et al 2014), namely actin plaques in non-expanding parts of the hyphae and actin cables with a net-longitudinally orientation to the length axis of hyphae. A similar actin organization was observed in hyphae that were skewering MsK8 cells (**figure 2.8a-b**). Also penetration structures of the other type of infection showed similar actin organization as in normal growing hyphae, i.e. with actin filament cables and plaques evenly distributed over the cortex of the cell (**figure 2.8c-d**). Thus, the actin organization of hyphae that penetrate MsK8 cells did not differ from that of hyphae growing in between cells or in the absence of host cells.

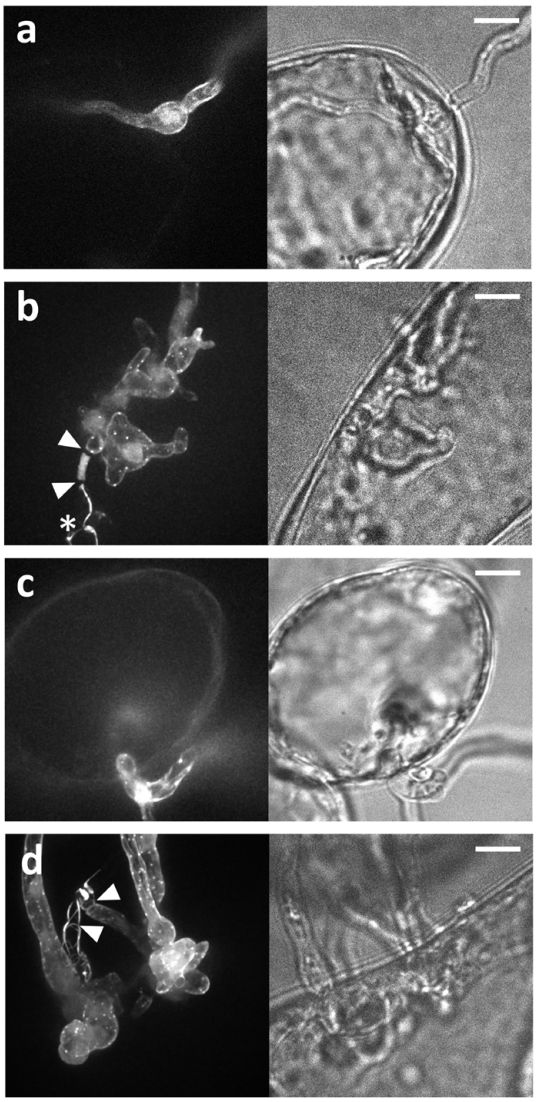

FIGURE 2.8 | Actin organization in *P. infestans* hyphae that have invaded MsK8 tomato cells. Images show the actin organization in different hyphal structures that develop within the MsK8 cells. a Growth directly through a plant cell without branching within the cell. b Hypha that has grown directly through a plant cell while producing irregularly shaped branches. c A hyphal side branch that has arrested growth briefly after the plant cell penetration. d A hyphal side branch that has produced irregularly shaped outgrowths within the plant cell after penetration. In (b) and (d) arrowheads point to plugs. In (b) the asterisk marks the cyst from which the hypha has emerged. The right panels of the images show the bright field and the left panels show the fluorescent channel. Bar = 10 µm.

2.5 Discussion

Previously, we have presented live cell imaging of the actin cytoskeleton in *in vitro* grown hyphae of *P. infestans* and revealed that actin plaques represent novel oomycete specific actin configurations (Meijer et al 2014). Here we have focused on the actin cytoskeleton in *P. infestans* in processes related to plant infection, including germ tube growth from encysted zoospores, appressorium formation and plant cell penetration, and identified additional novel actin configurations. We detected that actin filament accumulation correlates with cell

wall plug formation in germ tubes, and aster-like actin configurations that mark the barrier that appressoria encounter when attempting to penetrate. This aster-like actin configuration is prominently visible during the establishment of contact between an appressorium and the coverslip surface, and a similar transient accumulation of F-actin is also observed during plant cell penetration.

Why do *P. infestans* germlings form cell wall plugs? Generally, oomycetes are known as aseptate organisms. However, for a few oomycetes it has been shown that they have the ability to form septa that compartmentalize hyphae, i.e. *Peronospora tabacina, Pseudoperonospora cubensis* and *Pseudoperonospora humuli* (Kortekamp 2005). In addition, in some oomycete species cell wall structures have been reported that are deposited in response to wounding and during sporangium formation and function as sealant (Kortekamp 2005, Levina et al 2000). However, the plugs deposited in germinated cysts, also called false septa (Kramer et al 1997), are different from the wall material deposited after hyphal structural damage. In hyphae from the smut fungus *Ustilago maydis* (Steinberg et al 1998), so-called retraction septa are deposited that, similar to the plugs that we observed in *P. infestans*, seal off the basal part of the hypha after the depletion of cytoplasm. Also in angiosperm pollen tubes plugs that seal off compartments, are deposited and, similar to the plugs in *P. infestans*, pollen tube plugs expand centrifugally, i.e. from the periphery of the tube or hypha towards the central axis (Raudaskoski et al 2001). In pollen tubes the plugs consist of callose (Dumas & Knox 1983, Snow & Spira 1991, Williams 2008). Once these callose plugs are formed the apical part of pollen tube can advance independently of the pollen grain and the initial tube, and this reduces the risk of damage, limits the cell volume and allows growth over longer distances (Lord et al 2000, Williams 2008). The retraction septa in *U. maydis* seem to fulfil a similar function (Steinberg et al 1998). Mutants that are unable to form retraction septa produce much less appressoria and show severely reduced virulence and lower rates of plant penetration (Freitag et al 2011). We hypothesize that, similar to callose plugs in pollen tubes and retraction septa in smut fungi, plugs in *P. infestans* are deposited as a response to limitations in resources. Although this is supported by the finding that plugs in *P. infestans* hyphae are only deposited in hyphae emerging from cysts and not in hyphae emerging from sporangia, more research is needed to determine to what extent plug formation in *P. infestans* affects virulence.

The accumulation of F-actin associated with the leading edge of the extending plug that we observed suggests that the actin cytoskeleton is involved in plug deposition. In theory this could be tested by disrupting the actin cytoskeleton and analyse the effect on plug deposition. However, disruption of the actin cytoskeleton by actin depolymerizing drugs also causes inhibition of growth and cytoplasmic streaming (Ketelaar et al 2012, Meijer et al 2014), making it impossible to distinguish between cause and consequence: is the effect on plug formation caused by the actual actin depolymerisation or indirectly by inhibition of growth and cytoplasmic streaming resulting from actin depolymerisation? Occasionally,

some actin plaques remained associated with the cell cortex in the distal part of the hypha after plug deposition. These plaques showed a transient increase in fluorescence whereupon they disappeared. Since the intensity of surrounding actin cables did not change it is likely to be a plaque specific process. It could for example be due to stabilization of the actin associated with the plaques that may initially cause Lifeact-GFP to accumulate whereafter it is outcompeted by binding of endogenous actin binding proteins, or to a localised, transient pH increase (> pH 10), that causes GFP to become more brightly fluorescent (Balint et al 2013, Heikal et al 2001). Alternatively, a rapid pulse of actin polymerization followed by complete depolymerization of plaques may explain the transient increase in fluorescence. From previous studies we know that actin plaques are unique oomycete-specific actin structures. In growing hyphae they have a relatively long lifetime and tend to be highly immobile (Meijer et al 2014). Here we showed that during plug formation their lifetime is shorter and that they are more dynamic. As yet, we have no clue what the composition is of actin plaque and how dynamic this composition is. Are the plaques in hyphae the same as the plaques associated with plug formation and what exactly determines their behaviour? Isolating the actin plaques, with the aim to identify proteins associated with F-actin, would be the logical next step towards identifying their function and may help to increase our insight in plaque formation and in their role of the overall actin cytoskeleton in *P. infestans*.

When germlings face a physical barrier (in our experimental set-up a coverslip) we observed the assembly of actin that resulted in an aster-like structure at the point of contact. We hypothesize that the observed aster-like actin configuration in appressoria of *P. infestans* is induced by physical contact. Also during penetration of tomato MsK8 suspension cells we consistently observed a transient accumulation of F-actin that was reminiscent of the aster-like structures observed in appressoria at the contact point with the coverslip (**figure 2.5**). However, the prominence of the actin structures in the *in vivo* infection system, so during penetration of MsK8 cells (**figure 2.7**), was much lower in comparison to the actin asters in appressorium formed on glass. This reduced prominence might reflect a correlation between surface strength and the amount of actin that is recruited to breach the surface. In the rice blast fungus *Magnaporthe oryzae,* a torodial actin filament network has a function in the assembly of a septin diffusion barrier. This barrier is essential for increasing the pressure in the appressorium to the level that is required for plant cell penetration (Dagdas et al 2012). Also in the maize pathogen *Colletotrichum graminicola* Lifeact-GFP accumulates in appressoria at the spot where the penetration peg will form (Wang & Shaw 2016). Compared to fungal appressoria, *P. infestans* appressoria are understudied. It is not known to what extent pressure is important for penetration and how much pressure a *P. infestans* appressorium can handle. Moreover, *P. infestans* lacks genes encoding septins, the GTP-binding proteins that are conserved in many eukaryotes, and form protein complexes that are considered to be part of the cytoskeleton. So besides the shape also the envisioned composition of such a diffusion barrier, if it exists, will differ from the one present in *M. oryzae*. The location and organisation of the aster-like actin configuration in *P. infestans* appressoria suggests that it

may have a function in cargo transport rather than in assembling or supporting a diffusion barrier. This hypothetical function in cargo transport is supported by the fact that the centre of the actin aster is the exact spot from where plant cell penetration is initiated.

In this study we have identified two novel actin configurations in *P. infestans* and both associate with structures that are important for plant infection. Firstly, we found an accumulation of actin during cell wall plug formation. These plugs allow a hypha emerging from a cyst to extend its range while searching for a suitable entry point on the plant surface. Secondly, we found an actin network in the appressorium, the infection structure from which a penetration peg is formed that pierces the plant cells. More knowledge about these structures and the role of actin and the novel oomycete-specific actin configurations in assembling these structures may be a first step towards identifying agents that disrupt the assembly processes. The strategy to first pinpoint potential oomycete-specific targets and then develop methods to interfere with these targets holds promise for oomycete disease control in the future.

2.6 Supplemental material

VIDEO S2.1 | A *P. infestans* hypha in a stage just prior to plug formation which starts 7 min after this video ends. The cytoplasm is retracting and Lifeact-GFP labelled plaques disappear with the retracting cytoplasm. Hyphal tip and position of plug formation are located outside the field of view. Z-stacks were collected every 30 s and are displayed as maximal intensity projections. Total video duration is 15 min. Bar = 5 µm. Avi file: 5 frames/second.

VIDEO S2.2 | A *P. infestans* hypha during plug formation. Lifeact-GFP accumulates at the site of plug formation. The Lifeact-GFP signal stays associated with plug formation site until the process is completed. Hyphal tip is located outside the field of view. Structure on the left of the plug is an adjacent appressorium. Z-stacks were collected every 30 s and are displayed as maximal intensity projections. Total video duration is 31 min. Bar = 5 µm. Avi file: 5 frames/second.

VIDEO S2.3 | An appressorium formed by *P. infestans* that grows against the coverslip shows a Lifeact-GFP signal at the contact point. Z-stacks were collected every 30 s and are displayed as maximal intensity projections. Total video duration is 15 min. Scale bar = 5 µm. Avi file; 5 frames/second.-

VIDEO S2.4 | A non-expanding *P. infestans* appressorium expressing Lifeact-GFP located against the cover slip. Video also shows the start of the formation of a plug just below the appressorium. Z-stacks were collected every 30 s and are displayed as maximal intensity projections. Total video duration is 15 min. Scale bar = 5 µm. Avi file; 5 frames/second.

VIDEO S2.5 | A *P. infestans* appressorium expressing Lifeact-GFP showing a new outgrowth. Z-stacks were collected every 60 s and are displayed as maximal intensity projections. Total video duration is 12 min. Scale bar = 5 µm. Avi file; 3 frames/second.

VIDEO S2.6 | *P. infestans* expressing Lifeact-GFP penetrating a plant cell. Z-stacks were collected every 60 s and are displayed as maximal intensity projections. Total video duration is 20 min. Scale bar = 10 µm. Avi file; 3 frames/second.

Chapter 3

F-actin in *Phytophthora infestans*; plaques anchored to the cell wall and asters induced by physical stimuli

Kiki Kots,
Francine Govers*
Tijs Ketelaar*

* Equal contribution

Parts of this chapter are integrated in a broader study that is published as:
Bronkhorst J, Kots K, De Jong D, Kasteel M, Van Boxmeer T, Joemmanbaks T, Govers F, Van der Gucht J, Ketelaar T, Sprakel J (2022). An actin mechanostat ensures hyphal tip sharpness in *Phytophthora infestans* to achieve host penetration. *Science Advances* 8(23), eab00875

3.1 Abstract

Filamentous actin is part of a complex dynamic intracellular network that has a multitude of functions and is essential for viability of eukaryotic cells. In hyphae of the oomycete plant pathogen *Phytophthora infestans* F-actin is organized in cables and plaques while in the tips of hyphae facing a barrier, an aster-like actin configuration is formed. Unlike the ubiquitous actin cables, actin plaques are unique for oomycetes and present in every life stage except zoospores, the wall-less, flagellated motile propagules. The actin aster, so far only described in *P. infestans,* was observed during attempted host invasion. Here, we further studied the dynamics of plaques and asters using a *P. infesta*ns Lifeact-GFP expressing strain. In protoplasts, cells devoid of cell walls, plaques display a clear change in behaviour; movement is accelerated while lifetime is shortened. This suggests that actin plaques are anchored to the cell wall and play in role in establishing and/or maintaining the cell wall-plasma membrane continuum. In an attempt to artificially trigger aster formation in hyphae, we applied physical stimuli, including micromanipulation with a glass needle and laser ablation. Upon laser ablation asters appeared and disappeared within a timeframe of 40 seconds suggesting a role for actin asters in local cell wall modification or repair. These findings broaden our insight om oomycete actin dynamics and functioning.

3.2 Introduction

The actin cytoskeleton is essential for the growth and survival of all eukaryotes and consists of dynamic, filamentous polymers of actin proteins (Erickson 2007). Although the basic building blocks of actin filaments are conserved, the functions of the actin cytoskeleton may differ in different organisms depending on their evolutionary position, morphological features or tissue organization. For example, in mammalian and amoebal cells the actin cytoskeleton provides mechanical structure and mobility (Pollard & Cooper 2009), while in eukaryotes that have a cell wall, like plants and fungi, it functions in mediating intracellular transport, shaping the cytoplasm, and/or, facilitating endocytosis (Hussey et al 2006, Moseley & Goode 2006, Pollard & Cooper 2009). Actin exists as actin monomers (G-actin) and polymerized actin filaments (F-actin). Actin configuration, stability and dynamics are highly dependent on a variety of actin binding proteins (ABPs; Hussey et al 2006). Many ABPs are conserved across kingdoms, while some are species specific or limited to certain lineages (Pollard 2016).

Our research focusses on the cytoskeleton in *Phytophthora* species, filamentous oomycete plant pathogens that cause substantial damage in agriculture, forestry, and natural ecosystems (Kamoun et al 2015). One of the most notorious oomycetes is *Phytophthora infestans,* the late blight pathogen that triggered the Irish potato famine in the mid-19th century and is still a threat for potato and tomato crops worldwide (Haverkort et al 2008).

In terms of morphology, mode of dispersal and ecology, oomycetes strongly resemble fungi but they evolved independently from fungi. Oomycetes belong to the stramenopiles, a supergroup in the eukaryotic tree of life that comprises, amongst others, brown algae, diatoms, and a wide range of mostly unicellular marine organisms (Keeling & Burki 2019). Cytological studies using rhodamine-phalloidin staining have shown that all oomycetes analysed so far have at least two kinds of higher order F-actin organizations, actin filament cables and actin filament plaques (Chitcholtan et al 2012, Deora et al 2010, Kaminskyj & Heath 1994, Ketelaar et al 2012, Tsirigoti et al 2013). In mycelium these two dominant F-actin organizations occur in co-existence or on their own; so hyphae may consist of parts that have both cables and plaques, and parts that have only cables or only plaques (Ketelaar et al 2012). Subsequent studies using advanced live cell imaging microscopy and a transgenic line of *P. infestans* expressing Lifeact-GFP (Kots et al 2017, Meijer et al 2014) enabled us to show that the F-actin foci in *P. infestans* are quite distinct from the highly mobile F-actin foci in fungi (Meijer et al 2014). The latter, named actin patches, have a short lifetime and are known to play a role in endocytosis. In yeast their formation is linked to endocytotic vesicle formation and they move inwards away from the plasma membrane. as they move inwards, away from the plasma membrane (Lu et al 2016). In contrast to actin patches in fungi, actin plaques in *P. infestans* do not appear to be linked to endocytic events; they stay at the cortex, are immobile and have long lifetimes (Meijer et al 2014).

Actin plaques are actin configurations that have been found in all oomycetes in which the actin cytoskeleton was visualized by microscopy (Deora et al 2010, Harold & Harold 1992, Kaminskyj & Heath 1994, Tsirigoti et al 2013). Plaques seem to be unique for oomycetes as they were never observed in other stramenopiles such as brown algae and diatoms (Edgar & Zavortink 1983, Katsaros et al 2003). Yet, their function is unknown but since they are present in all life stages except zoospores (Deora et al 2010, Harold & Harold 1992, Kaminskyj & Heath 1994, Tsirigoti et al 2013), it is likely that they play an essential role in oomycetes.

Besides these unique actin plaques, we observed another actin configuration in *P. infestans,* namely the actin aster that appears in the tip of a germ tube approaching a barrier that it wants to penetrate (Kots et al 2017). In a recent study we showed that *Phytophthora* species use a slicing mechanism for host invasion (Bronkhorst et al 2021). The tip of the germ tube changes into an invasive hypha, that acts as a kind of knife, cutting through the plant surface under an oblique angle. The built-up pressure should cause flattening of the tip that might be counteracted by the actin cytoskeleton, more specifically the actin aster. This so-called 'naifu' invasion strategy differs from the 'brute force' approach in fungi that use melanized appressoria for host cell penetration. Strikingly, a brief flash of actin polymerization reminiscent of the actin aster dynamics in tips attempting to penetrate a barrier, was also observed just prior to plant cell penetration (Kots et al 2017). Taken together these observations strengthen the idea that the actin aster is linked to penetration; yet, the role of the actin aster is still a mystery. The question whether actin aster formation is triggered by mechanosensing when encountering a physical barrier or by cellular signalling

components that initiate the penetration process prior to physical contact, remains to be answered. In plants reorganization of the actin cytoskeleton was observed as a response to local mechanical stress (mechanosensing) and upon pathogen attack (Hardham et al 2008, Overdijk et al 2016, Sassmann et al 2018). In the rice blast fungus *Magnaporthe oryzae*, actin also plays an important role during plant cell invasion and co-localizes with septins in the appressorium (Dagdas et al 2012).

In this study our first aim was to test the hypothesis that actin plaques function in anchoring the actin cytoskeleton to the cell wall-plasma membrane continuum. We made use of the *P. infestans* Lifeact-GFP strain in a series of experiments aimed at visualizing the behaviour of the actin cytoskeleton in (regenerating) protoplasts, and in hypha exposed to a mechanical trigger and laser beam irradiation. Our analyses show that the extremely high mobility of plaques in protoplasts disappears after regeneration and cell wall formation, supporting the hypothesis that plaques function as anchors. Secondly, we aimed to investigate whether actin asters are restricted to penetration events. When searching for stimuli that trigger the formation of actin asters, we observed actin asters in hypha upon mechanical damage and laser ablation-mediated damage. This suggests that this actin reorganization might be linked to local cell wall modifications or repair events. Together these findings further our insight into actin cytoskeleton dynamics and organization in oomycete pathogens.

3.3 Materials and Methods

P. infestans cultivation

Phytophthora infestans was maintained on rye sucrose agar (RSA; Caten & Jinks 1968) in the dark at 20°C. Strains used are wild type 88069 and Lifeact-GFP transformant PiLA-GFP (Meijer et al 2014). Strains were maintained as described in Meijer et al (2014).

Generating protoplasts for imaging

Protoplasts were generated as described by Ah Fong and Judelson (2011) by incubating mycelium in protoplasting buffer containing 5 mg/ml Cellulysin® (Sigma-Aldrich) and 10 mg/ml Lysing Enzymes from *Trichoderma harzianum* (Sigma-Aldrich)]. After the final wash, the protoplasts were resuspended in RSM containing 1 M mannitol. For microscopic imaging, the protoplast suspension was transferred to glass bottom imaging dishes (Cellvis, USA).

Generating germinated cysts for imaging

Zoospore release was induced by flooding sporulating cultures with 10 ml cold tap water and subsequent incubation at 4 °C for 3 hours. The zoospore suspension was collected, filtered through Miracloth (Calbiochem, Germany) and vortexed for 5 min to encyst the zoospores.

Cyst suspensions (5 x 10^6 per ml) were then transferred to glass bottom imaging dishes and incubated for 3 h at 20 °C to allow cyst germination.

Plant cell infection

Zoospores were collected as described above and 2 ml of the zoospore suspension (5 x 10^6 per ml) were added to 2 ml of a 5 day old tomato MsK8 cell suspension culture (Schoina et al 2017). For imaging, 30 µl of this mixture was enclosed in a bio-foil slide and incubated overnight at room temperature in the dark. Inoculation of potato plantlets was done by applying one droplet (10 µl) containing 5 x 10^4 zoospores to etiolated stems (Bouwmeester 2010). After incubation overnight in the dark at room temperature, the plantlets were transferred to a glass bottom imaging dish (MatTek, Ashland, USA) and covered with an agar pad (1 cm diameter, 1% agar).

Laser ablation and mechanical stimulation

For laser ablation we made use of a high-wattage pulsed Teem Photonics SNG-03E 532 nm laser (Meylan, France) with a 1000 ns pulse length, which was fed into the microscope using an iLas 2 FRAP/PA illumination setup (Roper Scientific, Evry, France). Microscope slides containing germinating sporangia were prepared as described in Meijer et al (2014).

For mechanical stimulation we used glass micro-needles pulled on a List-Medical-Electronic L/M-3P-A Vertical Pipette Puller. The needles were loaded with the fluorescent dye Cy3. A Narashige micromanipulator was used to position the needle (Esseling-Ozdoba et al 2008).

Microscopic imaging and data analysis

A Roper Spinning Disk Confocal System (Evry, France) consisting of a CSU-X1 spinning disk head (Yokogawa, Japan) mounted on a Nikon Eclipse Ti microscope (Tokyo, Japan) equipped with Perfect Focus system and a 100× Plan-Apochromat 1.4 N.A. oil immersion objective was used for imaging. Fluorescence imaging was performed using a 491 nm or 543 nm laser line combined with band pass or long pass emission filtering (530/50 nm or 560 nm; Chroma Technology). Images were acquired with a Prime 95B Scientific CMOS camera (Photometrics), controlled by Metamorph software (Molecular Devices, California). Z-stacks were collected using a 0.5 µm step size. Images were processed in FIJI (https://imagej.net/Fiji; background subtraction, rolling ball radius 50.0 px and linear contrast stretching). Actin plaque intensities and positions were determined as pixel intensities through a maximum intensity Z-projection of the region of interest using Manual Tracker (https://imagej.nih.gov/ij/plugins/track/track.html). Actin plaque movement was tracked using the Temporal Color_Code plugin (https://imagej.net/Temporal-Color_Code). Drift was corrected for by the plugin StackReg (https://imagej.net/StackReg). Average plaque lifetime was determined as described in Meijer et al (2014).

3.4 Results

Protoplasts have a cortically arranged actin cytoskeleton

As a first step for testing the feasibility of visualising the actin cytoskeleton in protoplasts by live cell imaging, we removed to cell wall of mycelium of a Lifeact-GFP expressing *P. infestans* strain (hereafter called PiLA-GFP; Meijer et al 2014). The treatment with cell wall degrading enzymes yielded protoplasts defined as perfectly rounded fragments of the coenocytic mycelium, that we refer to as cells, lacking a cell wall and varying in size. Those cells that had failed to shed the cell wall completely, displayed a variety of shapes. Even though the mycelium of *P. infestans* is coenocytic, the protoplasting procedure caused fragmentation of the tissue into protoplasts that mostly contained a single nucleus and often also vacuoles. In live protoplasts, LA-GFP fluorescence remained visible (**figure 3.1**) and the actin dynamics could be recorded. We focussed on protoplasts that contained a single nucleus. All protoplasts possessed cortical actin plaques (**figure 3.1**), but their densities differed among cells (from 3 to >50 plaques per protoplast, n=21). Actin cables were observed in approximately half of the protoplasts (52%; n=21). When present, actin cables often aggregated in a ring-shaped configuration (**figure 3.1**; **video S3.1**). Both the actin cables and plaques localized to the most peripheral layer of the protoplasts, i.e. the cortex, while most nuclei and vacuoles had a non-cortical localization (**figure 3.1**). We never detected F-actin at locations other than at the cortex.

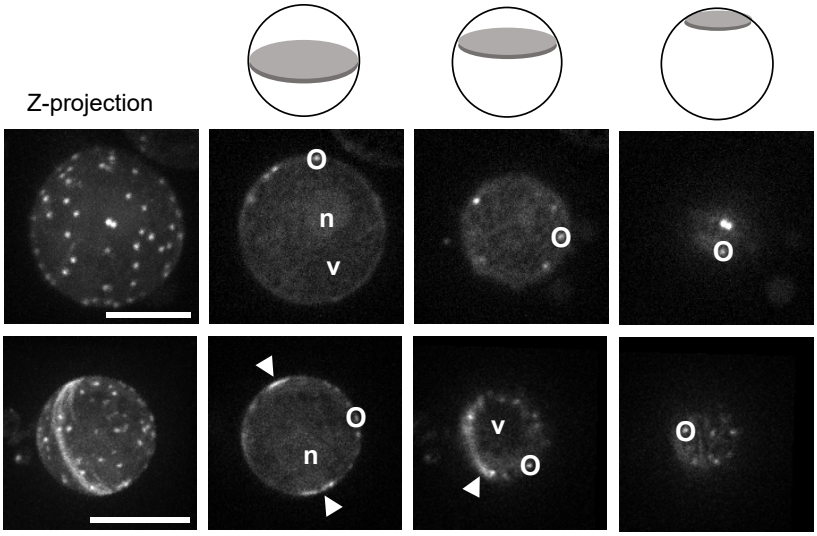

FIGURE 3.1 | Actin cables and plaques in *P. infestans* protoplasts are cortically localized. Live cell imaging of PiLA-GFP showing a protoplast with only actin plaques (top) and a protoplast with actin plaques and a ring consisting of actin cables (bottom). The most left panels show Z-projections. The others show single plane images of the Z-stack with positions as indicated in the top row spheres and with a few plaques encircled (o). Actin cables (arrowhead), nuclei (n), vacuoles (v) are indicated in the single plane images. Scale bars are 10 µm.

Actin plaques in protoplasts display increased mobility and shorter lifetimes

To follow the behaviour of plaques in protoplasts, we imaged the protoplasts (n=21) over time during 15 minutes with a 15 second time interval. While tracking the localization of the actin plaques over time, we noted the presence of actin cables in the cortical cytoplasm. In half of the protoplasts the actin cables were organized in a ring that in some cases was only visible in a few time frames while in other cases the ring remained visible for minutes and even during the entire time series of 15 minutes. When this ring was tracked over time, we observed in most cases a rapid rotation, or motion, of the ring (**figure 3.2**; **video S3.1**). A previous study showed that in hyphae, plaques are immobile with lifetimes often exceeding one hour (Meijer et al 2014). Here we observed that in protoplasts some plaques remained immobile, while others were highly mobile (**figure 3.2**). By tracking plaques and measuring their movements and lifetimes, it was noted that the mobile plaques were always localized in the vicinity of the ring structure while the immobile plaques were more distal from the actin cables **(figure 3.2**). The lifetimes of the plaques in protoplasts were significantly shorter when compared to the lifetimes of plaques in regenerated hyphae (**figure 3.2**), however, lifetime was neither affected by the presence, nor the location of an actin cable ring (**figure 3.2**). To test if the plaques regained their normal behaviour after synthesis of a new cell wall, we allowed protoplasts to recover while monitoring cell wall deposition and plaque behaviour (**figure 3.2**). After 2 hours the first signs of cell wall deposition were visible (n=24). After 24 hours the shape of the original protoplasts had not changed but in many cases a cell wall, occasionally patchy in appearance, had formed and filamentous outgrowth could be observed (**figure 3.3**; n=10). In these regenerated parts (hereafter called regenerated hyphae), plaques regained their regular immobility (**figure 3.2**), with average lifetimes up to 25 minutes. It should be noted that the plaque lifetime in regenerated hyphae is shorter than we reported previously in mature mycelium, with an average lifetime of over an hour in distal parts of the hypha (Meijer et al 2014). Possibly, this difference is caused by the difference in tissue studied; young, regenerated tissue versus old, highly vacuolated tissue. Taken together, the results show that the removal of the cell wall strongly affected both the mobility and the lifetime of actin plaques.

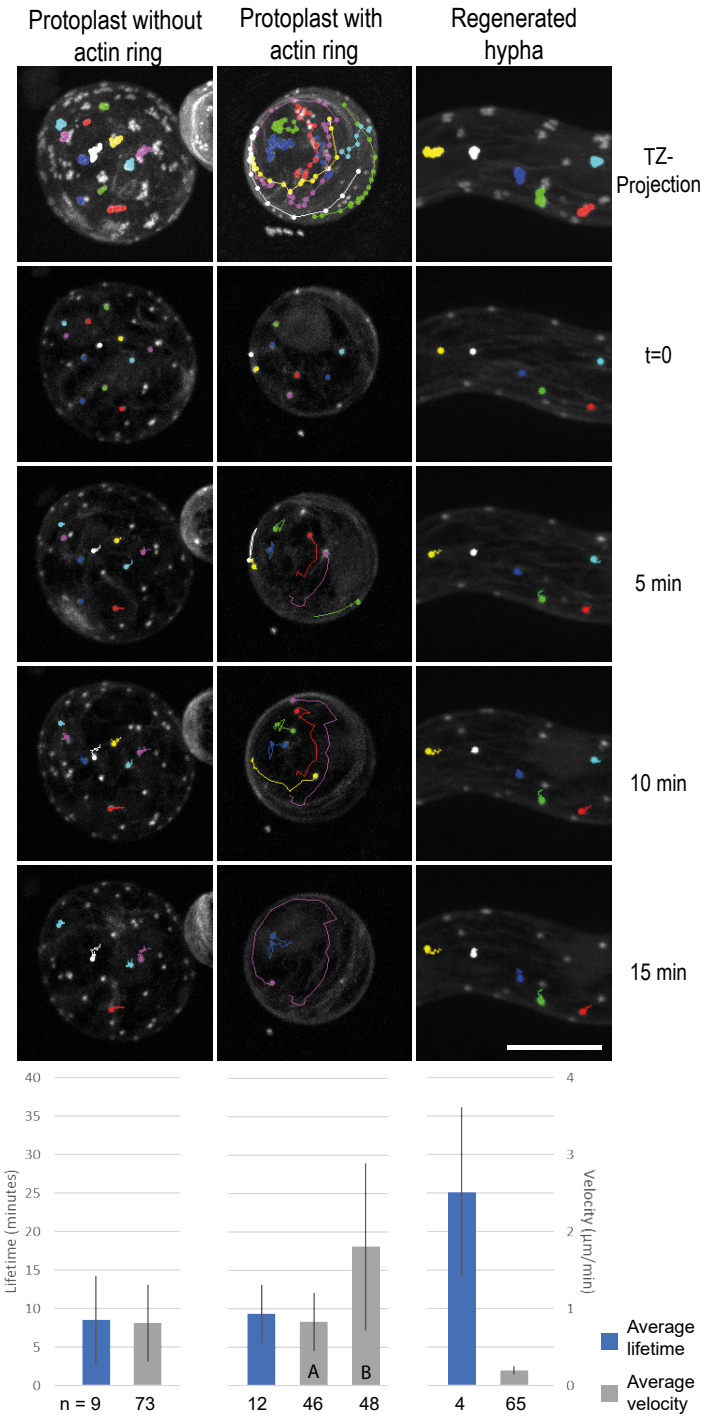

FIGURE 3.2 | Actin plaques in *P. infestans* protoplasts display increased mobility. Live cell imaging of protoplasts and a regenerated hypha of PiLA-GFP. Plaque displacement tracked during 15 minutes in a protoplast lacking actin cables (left), a protoplast containing both plaques and an actin ring assembled from actin cables (middle) and a regenerated hypha 24 hours after protoplasting (right). The top row images show time-Z-projections (TZ-

projection) of the total duration of the time series. The following rows show z-projections with the position of the plaques (coloured dots) at t=0, 5, 10 and 15 min, respectively, and their tracks over time (coloured lines). Each colour marks the position and the track of a single plaque as long as it is present. Scale bar is 10 µm. The graphs at the bottom show the average lifetime (blue bars) and average velocity (grey bars) of plaques. In protoplasts with an actin ring, plaques associated with the actin ring (A) were separately measured from plaques not associated with the actin ring (A).

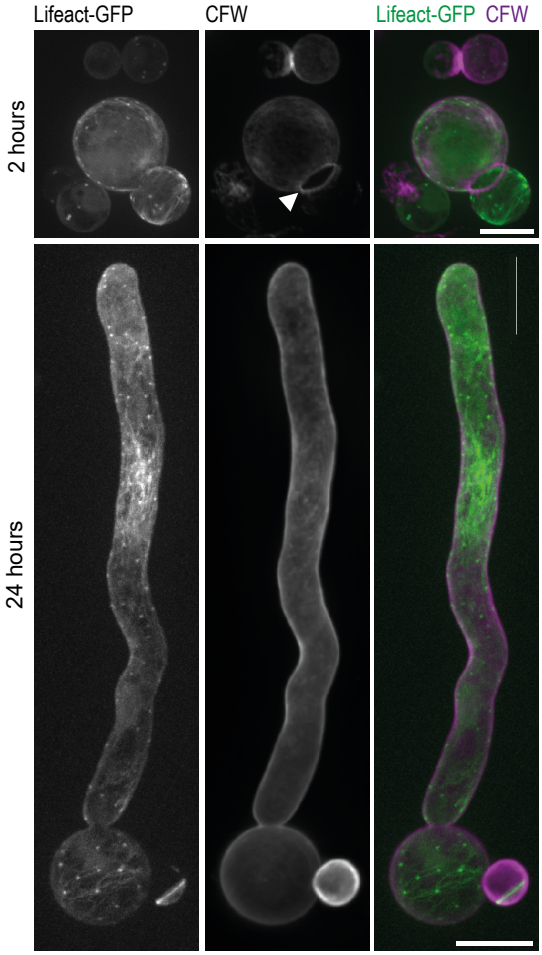

FIGURE 3.3 | Outgrowth and cell wall deposition during regeneration of *P. infestans* protoplasts. Protoplasts of PiLA-GFP were kept in regeneration medium and monitored after 2 hours and 24 hours. Calcofluor white (CFW) staining shows cell wall deposition in particular at the site where a globular outgrowth emerges (arrowhead) and all over the globular outgrowth and along the tubular outgrowth that is reminiscent of germ tubes emerging from cysts. Scale bars are 10 µm.

An actin aster appears at the penetration location prior to plant cell infection

We previously reported the presence of an actin aster during an invasion attempt by *P. infestans* on glass (Kots et al 2017). We then hypothesized that the actin aster would also be present during plant cell infection but were not able to detect a clear actin aster in hyphae attempting to penetrate viable cells of the tomato MsK8 cell line (Schoina et al 2017). In a more thorough analyses of the inoculated MsK8 cells we observed a hypha attempting to penetrate a dead cell that had lost its turgor pressure. The penetration attempt caused the cell wall of the dead tomato cell to deform inwards, but penetration was unsuccessful (**figure 3.4**). Nonetheless, an actin aster was clearly visible suggesting that the appearance of the aster correlates with physical interaction and not invasion. In addition, we imaged penetration events on stems of potato plantlets that were grown in *in vitro* the dark to suppress the differentiation of chloroplasts, thereby avoiding autofluorescence. Upon inoculation of etiolated plantlets we observed an actin aster in the tip of a germ tube emerging from an encysted PiLA-GFP zoospore, with the centre of the aster localized to the penetration location prior to the penetration event. After penetration, the actin aster briefly remained present, and then it disappeared (**figure 3.5**). This demonstrates that the timing of appearance and the localization of the actin aster coincide with the penetration event.

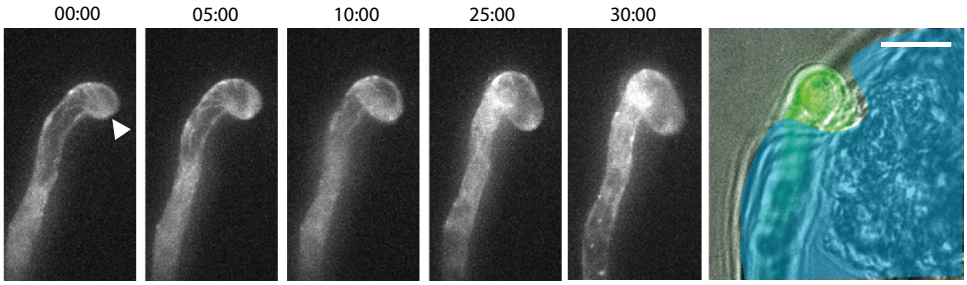

FIGURE 3.4 | Spatiotemporal correlation of an actin aster with an attempted penetration of a tomato cell by *P. infestans*. Live cell imaging of PiLA-GFP during an attempt to penetrate a dying cell in a tomato MsK8 cell suspension culture over time (0-30 min). The overlay (right panel) shows the dead tomato cell (traced in blue) which has lost its turgor pressure. The cell wall easily gives way to the invading *P. infestans* hypha (traced in green), causing an indentation in the plant cell wall. An actin aster (indicated with an arrowhead) is present from the onset of the penetration attempt and localizes to the attempted penetration site. Scale bar is 10 µm.

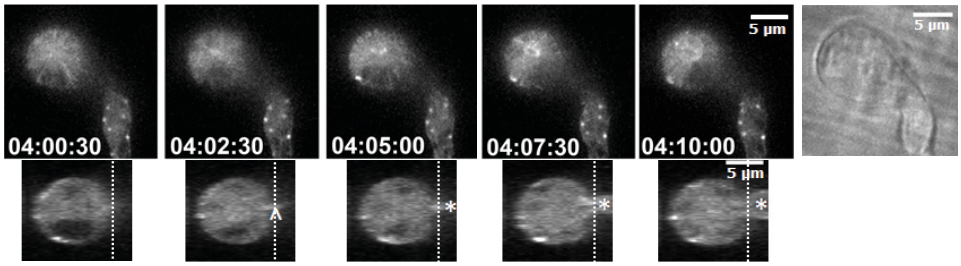

FIGURE 3.5 | Spatiotemporal correlation of an actin aster with penetration of *P. infestans* in an etiolated potato stem. Live cell imaging of PiLA-GFP during a time series of 10 minutes showing a penetration event and in the rightest panel the accompanying bright field image. The micrographs in the bottom row are Z-projections showing an orthogonal view (90° rotation) of the visualizations in the top row. Aster and penetration point (Λ) and infection hypha inside the plant cell (*) are indicated. The dashed line reflects the plant cell wall. Scale bar is 5 µm.

Actin asters can be induced by physical triggers

The presence of an actin aster on glass surfaces and during host cell penetration led us to hypothesize that the trigger to form the aster may be of physical nature. To test this hypothesis, we exposed hyphae to a mechanical trigger and analysed the actin cytoskeleton during this process. We loaded microneedles with Cy3 dye and positioned these in the vicinity of the tip of a growing hypha. We then repositioned the needle in such a way that it touched the hyphal tip. Now and then application of the needle damaged the hypha, but only events in which there was no damage were used for analysis. We observed three different types of responses. (i) inhibition of growth accompanied with rapid plaque formation in the tip (**video S3.2**; n=3). (ii) the formation of an actin aster or local actin accumulation close to the needle tip (**video S3.3**; n=1). (iii) no detectable response (**video S3.4**; n=3). In the latter case, the touch by the needle tip was ignored and the hypha continued to grow, enclosing the needle tip. These observations show that it is possible to induce actin reorganization upon physical manipulation of hyphae and that one of these responses is the formation of an actin aster. This approach, however, is very time consuming and since we were not able to increase the efficiency of 'touch' experiments, we abandoned it.

Actin asters can be induced by laser ablation

An alternative for physical manipulation is laser ablation. Targeting a laser beam at specific subcellular regions causes localized heat damage in hyphae. We focussed either on the hyphal tip region or a region distal from the tip (**figure 3.6**) and in each region we pointed the ablation laser at two targets, one with a plaque and one without. Strikingly, in all cases and independent of the position of the targeted plaques or regions within the hypha, laser ablation led to the formation of an actin aster. Rapidly after the laser pulse hit the surface of the hypha, i.e. within a 10 seconds time frame, a transient actin aster assembled that remained present for less than a minute before disappearing (**figure 3.6**, 100%; n=10 in

distal region and n=10 in tip region). In all cases the centre of the aster was located exactly at the spot of laser ablation. These observations show that the formation of an actin aster correlates with physical disruption or wounding of the hypha.

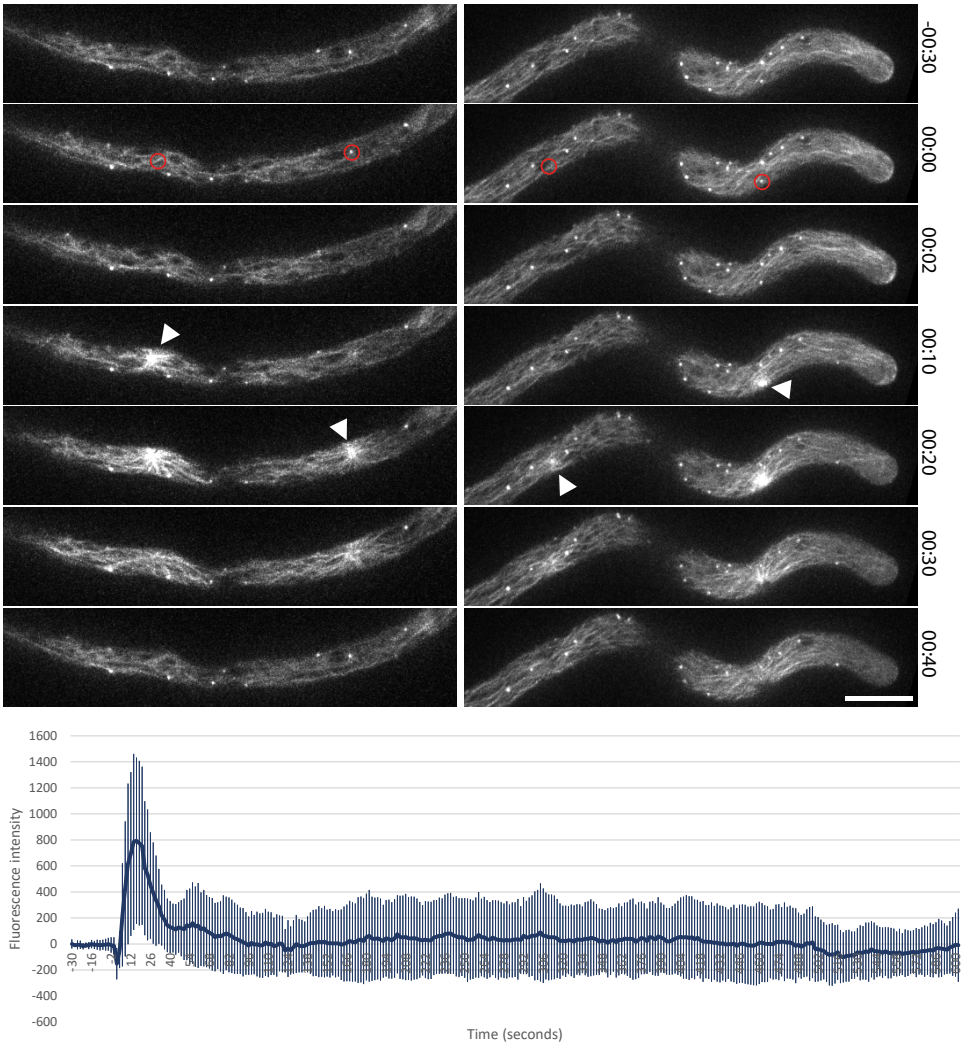

FIGURE 3.6 | Local damaging of *P. infestans* by laser ablation induces actin aster formation. Live cell imaging of PiLA-GFP upon laser ablation at t= 0 in a distal area of the hypha (left) and a tip area of the hypha (right) during a time frame of 40 seconds. In each hypha the ablation laser was targeted to a plaque and a plaque-free region of the cytoplasm (indicated with red circles). Asters are indicated with arrowheads. Scale bar is 10 µm. The graph shows the average fluorescence intensity of the ablated regions shown in the top images in the red circle (n=19). The first 10 frames (pre-ablation) were averaged and subtracted from each timepoint to normalise fluorescence intensity differences. Ablation at 00:00.

3.5 Discussion

This study focusses on two previously identified actin configurations in *P. infestans* with unknown function: actin plaques and actin asters. Actin plaques are unique for oomycetes as they have not been reported in any other organism, not even in other stramenopiles such as brown algae (Katsaros et al 2006). They are present in different life stages, but are more abundant in sporangia and older, less active parts of hypha while they are not or rarely found in the actively growing hyphal tips (Meijer et al 2014) and in zoospores (Islam 2008), the only life stage completely lacking a cell wall. Also actin asters seem to be unique, but unlike actin plaques they were so far only found during attempted invasion (Kots et al 2017). We are not aware of studies describing similar shaped aster-like actin configurations in organisms other than *Phytophthora*.

When monitoring the *P. infestans* actin cytoskeleton after protoplasting we found that actin plaques are retained despite the removal of the cell wall, however, their behaviour changes. They become much more mobile than in hyphae. Highest plaques velocities are observed when a ring of actin cables is present in their vicinity while plaques located distal from the actin cables are less mobile. The correlation between high plaque mobility and the presence of an actin cable ring suggests that the ring exerts a force on the plaques. In contrast to the static actin cables in hypha, the actin ring in protoplasts displays a rotating motion. Moreover, the longevity of plaques is shorter in protoplasts than in hypha and thus depends on the presence of a cell wall. In plants there is ample evidence for links between the cell wall, the plasma membrane and the cytoskeleton; the so-called cell wall–plasma membrane–cytoskeleton continuum (Liu et al 2015). The plant cell wall is thought to provide stable anchor points around which the actin cytoskeleton can remodel. This is supported by the study of Tolmie et al (2017) who found that in *Arabidopsis* disruption of the linkage between the cytoskeleton and the cell wall by either plasmolysis or treatment with the cell wall biosynthesis disturbing drug isoxaben, interferes with actin cytoskeleton remodelling. Our observations in *P. infestans* protoplasts on the loss of immobility of plaques and the spinning of the actin cable ring support the hypothesis that actin plaques function as cell wall anchors that establish the linkage between actin cables and the cell wall, and that this linkage is important to their stability and longevity.

Actin asters were previously observed during attempted invasion on glass surfaces (Kots et al 2017). We then hypothesized that they have a role in facilitating penetration, for example by focussing growth or by supporting targeting delivery of vesicles or substances needed for plant cell invasion (Kots et al 2017). In this previous study we also observed accumulation of actin during attempted penetration of plant cells but this accumulation was never as pronounced as during attempted invasion on a glass surface (Kots et al 2017). Possibly, the level of resistance encountered on glass is higher than on plant cells and hence the force on glass needs to be higher. In this study we revisited the invasion attempts of *P. infestans* and

observed a very clear actin aster during attempted invasion of a dead cell in a tomato cell suspension culture. The prolonged presence of an actin aster in this case may reflect the failure to penetrate the dented cell wall of the dead cell which leads to prolonged physical interaction with the wall. Also, during successful penetration of thin stems of etiolated potato plantlets a bright actin aster was visible during at least 10 minutes while penetration proceeded. Thus, the actin aster not only correlates to the infection site in space, but also in time.

The appearance of actin asters at the site of penetration prompted us to test if physical stimulation plays a role in triggering and assembling an actin aster. When touching *P. infestans* hyphae with a glass needle we noticed actin accumulations at the site of needle contact but this was not always the case. Sometimes there was no visible response of the actin cytoskeleton and apparently the hypha did not notice the presence of the needle. In other cases, the hyphae simply stopped growing. Since these touch experiments did not allow us to draw firm conclusions, we switched to laser ablation. With a laser we managed to administer a more precise kind of damage to the hyphae. Strikingly this method had a 100% success rate in forming asters in hyphae. These findings demonstrate that physical stimuli are sufficient to trigger actin aster formation. In plants, a similar polarization of the actin cytoskeleton towards the site of application of external, physical stimuli was observed (Hardham et al 2008, Sassmann et al 2018). As such, actin asters may indeed have a role in supporting targeted delivery of vesicles or substances to a specific site; in the case of damage the transported items might be needed for the cell repair machinery while invasion organs likely need substances that foster the infection process. Although our data show that actin aster formation is triggered by mechanosensing it cannot be excluded that cellular signalling pathways also play a role in this process.

This research has broadened our understanding of the acting and reacting of the actin cytoskeleton in *P. infestans,* however, it also raised new questions. The finding that the actin plaques play a role in anchoring actin cables to the cell periphery implies that there is a protein complex that next to ABPs, likely contains proteins that establish links with the cell wall. This protein complex is a black box yet to be deciphered. Similarly, actin asters are dynamic protein complexes that need to be characterized in order to better understand how invasion hyphae are formed and how they function. A better insight into the composition and the stability of the complexes associated with the oomycete-specific actin configurations might lead to new targets that can be exploited for controlling late blight or other *Phytophthora* diseases.

3.6 Supplemental material

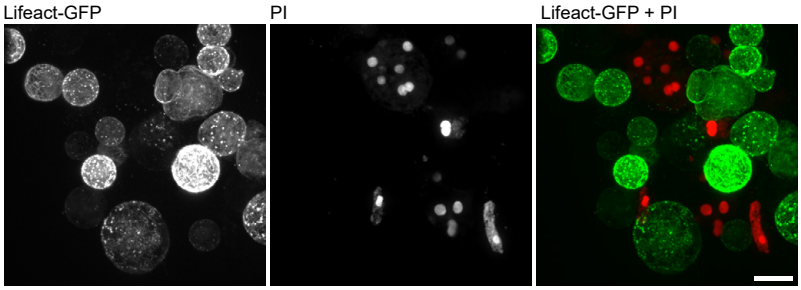

FIGURE S3.1 | *P. infestans* PiLA-GFP protoplasts stained with propidium iodide (PI). Lifeact-GFP is only visible in living protoplasts. Z-projection of a PiLA-GFP protoplast suspension containing 40 µM propidium iodide. Living protoplasts display Lifeact-GFP in green (491 nm) and dead protoplasts display a propidium iodide-stained nucleus in red (561 nm). Scale bar is 10 µm.

VIDEO S3.1 | A PiLA-GFP protoplast displaying actin plaques and actin cables in a ring formation. Total video duration is 15 min. Bar = 10 µm. Avi file: 7 frames/second.

VIDEO S3.2 | A PiLA-GFP hypha micromanipulated and responding with a growth arrest. Total video duration is 7 min. Bar = 10 µm. Avi file: 5 frames/second.

VIDEO S3.3 | A PiLA-GFP hypha micromanipulated and responding with a local actin aster. Total video duration is 7 min. Bar = 10 µm. Avi file: 5 frames/second.

VIDEO S3.4 | A PiLA-GFP hypha micromanipulated and not responding. Total video duration is 7 min. Bar = 10 µm. Avi file: 5 frames/second.

Chapter 4

Effect of flumorph on F-actin dynamics in the potato late blight pathogen *Phytophthora infestans*

Chenlei Hua*
Kiki Kots*
Tijs Ketelaar
Francine Govers
Harold J. G. Meijer

* Equal contribution

This chapter is published in 2015 in *Phytopathology* 105(4): 419-423

4.1 Abstract

Oomycetes are fungal-like pathogens that cause notorious diseases. Protecting crops against oomycetes requires regular spraying with chemicals, many with an unknown mode of action. In the 1990s, flumorph was identified as a novel crop protection agent. It was shown to inhibit the growth of oomycete pathogens including *Phytophthora* spp., presumably by targeting actin. We recently generated transgenic *Phytophthora infestans* strains that express Lifeact-GFP, which enabled us to monitor the actin cytoskeleton during hyphal growth. For analysing effects of oomicides on the actin cytoskeleton *in vivo*, the *P. infestans* Lifeact-GFP strain is an excellent tool. Here, we confirm that flumorph is an oomicide with growth inhibitory activity. Microscopic analyses showed that low flumorph concentrations provoked hyphal tip swellings accompanied by accumulation of actin plaques in the apex, a feature reminiscent of tips of nongrowing hyphae. At higher concentrations, swelling was more pronounced and accompanied by an increase in hyphal bursting events. However, in hyphae that remained intact, actin filaments were indistinguishable from those in nontreated, nongrowing hyphae. In contrast, in hyphae treated with the actin depolymerizing drug latrunculin B, no hyphal bursting was observed but the actin filaments were completely disrupted. This difference demonstrates that actin is not the primary target of flumorph.

4.2 Introduction

Phytophthora infestans is a notorious plant pathogen that causes late blight on potato and tomato and was responsible for the Great Famine in Ireland in the mid-19th century. It is one of the more than one hundred species in a genus that comprises exclusively plant pathogens (Kroon et al 2012). For managing *Phytophthora* diseases, farmers often make use of synthetic agrochemicals and spray their crops with regular intervals in order to prevent or reduce yield losses. For controlling potato late blight, for example, the number of sprays per growing season can reach up to fifteen (Hijmans et al 2000).

Phytophthora species resemble fungi in many ways; they show hyphal growth, disperse via spores and exploit similar strategies to infect plants. Yet, evolutionarily they are not related to fungi (Latijnhouwers et al 2003). *Phytophthora* belongs to the oomycetes, a stramenopile lineage in the supergroup Chromalveolates whereas fungi are members of the supergroup Unikonts (Baldauf 2003, Lee et al 2012). This difference in origin is reflected in differences in structural and biochemical properties. Two prominent examples that relate to the sensitivity to agrochemicals are cell wall composition and ergosterol biosynthesis. Cell walls in fungi are mainly composed of chitin while *Phytophthora* has cell walls that contain primarily cellulose and β-glucans (Badreddine et al 2008, Grenville-Briggs et al 2008, Meijer et al 2006). Hence, chitin synthase inhibitors such as the fungicide nikkomycin Z, have no inhibitory effect on *Phytophthora* (Latijnhouwers et al 2003). The same holds for azole fungicides. They target

the sterol biosynthesis pathway and unlike fungi, *Phytophthora* spp. do not synthesize sterols (Latijnhouwers et al 2003). The lack of these common targets explains why many of the agrochemicals marketed as general fungicides are less effective in controlling diseases caused by *Phytophthora* and other oomycetes, including downy mildews and *Pythium* spp. (Cohen & Coffey 1986). Genome-wide analyses have shown that oomycetes have quite a number of genes encoding proteins with unique combinations of protein domains (Bakthavatsalam et al 2006, Meijer & Govers 2006, Seidl et al 2011). These novel proteins are not found in other eukaryotes and could be exploited for finding novel drug targets in oomycetes. The term oomicide was introduced to distinguish compounds with activity against oomycetes from those active against fungi (Govers 2001).

In the 1990's a novel systemic compound with the common name flumorph, was introduced (Liu et al 2000, Zhang et al 2014). The active ingredient of flumorph is 4-[3-(3,4-dimethoxyphenyl)-3-(4-fluorophenyl)-1-oxo-2-propenyl] morpholine. It belongs to the carboxylic acid amides (CAA's) and was shown to act as a strong oomicide effective against certain *Peronospora* and *Phytophthora* species (Hu et al 2008, Yuan et al 2006, Zhu et al 2008, Zhu et al 2007b). In China flumorph is registered as a crop protection agent and currently applied in several crops to control oomycete diseases. As yet, however, the mode of action of flumorph is unknown. In *Pseudoperonospora cubensis,* Zhu and co-workers (Zhu et al 2008) observed some cross-resistance of flumorph with dimethomorph, a structural CAA analogue, and with iprovalicarb, a structurally unrelated CAA, suggesting an interference with cell wall synthesis (Zhu et al 2008). In another study the same authors observed that treatment of *Phytophthora melonis* with flumorph resulted in impairment of polar growth and cell wall deposition and suggested that flumorph disrupts F-actin organization (Zhu et al 2007b).

The actin cytoskeleton consists of filamentous actin polymers (filamentous or F-actin). The actin cytoskeleton is highly dynamic and continuously reorganizes. It is essential for many cellular processes including cell motility and cell shape changes during the cell cycle or in response to extracellular stimuli in vertebrate and invertebrate cells (Ketelaar 2013). This dynamicity of the actin cytoskeleton has been observed in several eukaryotes but until recently, not in oomycetes. So far, the studies in oomycetes were mainly based on phalloidin staining of actin in hyphae or sporangia with only static images as result. In a recent study, Meijer and co-workers analysed the dynamics of the actin cytoskeleton in *P. infestans in vivo* by introducing a DNA fragment encoding the actin binding peptide Lifeact-GFP into *P. infestans* (Meijer et al 2014). In transgenic Lifeact-GFP strains, cortical actin filament plaques and actin filament cables were visualized *in vivo* and over time without affecting hyphal growth and virulence. The study of Meijer et al (2014) further revealed that, in contrast to actin filament patches in fungi, the actin filament plaques in *P. infestans*, are highly immotile, they are not internalized prior to their disassembly, and are relatively insensitive to actin depolymerization. As experimental set-up, flow cells were used for microscopic observation of living hyphae. With this set-up it is easy to expose the hyphae to

drugs and immediately analyse the effect of the drug treatment *in vivo* with the microscope. In this way, the effect of latrunculin B (latB), a drug that affects free actin polymerization by binding actin monomers was monitored (Meijer et al 2014). Thus, the Lifeact-GFP strains are instrumental for visualising *in vivo* changes in the actin cytoskeleton.

In this study, we exploited the *P. infestans* Lifeact-GFP strains to investigate the mode of action of flumorph and to test the hypothesis put forward by Zhu et al (2007b) that the actin cytoskeleton is the primary target of flumorph in *P. infestans*.

4.3 Materials and methods

Phytophthora infestans strains and cultivation

P. infestans strains 88069-mRFP (Hua et al 2013) and Lifeact-GFP (Meijer et al 2014) were maintained on rye sucrose agar (RSA) plates supplemented with 5 µg/ml geneticin as described (Meijer et al 2014).

Flumorph and latB solutions

A stock solution of 10 mM latB (Sigma-Aldrich, Zwijndrecht, The Netherlands) was prepared in dimethylsulfoxide (DMSO), and diluted to the desired concentration in rye sucrose liquid (RS) medium as previously described (Ketelaar et al 2012). A stock solution of 1 mg/ml flumorph (generously provided by Junli Liu, Shenyang Research Institute of Chemical Industry, Shenyang, China) was prepared in methanol (Zhu et al 2007a) and diluted in RS medium to the desired concentration.

Flumorph sensitivity assays

Growth assays were performed in triplicate on RSA medium in six-well plates (CELL STAR, Greiner bio-one). A 5 mm-diameter fresh mycelial plug was inoculated in each well and the six-well plates were incubated at 18°C in the dark. The mycelial growth rate was determined by measuring the diameter of mycelial colony on RSA with and without flumorph each day after inoculation. The colony outgrowth was determined by comparing colony diameters of each strain on flumorph plate to that on non-flumorph plate at six days post inoculation. The statistical data analysis was performed using Student's t-test. The EC_{50}, indicative for the concentration that results in 50% growth reduction, was determined based on the data points after 6 dpi.

Sample preparation for microscopy

Samples for microscopic imaging using either biofoil slides or flow cell slides were prepared as described previously (Meijer et al 2014). Germinating sporangia were incubated in the presence of latB or flumorph for the time indicated and then transferred to biofoil slides. To study the immediate effect of flumorph on actin organization flow cells containing germinating sporangia were prepared before flumorph was added.

Microscopy and data analysis

P. infestans hyphae were monitored using a Roper (Evry, France) Spinning Disc Confocal System on a Nikon Eclipse Ti microscope using a 100x Plan apo oil immersion objective (NA 1.4) and a 491 nm laserline. Optical sections were collected with 0.5 µm Z-intervals. The images were taken by Metamorph software (http://www.moleculardevices.com/products/software/meta-imaging-series/metamorph.html) and processed using ImageJ software (http://rsbweb.nih.gov/ij/).

4.4 Results and discussion

Flumorph inhibits growth and stimulates sporangial development of *P. infestans* strain 88069

To determine the sensitivity to flumorph of the *P. infestans* strains used in this study, the mycelial growth rate was measured. In the absence of flumorph, no significant differences in growth were observed between the strain 88069 expressing Lifeact-GFP (hereafter named Lifeact-GFP) and the control strain 88069-mRFP (**figure 4.1A**). The 88069-mRFP strain expresses mRFP that was shown not to interfere with cellular processes (Meijer et al 2014). The result of this sensitivity assay suggests that, at the expression level we used, the actin binding capacity of Lifeact does not interfere with normal functioning of the actin cytoskeletal during growth and confirms previous observations (Meijer et al 2014). Adding flumorph to concentrations of up to 0.25 µg/ml did not affect the mycelial growth on agar medium. However, in the presence of 0.5 µg/ml flumorph, a 10.2±4.0% growth reduction was observed and at 0.75 µg/ml flumorph, a 50% growth reduction was reached. This EC_{50} value of 0.75 µg/ml was significantly higher than the EC_{50} values reported for other *P. infestans* strains, which were in the range of 0.10-0.33 µg/ml (Yuan et al 2006). We are not aware of any reports describing the flumorph sensitivity of *P. infestans* strain 88069, the recipient strain of the two transformants used in this study. It is possible that these differences in flumorph sensitivity are caused by strain and/or medium specific effects, a phenomenon that has been described before in sensitivity tests of *P. infestans* for certain compounds (Matuszak et al 1994, Yuan et al 2006). When analysing the mycelium of the Lifeact-GFP and 88069-mRFP

strain (**figure 4.1B**) by microscopy, we observed that flumorph at high concentrations (1 µg/ml) provoked aerial outgrowth of numerous escaping hyphae carrying multiple sporangia. This abnormal morphology might explain the observations made by Yuan et al (2006) that flumorph-resistant *P. infestans* strains produce less sporangia than sensitive strains. The morphological aberrations were not observed when the mycelium was exposed to actin depolymerising drug latB (**figure 4.1B**), and hence, it is unlikely that actin depolymerization is causing the change in morphology.

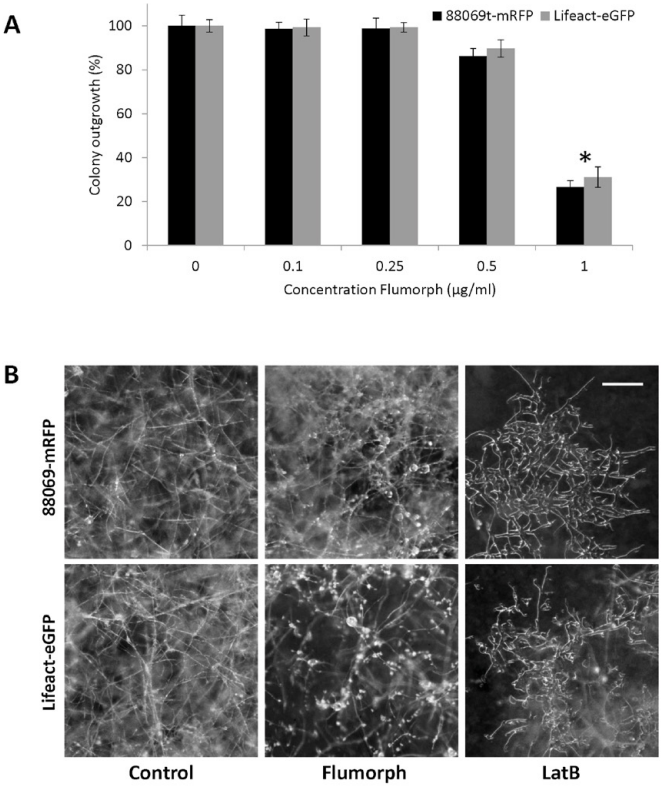

FIGURE 4.1 | Growth and morphology of *a Phytophthora infestans* Lifeact-GFP strain in the presence and absence of flumorph. A) Relative colony sizes of *P. infestans* strains 88069-mRFP or Lifeact-GFP on six-well plates containing rye sucrose agar (RSA) medium without additives (set at 100%) or in the presence of flumorph at 0.1, 0.25, 0.5, and 1 µg/ml (* indicates $P < 0.05$) B) Morphology of 88069-mRFP and Lifeact-GFP hypha grown on RSA without additives (Control) and with flumorph at 1 µg/ml (Flumorph) or 750 nM latB (LatB) visualized by light microscopy. Recipient strain 88069 showed a similar morphology. Photos were taken from 7-day-old colonies. Scale bar is 200 µm and representative for all images.

Flumorph affects *P. infestans* morphology but not the actin cytoskeleton

Previously, Zhu et al (2007b) described that flumorph treatment of *P. melonis* resulted in tip-swelling morphology and disruption of F-actin organization. For visualizing of the actin cytoskeleton they used phalloidin staining and confocal microscopy. We first monitored the

hyphae with abnormal morphology during flumorph treatment for the 88069-mRFP control strain and the Lifeact-GFP transformant. The EC_{50}, determined from solid RSA medium assays, was selected as flumorph concentration in liquid medium although the sensitivity of hyphae could differ between solid and liquid medium. Within 30 minutes after 0.75 µg/ml flumorph treatment, 50% of hyphae showed tip swelling (n=70). These swelling tips showed at least 40% increase of tip diameter compared to the original hyphal diameter. The availability of a *P. infestans* Lifeact-GFP strain allowed us to monitor the effect of flumorph on hyphal morphology in much more detail and, more intriguingly, to visualize the actin cytoskeleton dynamics in the same hyphae during flumorph treatment. In this set-up we compared the effects induced by flumorph with those induced by treatment with latB, a known actin depolymerizing drug that, similar to flumorph, causes hyphal tip swelling (Ketelaar et al 2012, Meijer et al 2014). Our previous studies showed that the consequences of latB treatment are concentration dependent (Ketelaar et al 2012, Meijer et al 2014). At low concentrations most hyphae stopped growing and developed apical actin plaques (**figure 4.2D-E** and **video 4.2**). At intermediate concentrations there was an initial total loss of actin cables and plaques but within minutes plaques reappeared. At high concentrations, all actin cytoskeletal structures were permanently lost but cytoplasmic streaming (**figure 4.2F**) and tip-swelling were still observed (Meijer et al 2014). Similar to latB, flumorph caused a severe reduction of growth speed (**figure 4.1A**). Within 30 minutes after the adding of 0.75 µg/ml flumorph in many hyphae plaques appeared up to the apical zone while maintaining the actin cytoskeleton structures (**figure 4.2G-H**). The presence of plaques in the apical area of hyphae is reminiscent of non-growing hyphae (**figure 4.2C**). Plaque recruitment was often accompanied by swelling of the hyphal tip (**figure 4.2G-H**, **figure 4.3C** and **video 4.3**). This swelling is characteristic for *Phytophthora* isolates exposed to flumorph and might be due to an effect on the cell wall (Zhu et al 2007b). We tested for local changes in cell wall composition, induced by flumorph treatment, by calcofluor white staining but did not detect an obvious difference in the amount and/or accessibility of cellulose in the cell wall at the hyphal tip (**figure S4.1**). After overnight exposure to 0.75 µg/ml flumorph many hyphae had regained growth. These hyphae were devoid of plaques in the apical zone (**figure 4.2I-J**) and in that respect they resembled growing hyphae in non-treated cultures (**figure 4.2A-B** and **video 4.1**). In contrast, the non-apical parts of the hyphae contained many plaques (**figure 4.2J**) reflecting an actin plaque organization known from non-growing hyphae (**figure 4.2C**). When hyphae were treated with 1 µg/ml flumorph, rapid tip swelling was more prominent. **Figure 4.3C** shows a time series of a hyphal tip that responded within two minutes after exposure to 1 µg/ml flumorph. The rapid tip swelling was accompanied with recruitment of actin plaques into the apical zone as clearly observed at the later time points (**figure 4.3C** and **video 4.3**). Besides hyphae with swollen tips, hyphae with burst tips were also occasionally observed, in particular at higher flumorph concentrations. An example is shown in **figure 4.3D** where exposure to 1.5 µg/ml flumorph resulted in a loss of fluorescence, accompanied with bursting of the hyphal tip. This differs from latB treatment where we observed that the fluorescence signal was not lost (**figure 4.2F**) and apparently

the cytoplasmic streaming was not disrupted (Meijer et al 2014). Since latB depolymerizes actin the loss of fluorescence cannot be considered as a hallmark for the disruption of actin structures. We hypothesize that the burst hyphae die, which causes a rapid drop in GFP fluorescence, possibly due to protein degradation or a drop in pH. Hyphae that display arrested growth during flumorph treatment regain growth after time. The actin filament plaques and actin filament cables shown in **figure 4.2** and **figure 4.3** were repeatedly observed in three independent experiments. Treatment with flumorph did not change the organization of the actin cytoskeleton. All actin filament plaques and actin filament cables behaved as under control conditions with the exception of a slight reduction in fluorescence levels. Aberrant actin structures, such as induced during latB treatment of hyphae (Meijer et al 2014), were not observed.

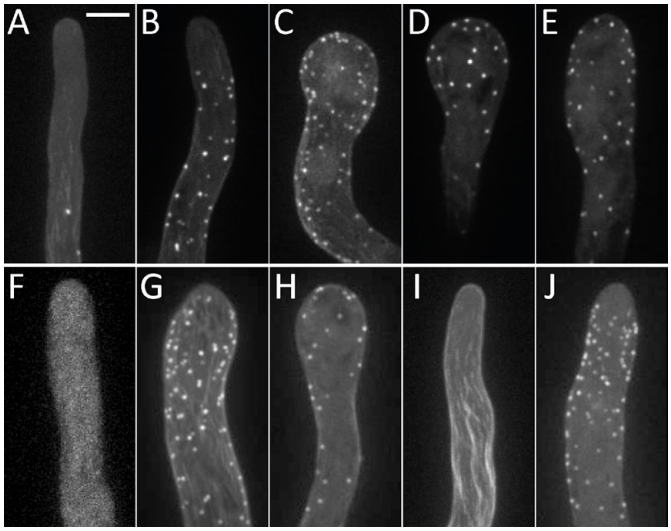

FIGURE 4.2 | Actin cytoskeleton organization and hyphal morphology of the *Phytophthora infestans* Lifeact-GFP strain under various conditions visualized by spinning disk confocal microscopy. A) Hypha growing in rye sucrose liquid (RS) medium without treatment with a relative fast growth speed of 155.4 µm/h. B) Hypha growing in RS medium without treatment with a relative slow growth speed of 57.1 µm/h. C) Nongrowing hypha in RS medium without treatment. D) and E) Hyphae treated for 30 min with 200 nM latB showing tip swelling. F) Hypha treated with 10 µM latB. The picture was taken at 3 s after latB was added. G) and H) Hyphae treated for 30 min with flumorph at 0.75 µg/ml. I) and J) Hyphae treated overnight with flumorph at 0.75 µg/ml. Bar is 5 µm.

In summary, no notable effect of flumorph on the actin cytoskeleton organization in *P. infestans* were detected. The actin cytoskeleton in the flumorph treated hyphae is reminiscent of that in non-growing untreated hyphae. At high concentrations flumorph there was a loss of fluorescence, which was accompanied with bursting of the hyphal tip. This is in contrast to the effect of LatB where at high concentrations, there was still fluorescence but this was dispersed throughout the cytoplasm and not confined to actin cytoskeleton structures due to their depolymerization (Meijer et al 2014). This difference suggests that instead of disrupting the actin cytoskeleton, flumorph induces hyphal death, frequently

accompanied by bursting of the hyphal tip. Based on our results we conclude that flumorph inhibits the growth of *P. infestans* and thus is effective as an oomicide for late blight control. However, its mode of action is still unknown and its primary target remains to be elucidated.

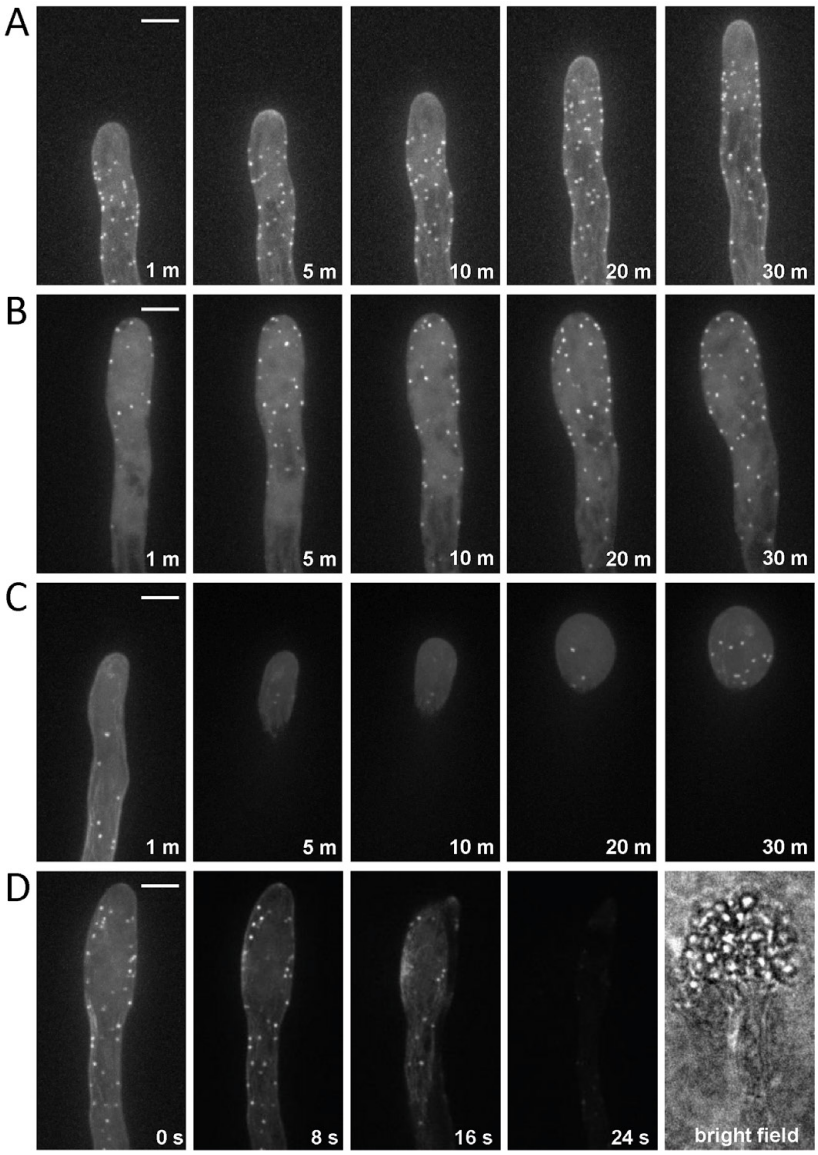

FIGURE 4.3 | Time series for actin cytoskeleton dynamics and hyphal development of the *Phytophthora infestans* Lifeact-GFP strain under various conditions visualized by spinning disk confocal microscopy. A) Time series of a hypha growing in rye sucrose liquid (RS) medium without treatment (control condition). B) Time series of a hypha treated with 200 nM latB. Time point 1 shows the hypha 1 min after latB addition. C) Hypha treated with flumorph at 0.75 µg/ml. Time point 1 shows the hypha at the moment of flumorph addition. D) Hypha bursting after addition of flumorph at 1.5 µg/ml. Images were taken 40 min after addition of flumorph, with 8-s time interval, and show the actin cytoskeleton organization directly before bursting. The bright-field image shows the hyphal tip 2 min after bursting. Bars are 5 µm.

4.5 Conclusions

In this study we used a Lifeact-GFP *P. infestans* marker strain to investigate the anticipated mode of action of the novel agrochemical flumorph. Flumorph was suggested to act by interfering with the actin cytoskeleton in *Phytophthora* spp. (Zhu et al 2007b) but under the conditions used in this study no such interference was observed. Our results illustrate that marker strains which allow real-time monitoring of vital signs such as the actin dynamics, are powerful tools for characterizing the effect of (new) agrochemicals at the cellular level. In our microscopic analyses of *P. infestans* hypha treated with flumorph we frequently observed hyphal bursting, which suggests that flumorph acts by interfering with the cell wall. The cell wall in oomycetes has a different composition than cell walls in other organisms (Grenville-Briggs et al 2010, Meijer et al 2006) and therefore could be an interesting target for oomicides. In fact, the recently developed drug mandipropamid was found to inhibit an enzyme involved in cell wall biosynthesis in *P. infestans* (Blum et al 2010). Generated CAA fungicide resistant *P. melonis* strains were found to share a mutation in a cellulose synthase gene, suggesting that this compound also has a cell wall biosynthesis-influencing mode of action (Chen et al 2012). Apart from the Lifeact-GPF marker strain various other *P. infestans* marker strains have been generated (Ah-Fong & Judelson 2011), but they remain to be exploited as tools for analysing the mode of action of oomicides and guiding the development of new compounds. The availability of additional *P. infestans* marker strains, for example to study the effects on the cell wall, can support the discovery of new, species specific compounds with a known mode of action.

4.6 Supplemental material

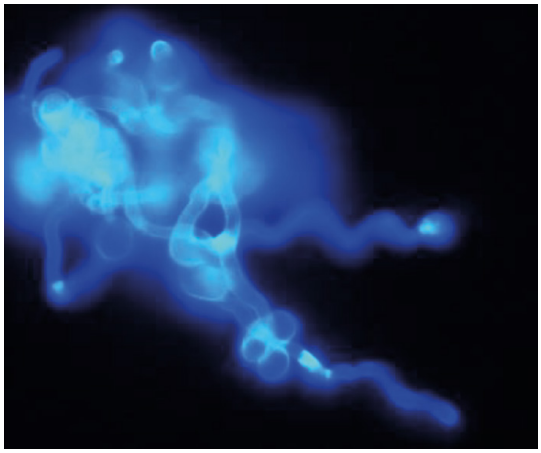

FIGURE S4.1 | Calcofluor white staining of flumorph (0.75 µg/ml, 30 min) treated *Phytophthora infestans* hyphae. Hyphae were stained with calcofluor white (0.015% in PBS), and imaged by fluorescent microscope with DAPI channel.

VIDEO S4.1 | shows confocal fluorescence time series of nontreated hypha visualized in the Lifeact-GFP-expressing strain. The time interval per frame is 8 seconds.

VIDEO S4.2 | shows confocal fluorescence time series of hypha treated with 200 nM latB visualized in the Lifeact-GFP-expressing strain. The time interval per frame is 8 seconds.

VIDEO S4.3 | shows confocal fluorescence time series of hypha treated with flumorph at 0.75 µg/ml visualized in the Lifeact-GFP-expressing strain. The time interval per frame is 8 seconds.

Chapter 5

Live cell imaging of the oomycete *Phytophthora palmivora* shows a role for microtubule-based force generation in nuclear positioning and tip growth directionality

Kiki Kots
Johan van den Hoogen
Michiel Kasteel
Tijs Ketelaar
Francine Govers

5.1 Abstract

The microtubule (MT) cytoskeleton is a well-organized, dynamic system of intracellular filaments. It is shared in all eukaryotes and is involved in numerous processes, ranging from nuclear division to intracellular transport. Here we focus on the MT cytoskeleton of oomycetes in the genus *Phytophthora*, a group of harmful plant pathogens. On the one hand, we provide an inventory of MT-associated proteins in *Phytophthora infestans*, which reveals the presence of unique dynein and kinesin types, some with accessory domains not found elsewhere. On the other hand, we obtained GFP-tubulin-tagged *Phytophthora palmivora* lines which enabled us to gain insight in the temporal and spatial organization of the MT cytoskeleton. By life-cell imaging we visualized MT organization and dynamics in hyphae and during the sequential steps of nuclear division in *Phytophthora*, for the first time ever in an oomycete. We also showed that *Phytophthora* MTs are sensitive to the MT depolymerizing drug oryzalin and used this drug to investigate if MTs have a role in nuclear positioning and distribution. Altogether, this study provides an important basis for further research on the MT cytoskeleton in *Phytophthora* and other oomycetes.

5.2 Introduction

Oomycetes are classified as Stramenopiles, a lineage that also harbours brown algae and diatoms (Levesque 2011). Although some are free-living harmless saprophytes, most oomycetes known to date are pathogens, mainly on plants but also on animals, insects, or other microbes, (Govers & Gijzen 2006). Their morphology resembles that of fungi; filamentous hyphae with tip growth and spores for dispersal. Nonetheless, in the evolutionary tree of life they are far away from unikonts, the supergroup that harbours the fungi (Koonin 2010). One of the most notorious oomycetes is *Phytophthora infestans*, the Irish potato famine pathogen that was introduced in Europe in the mid-19th century (Fry 2008). It causes late blight, a disease that even to this day is a huge problem in potato cultivation worldwide. The *Phytophthora* genus comprises over 120 species, all plant pathogens (Kroon et al 2012). Another devastating species is *Phytophthora palmivora*, the causal agent of black pod in cacao. It has a broad host range, infecting over 170 plant species mainly in the (sub)tropics, including cacao, citrus, rubber, coconut, and oil palm (Torres et al 2016). Our research aims to gain more insight into the biology of *Phytophthora* and to exploit this to identify novel targets for disease control. In this study we focus on gaining new insights in the microtubule (MT) cytoskeleton of these devastating pathogens.

The cytoskeleton is a dynamic and complex system of filamentous protein polymers, that is present in all eukaryotes (Wickstead & Gull 2011) and functions in numerous processes (Erickson 2007). The main components of the eukaryotic cytoskeleton are actin filaments and microtubules (MTs). MTs are hollow, 25 nm wide tubes assembled from heterodimeric

subunits consisting of α- and β-tubulin (Desai & Mitchison 1997). The uniform orientation of the heterodimers incorporated into a MT leads to an intrinsic polarity, which is reflected in a distinct plus (+) and a minus (-) end. MTs alternate phases of polymerisation and depolymerisation, a process referred to as dynamic instability. Most of the dynamic instability occurs at the + end, while the – end is stabilized or shrinks under physiological conditions (Horio & Murata 2014). Due to their dynamic instability and their association with proteins that can modulate MTs behaviour, so called Microtubule Associated Proteins (MAPs), MTs can rapidly restructure in response to intra- and extracellular cues. Besides proteins involved in nucleating, stabilizing and bundling MTs, MAPs include the motor proteins, dyneins and kinesins (Wade 2009). These proteins may have a role in directionally translocating cargo along MTs, but may also function in structuring the MT cytoskeleton for example by sliding MTs apart or by inhibiting polymerisation (Bodakuntla et al 2019). Although some functions of MTs, including chromosome positioning and segregation during mitosis and flagellar movement (Xiang & Plamann 2003), are conserved in many, if not all eukaryotes, other functions differ between evolutionary groups (Gardiner 2013).

Studies on the MT cytoskeleton in oomycetes are scarce, limited to a few species and solely based on microscopic analyses of fixed tissues. Immunolocalization studies showed that MTs in *Saprolegnia ferax* are mostly oriented parallel to the long axis of the hyphae (Heath & Kaminskyj 1989) while electron microscopy studies in the same species revealed that MTs originate from microtubule organizing centres (MTOCs) associated with the nuclear membrane (Heath & Greenwood 1968) and are most abundant in the nuclei-rich zones. Based on these observations it was hypothesised that MTs play a role in nuclear positioning (Heath & Kaminskyj 1989). Transmission Electron Microscopy studies revealed that in *P. infestans* cytoplasmic MTs appear in bundles of approximately ten MTs (Temperli 1990). In *S. ferax*, it was found that MTs rarely extend into the apex of hyphae (Heath & Kaminskyj 1989) and that application of MT depolymerising drugs did not appear to affect the growth velocity of hyphal tips (Heath et al 2000). Thus, it is unlikely that the MT cytoskeleton in oomycete hyphae mediates the transport of vesicles containing growth materials. However, since the directionality of hyphal growth becomes more erratic upon MT depolymerization, it was suggested that MTs have a role in maintaining growth directionality (Heath et al 2000). Similar growth defects caused by MT disruption have been observed in cells with tip growth in other organisms, amongst others in fungal hyphae (Riquelme et al 1998), in root hairs in *Arabidopsis thaliana* (Bibikova et al 1999) and in protonema cells in moss (Doonan et al 1988, Schmiedel & Schnepf 1980).

The aim of this study was to explore the MT cytoskeleton of *Phytophthora* by addressing issues related to its organization and dynamics. To assess whether oomycetes have unique features in their repertoire of MAPs, we mined the *P. infestans* genome for genes encoding putative MTs motor proteins and other MAPs and identified novel subfamilies of the motor proteins dynein and kinesin, in some cases with unique accessory domains. We classified the MAPs and show a cartoon with predicted cellular locations of the MAPs. To visualize the

MT cytoskeleton we generated GFP-tubulin tagged *P. palmivora* lines for live cell imaging and show MT dynamics during mitosis. After nuclear division, MTs extend from MTOCs that polymerize to spatially separate the daughter nuclei, a process that is disrupted when depolymerising MTs with oryzalin. Altogether, this study gives us a unique insight in the MT dynamics in *Phytophthora* and provides an important basis for future research on the oomycete MT cytoskeleton.

5.3 Materials and methods

Data collection and identification of oomycete tubulin subunits and MAPs

The genome of *P. infestans* strain T30-4 (Haas et al 2009) was screened for genes encoding α- and β-tubulin subunits by BLAST search using previously annotated genes from *P. sojae* and *P. ramorum*. In addition, 19 oomycete species (**figure S5.1**) were analysed for homologs using BLAST and orthology searches on FungiDB (Stajich et al 2012). Protein domains were predicted using SMART (Letunic et al 2015) and InterProScan (Jones et al 2014).

Kinesin and dynein heavy chain classification

P. infestans kinesins and dynein heavy chain (DHC) subunits were categorized according to previously described kinesin and DHC families (Kollmar 2016, Wickstead et al 2010) based on sequence similarity. To this end, a multiple sequence alignment was made of putative *P. infestans* kinesins and 1188 eukaryotic kinesin protein sequences (Kollmar 2016, Wickstead et al 2010) using MAFFT v7 (Katoh & Standley 2013) and resources available from the CIPRES Science Gateway (Miller et al 2010). Next, alignment positions that contained more than 25% gaps were trimmed using TrimAL (Capella-Gutierrez et al 2009). A phylogenetic tree was reconstructed using the WAG amino acid substitution model with gamma model of rate heterogeneity, and bootstrapping (100 replicates) was performed with rapid bootstrap analyses on RAxML v8 (Stamatakis 2014). A similar approach was used for DHC subunits, were 3540 eukaryotic DHC subunits and 19 putative *P. infestans* DHC subunits were included in the tree. All DHC sequences were obtained from CyMoBase (Odronitz & Kollmar 2006). Putative *P. infestans* kinesins not readily categorized were annotated as 'ungrouped'. Protein domains were predicted using InterProScan (Jones et al 2014).

Plasmid construction and transformations

To obtain N-terminally GFP-tagged constructs for expression in *P. palmivora*, α-tubulin genes *PiTubA2* (PITG_07960) and *PiTubA5* (PITG_07999) were amplified from *P. infestans* strain NL88069 genomic DNA using primers PITG_07960_NotI_F, PITG_07960_AscI_R, PITG_07999_NotI_F, and PITG_07999_AscI_R (**table S5.5**). Next, the respective PCR

amplicons were cloned in pGFP-N (Ah-Fong & Judelson 2011) using the restriction sites NotI and AscI, resulting in constructs pGFP-07960 and pGFP-07999 (**figure S5.2**). Additionally, the Lifeact-GFP construct (Meijer et al 2014) was included in the transformations to obtain *P. palmivora* F-actin labelled lines. Stable transformants of *P. palmivora* were generated using PEG/$CaCl_2$-mediated protoplast transformation using a modified version of earlier described methods (van West et al 1999). Germinating sporangia (10^5/ml) were incubated on a large petri dish (ø 15 cm) containing 25 ml 10% V8 broth for 18 h at 28°C in the dark. Mycelia were washed in MQ to remove sporangia and incubated in 0.8 M mannitol for 10 min to induce plasmolysis, and subsequently protoplasted by incubation in protoplasting buffer [0.4 M mannitol, 20 mM KCl, 20 mM MES pH 5.7, 10 mM $CaCl_2$, 5 mg/ml CELLULYSIN (Sigma-Aldrich) and 10 mg/ml Lysing Enzymes from *Trichoderma harzianum* (Sigma-Aldrich)] for 30-45 minutes at room temperature in the dark. After removing residual mycelial fragments by filtration (50 µm mesh), protoplasts were pelleted by centrifugation (4 minutes, 700 g). The protoplasts were resuspended in MT buffer (1 M mannitol, 10 mM Tris-HCl pH 7.5) and after a second centrifugation step in MTC buffer (MT + 25 mM $CaCl_2$), then diluted with MTC to $1{\cdot}10^6$ - $5{\cdot}10^6$ protoplasts per ml. 700 µl of the protoplast suspension was mixed with 30 µg circular plasmid DNA in 50 µl MQ. After incubation for 10 minutes at room temperature, 700 µl of freshly prepared PEG solution (50% PEG-3350, 10 mM Tris-HCl pH 7.5, 25 mM $CaCl_2$, sterilized by filtration) was slowly added to the DNA-protoplast mixture. Protoplasts were regenerated overnight at 28°C in 25 ml rye sucrose medium (Caten & Jinks 1968) containing 1 M mannitol, without antibiotics. Regenerated protoplasts were pelleted by centrifugation (5 minutes, 1000 g), resuspended, and plated on selective plates containing 25 µg/ml geneticin. Plates were incubated at 28°C in the dark. Colonies appeared within 4 days.

Strains, culture conditions and life stages

P. palmivora strain P6390 (McHau & Coffey 1994) was routinely grown on 10% V8 medium (10% V8 juice, 1 g/l $CaCO_3$, 1.5% technical agar) containing 20 µg/ml vancomycin, 100 µg/ml ampicillin and 50 µg/ml amphotericin B at 25 °C under continuous light. For selection of transgenic lines the medium was supplemented with 25 µg/ml geneticin. For zoospore release, 4 to 6 day old plates were flooded with V8 broth (10 ml per plate) and incubated in the light for 5 to 20 minutes. Zoospores were encysted by vigorous shaking for 5 minutes, subsequently 100 µl cyst suspension was pipetted in 35 mm glass bottom dishes (MatTek, Ashland, USA) and before microscopic imaging cysts were allowed to germinate for 1-24 hours, depending on the aim of the experiment. For the oryzalin assay, cysts were supplemented with desired concentration of oryzalin (100mM stock in DMSO). In these assays control samples were treated with equal amounts of DMSO, never exceeding 1% of the total volume. Individual hyphal apex positions were registered at each timeframe Δt. Each new position $zt+1$ is then subtracted from previous position zt to obtain a traversed distance. Averaging over the total number of timeframes yield average growth speed per hypha. Significant differences are determined with two-sided t-tests. MT organization was

observed using a Roper (Evry, France) Spinning Disc Confocal System on a Nikon Eclipse Ti microscope using a 100× Plan apo oil immersion objective (NA 1.4) and a 491 nm laserline. Z-stacks were collected with 0.5 µm Z-intervals. Images were analysed using FIJI (https://imagej.net/Fiji).

5.4 Results

Tubulins and MAPs are conserved in *Phytophthora*

Tubulins and MAPs are generally well conserved during evolution. Studies focused on comparative analysis of the MT cytoskeleton in a range of organisms, have identified *Phytophthora* genes encoding components of the MT cytoskeleton, and proteins associated with it, including α-, β-, and γ-tubulin subunits, and several MAPs (Kollmar 2016, Richardson et al 2006, Wickstead & Gull 2011). However, there is as yet no complete and detailed inventory of *Phytophthora* or oomycete MT proteins and MAPs available in literature. Hence, we set out to mine the *P. infestans* genome for genes encoding proteins with sequence similarity to known proteins associated with the MT cytoskeleton. In the *P. infestans* genome, we identified five gene models encoding an α-tubulin subunit (named *PiTubA1*-5), and one encoding a β-tubulin subunit (named *PiTubB1*; **tables S5.1 and S5.2**). These gene models were then used as a query to identify homologs in other oomycetes. Each oomycete species that we analysed has three to five α-tubulin genes and a single β-tubulin gene (**tables S5.1 and S5.2**). At the protein level, α- and β-tubulin sequences are highly similar in different oomycetes; α-tubulin subunits display 91.5% pairwise identity, and β-tubulins are essentially identical exhibiting 99.4% pairwise identity. Additionally, *P. infestans* has one gene encoding γ-tubulin and five encoding γ-tubulin complex proteins (GCP2-5). Together these proteins can form a γ-tubulin ring complex, necessary for MT nucleation (Tovey & Conduit 2018). Another MT nucleation factor gene, a homolog of *TPX2* (Targeting protein for Xklp2) is also present (**table S5.3**).

With the aim of providing a comprehensive overview of MT-associated motor proteins and other MAPs in *P. infestans*, we used a combination of Blast, HMM, and keyword searches, and included sequences of motor proteins and other MAPs previously described in fungi (Xiang & Plamann 2003) and plants (Krtková et al 2016) as queries for screening the genome. This resulted in a total of 186 *P. infestans* gene models that were classified into relevant (sub) families based on sequence homology to known MAPs. An overview of the MAPs identified in *P. infestans*, their predicted sub-cellular location and association with the MTs is depicted in **figure 5.1**. Putative MAP encoding genes and their expression profiles are listed in **table S5.3**. The inventory identified members of all major families of known MAPs, such as the motor proteins dynein and kinesin, as well as MT- and centrosome-associated protein kinases, tubulin assembly proteins, and kinetochore and centromere-associated proteins.

P. infestans has large families of MTs motor proteins with 58 genes predicted to encode kinesins and 39 predicted to encode dyneins (**table S5.3**). Most of the kinesins show similarity to members of described kinesin families in other eukaryotes and can be classified in existing subfamilies (Ali & Yang 2020). There is one protein, though, with a kinesin domain and a ZZ-type Zinc Finger domain. This combination of domains appears to be unique for oomycetes since a similar protein is found in other Peronosporalean oomycetes but not in other eukaryotes. The 39 dynein genes are divided into three groups, 15 encoding dynein light chain (DLC) subunits, 4 encoding dynein intermediate chain (DIC) subunits, and 20 encoding dynein heavy chain (DHC) subunits (**table S5.3**).

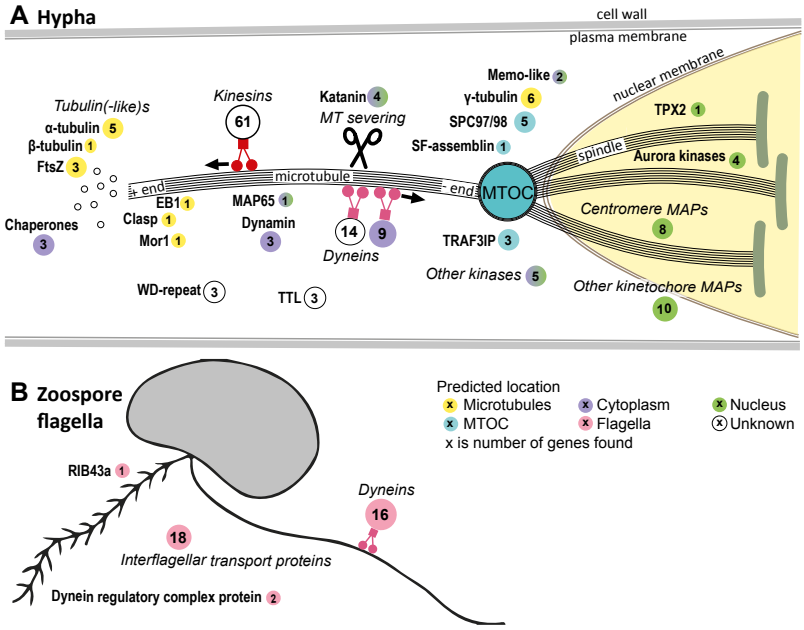

FIGURE 5.1 | Microtubule subunits and microtubule associated proteins (MAPs) in *P. infestans* and their predicted locations in hyphal compartments (A) or in zoospore flagella (B).

We found several genes encoding MT plus end binding proteins (**table S5.3**), which have important roles in several processes such as protein localization and regulating MT dynamics. A number of previously identified genes encoding intraflagellar transport proteins are also included in our inventory (Judelson et al 2012).

The augmin complex, present in plants and fungi, is able to bind to spindle MTs and is involved in MT nucleation (Edzuka et al 2014). We were not able to identify any augmin encoding gene in *P. infestans*. In several other oomycetes, including species from the genera *Phytophthora*, *Hyaloperonopspora*, *Peronospora*, and *Plasmopara,* augmin genes are also missing (**table S5.3**). However, in species belonging to the genera *Albugo*, *Pythium*, *Aphanomyces*, and *Saprolegnia*, there is a single gene encoding a homolog of the augmin subunit 4 (Aug4; **table S5.4**).

Expression of GFP-α-tubulin allows live cell visualization of MT organization and dynamics in *Phytophthora*

For live cell imaging of the MT cytoskeleton, we generated *P. palmivora* transformants expressing GFP-tagged α-tubulin, an approach that has been successfully implemented to visualize the MT cytoskeleton in a wide range of organisms (Goodson et al 2010). The transformation constructs contained the HAM35 promotor followed by a GFP coding sequence, the open reading frame of either *PiTubA2* (PITG07960) or *PiTubA5* (PITG07999), both highly expressed in all tissues, and the HAM35 terminator (**figure S5.2**). Transformation of *P. palmivora* strain 6391 resulted in a total of six independent transformants with a detectable fluorescent signal. In all six lines, designated GFP-TubA2#1-3 and GFP-TubA5#1-3, GFP labelled MTs were visible by microscopy and all showed a similar localisation pattern (**figure S5.3**). This localization included mitotic spindles, MTOCs and cytoplasmic MTs, and their dynamics (**figure 5.2A-B**). We used GFP-TubA2#1 and GFP-TubA5#1 for further experimentation. These lines behaved similarly as the wild type recipient strain in growth assays with no changes in viability and growth morphology (**figure S5.4**).

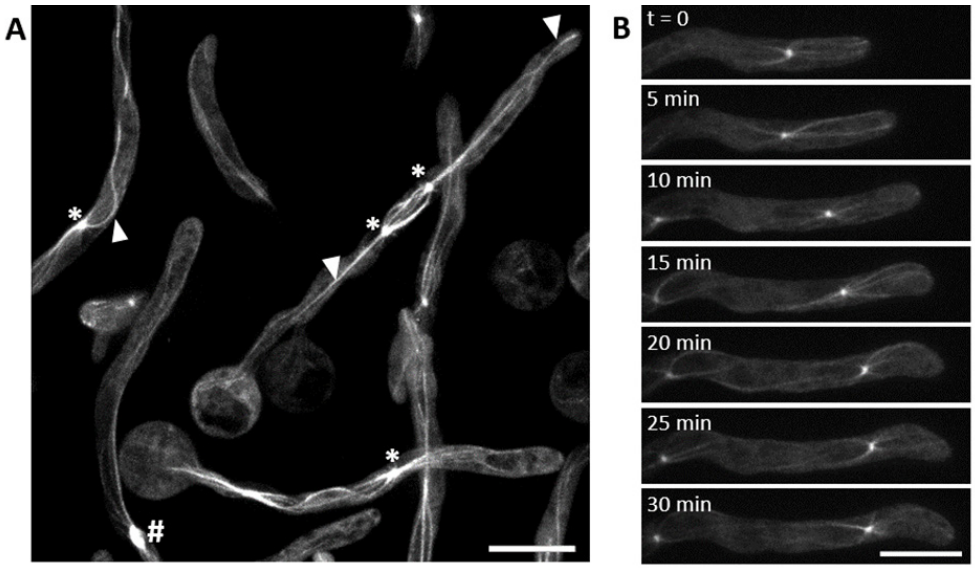

FIGURE 5.2 | *Phytophthora palmivora* GFP-α-tubulin transformants. A) MTs visible in GFP-TubA2. Arrowheads point to cytoplasmic MTs. Asterisks indicate MTOCs and the hashtag indicates a spindle. B) MT dynamics in a GFP-TubA2 hypha. Scale bars are 10 µm.

Phytophthora MTs are sensitive to the MT depolymerizing drug oryzalin

To assess the effects of MTs depolymerization on *Phytophthora* hyphae, we started by exposing the GFP-TubA lines to a range of concentrations of the MT depolymerizing drug oryzalin . We incubated cysts in V8 with increasing concentrations of oryzalin (1 - 10 µM) for two hours and examined the MT cytoskeleton in germ tubes by spinning disk microscopy. Cytoplasmic MTs were absent in samples treated with oryzalin concentrations of 2.5 µM and higher (**figure 5.3A-D**). However, MT fragments associated with the MTOCs, and MTs in spindles, were not affected, not even with the highest concentration tested (**figure 5.3D**). Possible reasons for this observation may be that mitosis in oomycetes is closed, i.e. with an intact nuclear membrane (Heath et al 1984), which may hamper the accessibility of spindle MTs to oryzalin, or that spindle MTs are less sensitive to oryzalin treatment. Based on these observations we selected 5 µM oryzalin for further experiments.

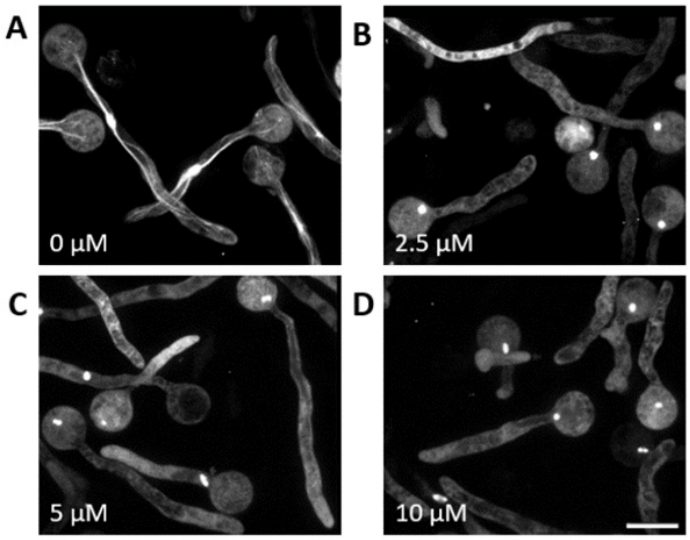

FIGURE 5.3 | *Phytophthora palmivora* MT organization in germinating GFP-TubA2 cysts treated with oryzalin. Germinating cysts treated with A) 0 µM, B) 2.5 µM, C) 5 µM and D) 10 µM oryzalin. Scale bars: 10 µm.

To identify the effects of oryzalin treatment on cyst germination and hyphal growth, we tracked these processes over a time frame of five hours. As shown in **figure 5.4** the percentage of germinating cysts and the hyphal growth velocities in the presence of oryzalin decreased significantly. The decrease in growth velocity may be caused by sudden growth arrests that we observed in oryzalin treated hyphae. These arrests were not observed in control hyphae. In 28% of the observed growth arrests, hyphal tip growth recovered eventually, whereas other growth arrest events resulted in the formation of a branch. Indeed, most branching events were observed in hyphae that had arrested growth (0.61±0.22 events h^{-1}, n=15), when compared to hyphae with an actively growing tip (0.05 ±0.09 events h^{-1}, n=15),

suggesting that branching often was the consequence of the initiation of a new hyphal tip in hyphae that had arrested growth.

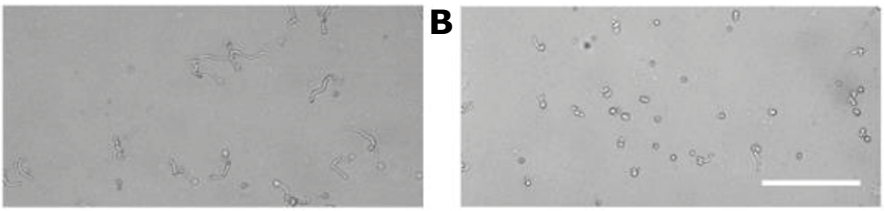

C

	Control	5µM oryzalin
Germination	85% (n=34)	63% (n=48)*
Time to germination	28.6 ± 13.3 (n=34)	61.3 ± 41.2 (n=48)*
Growth velocity (µM h^{-1})	32.8 ± 16.7 (n=15)	9.2 ± 8.1 (n=15)*
Growth arrests (events h^{-1})	0	0.8 ± 0.2 (n=15)*
Branching (events h^{-1})	0	0.64 ± 0.2 (n=15)*

FIGURE 5.4 | The effect of microtubule depolymerization on germination of *P. palmivora*. The fraction of germinated cysts over the course of 5 hours in the absence (A) or presence of 5 µM oryzalin (B). Scale bar indicates 15 µm. C) Germination percentages were determined at the end of this time frame and the other parameters were calculated over the 5 hours interval. *Significant (P<0.05 by a two-sided t-test).

Microtubule organization and dynamics in *P. palmivora* during mitosis

Oomycetes are coenocytes and hence, multiple nuclei reside in a shared pool of cytoplasm. Nuclei do not divide simultaneously and, as mentioned earlier, remain enclosed by the nuclear envelope during mitosis (Heath 1980). Using the GFP-TubA expressing lines, we were able to observe and time the different stages of mitotic events in *P. palmivora*. To this end, we monitored germinating cysts over time. Cysts typically have just one nucleus and based on the time-lapse imaging experiments (**figure 5.5A**), we know that the first mitotic event occurs within five hours after germination. The first detectable sign of an imminent mitotic event was the duplication of the MTOC. After this duplication, both MTOCs positioned themselves at opposite sides of the nucleus. During this phase, that usually occurred within the first 30 minutes after zoospore encystment, no spindle MTs could be observed yet (**figure 5.5A**). This stage lasted several hours and was referred to as early prophase by Heath and Greenwood (1970). To track mitosis, we started imaging 3 hours after cyst germination and focused on individual spindles to acquire sufficient temporal resolution. As the nuclear division proceeded, distinct phases could be distinguished (**figure 5.5C**; I-III). During the first phase a MT spindle assembled while the MTOCs remained positioned apart from each other at a constant distance of 1.73±0.19 µm (**figure 5.5C**; I-III). In general, this stage lasted at least 30 minutes, and in some nuclei even over an hour. Unfortunately we were unable to stain nuclei in *P. palmivora*. For this reason we were not able to link the MT organisation directly to mitotic stages, but it is likely that this stage corresponds to prophase and metaphase. During

the next phase (II), the MTOCs slowly moved apart with an average velocity of 16.44 (±21.08) μm h^{-1}. This stage lasted ~5 minutes. During the final phase (III), the separation of the MTOCs accelerated to a velocity of 40.74 (±99.31) μm h^{-1} (**figure 5.5B**). At the end of this phase, MTOC segregation velocities decreased until a constant distance between the MTOCs was established (18.96±6.15 μm, n=5). When linking these observations to mitotic stages, it is likely that stage II represents the anaphase where the MTOC displacement is caused by the elongation of interpolar MTs, referred to as anaphase B. During anaphase nuclear separation occurs. We hypothesize that at the onset of phase III nuclear separation, and hence mitosis, has been completed.

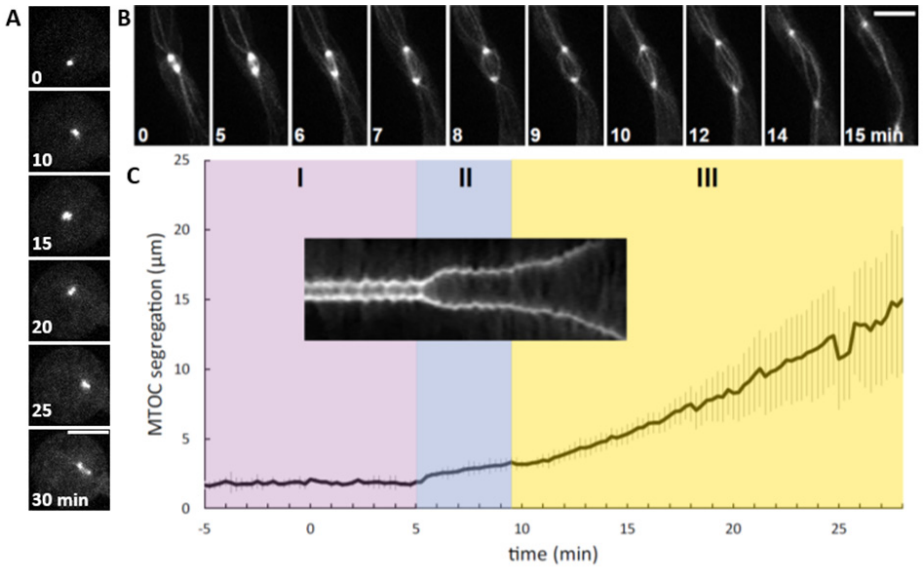

FIGURE 5.5 | *P. palmivora* MTs during nuclear division. A) MTOC duplication over time. B) Mitotic spindle over time. C) Average distance between two MTOCs during mitosis (n=11). Three different phases were distinguished based on the speed of microtubule segregation (I-III). T=0 is 3 hours after germination. Kymograph of spindle (B) showing the MTOC moving apart over time. Scale bars are 5 μm.

Dynamic cytoplasmic MTs interact to position nuclei

To understand the processes that may underlie the rapid MTOC separation and MTOC positioning in phase III it is important to take into account that, next to the MTs that form the spindle in the nucleus during closed mitosis, there are other MTs radiating from the MTOCs but residing in the cytosol (**figure 5.6A**). When we followed MTs organization over time, the cytoplasmic MTs in *P. palmivora* displayed dynamic instability; alternating stages of MT growth and shrinkage (**figure 5.6A**). When MTs that originated from MTOCs on adjacent nuclei encountered each other, the fused and the total length of the interacting MTs increased (**figure 5.6B**). If our hypothesis that this sequence of events occurs in phase III is correct, we should be able to observe two events: (i) Antiparallel MT bundles should

display occasional buckling caused by compressive forces generated by MT bundles that operate between other nuclei, and (ii) nuclear positioning should be disrupted upon MTs depolymerization. Firstly, we followed MT bundles between nuclei over time. It was clearly visible that these bundles occasionally buckled (**figure 5.6B**).

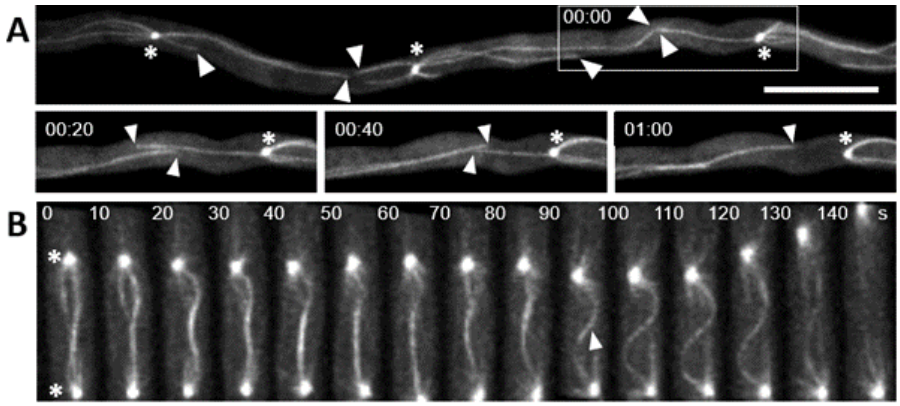

FIGURE 5.6 | Behaviour of cytoplasmic MTs in *P. palmivora*. A) MTs polymerizing and depolymerizing. Arrowheads point to plus-ends, asterisk indicate MTOCs. Scale bar is 10 µm. B) Buckling MTs over time. Asterisks indicate two daughter MTOCs moving apart. Arrowhead points to buckling MT. Sections are 5 µm wide.

MTs that extend into the hyphal tip may be involved in positioning the nucleus distal from the tip

In a previous study on the *P. infestans* cytoskeleton we observed that the nucleus closest to the tip of a hypha is positioned at a fixed distance from the tip and that the actin cytoskeleton is involved in this nuclear positioning (Ketelaar et al 2012). However, the actin induced changes in nuclear positioning may be indirect and caused by cessation of growth. To gain insight in the role of MT in positioning the most apical nucleus, we studied MT organization in the growing tip of hyphae expressing GFP-TubA. From the MTOC located closest to the tip, MTs radiated into the extreme tip that occasionally made contact with the apical cell boundary. To gain insight in the consequences of these interactions we performed a correlative study of nuclear positioning and the behaviour of the MTs extending into the apex. We found that MTs frequently buckled once they reached the cell boundary in the hyphal tip (**figure 5.7A**; arrowhead 120 s), whereas they are much straighter when not reaching the boundary (**figure 5.7A**; arrowhead 0 s). To quantify buckling behaviour, we determined the curvature by dividing the length of the MT extending into the apex by the shortest possible path length. Next, we determined if the MT interacted with the cell apex or not. This analysis showed that the curvature of MTs increased significantly (1.075±0.082, n=26) once they reached the tip when compared to that of free MTs (1.011±0.008, n=17; **figure 5.7B**). Moreover, the presence of a buckling MTs at the tip was frequently followed by either displacement of the MTOC away from the tip or an arrest of movement of the MTOC towards the tip (n=22; **figure**

5.7C), but almost never with a displacement towards the tip (n=2). Together these data show that the interaction of MTs with the apex may play a role in maintaining a distance between the apex and the closest nucleus.

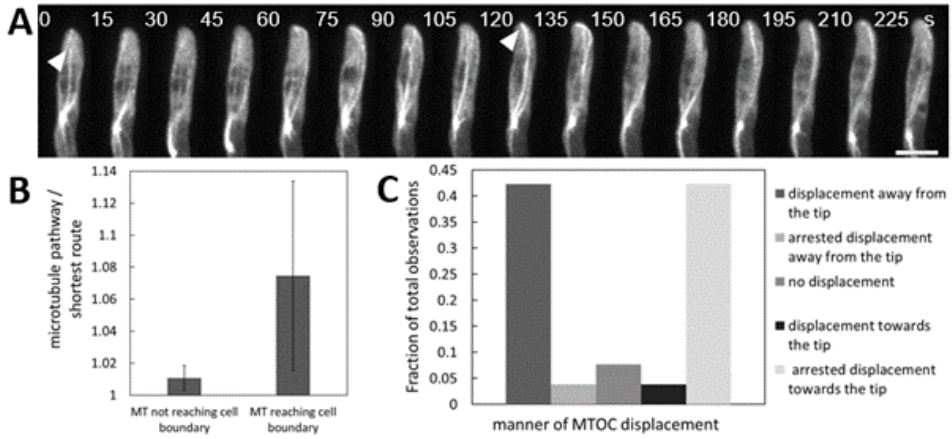

FIGURE 5.7 | *P. palmivora* cytoplasmic MTs during tip growth. A) Microtubules in the growing tip, without reaching the apex (arrowhead 0 s) and with reaching the apex (arrowhead in 120 s). B) Microtubules reaching the apex undergo more buckling than those that do not (P<0.05 by a two-sided t-test). C) Microtubule buckling results mainly in either the displacement of the MTOC away from the apex or an arrest of movement towards the tip (n=26). Scale bar is 5 µm.

Actin plaques appear in the tip during oryzalin induced growth arrests

In diverse systems, an interplay between actin and MT cytoskeleton has been reported. In tip growing cells of plants, MTs have been shown to provide polarity cues to the actin cytoskeleton (Ketelaar et al 2002, Wu & Bezanilla 2018) and in the tip growing fission yeast *Schizosaccharomyces pombe,* MTs deliver an actin nucleating machinery to the cell apex (Laporte et al 2015). To assess if MT depolymerisation affects the actin cytoskeleton, we generated a Lifeact-GFP expressing *P. palmivora* line (PP-LA-GFP) by introducing the Lifeact-GFP construct from Meijer et al (2014) by DNA transformation. We monitored growing PP-LA-GFP hyphae treated with oryzalin and found that during growth arrests there was an accumulation of actin plaques close to the tip (**figure 5.8A**). Next we looked at the correlation between the growth speed and the distance from the extreme tip to the first plaque and we found a shift in this correlation when we compare oryzalin treated with non-treated hyphae (**figure 5.8B**). Surprisingly, plaque lifetimes in oryzalin treated hyphae (8.9±4.4 min, n=10) decreased significantly (p=0.009, two-sided t-test) when compared to control hyphae (16.3±6.0 min, n=10), suggesting a link between MT based activities and plaque longevity.

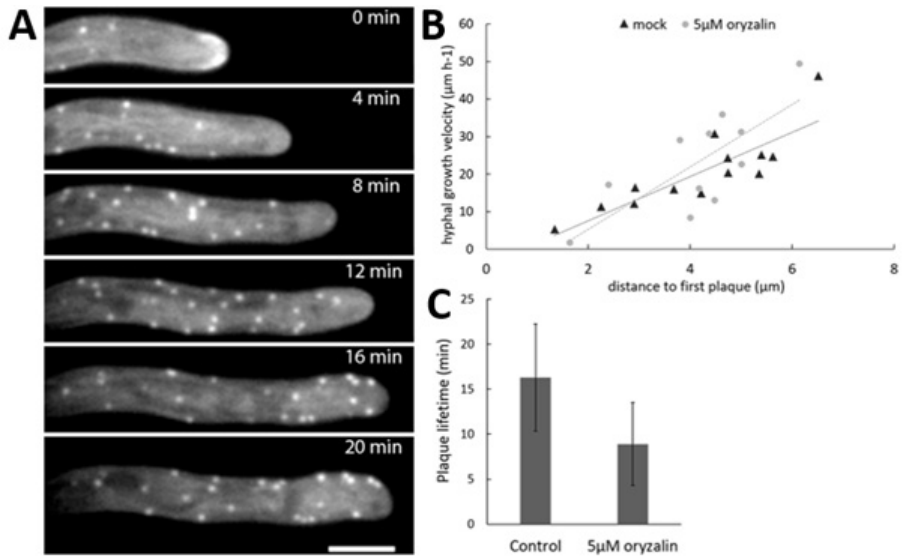

FIGURE 5.8 | The effect oryzalin on the actin cytoskeleton of *P. palmivora*. A. Hyphae treated with oryzalin often undergo a sudden growth arrest. B. The relation between the distance of the first plaque to the tip (µm) and hyphal growth velocity (µm/h). Calculated Pearson correlations of untreated (0.847) and hyphae treated with 5 µM oryzalin (0.751) were, by means of a Fisher r-to-z transformation, found to differ significantly ($P<0.05$ by a two-sided z-test). C. Microtubule depolymerization decreases actin plaque lifetime ($P<0.05$ by a two-sided t-test).

5.5 Discussion

In the current work we have focused on the composition, localization, dynamics and functions of the *Phytophthora* MT cytoskeleton, starting by making an inventory of the proteome associated with the *Phytophthora* MTs cytoskeleton. Using databases with known MAPs as a reference, we show that amongst the proteins associated with the MT cytoskeleton, next to the MAPs with common domain combinations, some *Phytophthora* MAPs have unique domain combinations. Proteins with unusual domain combinations have not only been identified in this study, but also in other genome analyses in *Phytophthora* species (Seidl et al 2011). The remarkable amount of proteins with unusual domain combinations may be linked to oomycetes being coenocytic. This allows oomycetes to overcome lethal mutations by using transcripts from multiple nuclei and it may also make it easier to stepwise evolve proteins with unusual domain combinations. Since species from the genus *Phytophthora* specialized in being plant pathogens, they would benefit from the ability to adapt rapidly to newly evolved defence strategies by high genomic plasticity (Kroon et al 2012).

By introducing a live cell MTs marker in *P. palmivora*, we were able to study MTs organization and dynamics in *Phytophthora*. Until now, most information about the oomycete MTs cytoskeleton originated from serial-sectioning electron microscopy of freeze-substituted

cells (Heath & Kaminskyj 1989) and immunofluorescence studies (Kaminskyj & Heath 1994, Temperli 1990). Although these studies have provided valuable information and had a pioneering nature, they lack information about dynamics and cannot be used for correlative studies that link growth and nuclear positioning to MTs dynamics. Using live cell imaging data, we were able to identify different stages in the mitotic process and show that after mitosis, MTs originating from different MTOCs interact with each other to separate nuclei and maintain this separation over longer time frames. In addition, we showed that MTs that polymerize into hyphal apices from the surface of the nearest nucleus contribute to maintaining a minimal spacing between apex and nearest nucleus. Why would a mechanism for uniform spacing between nuclei and spacing between the hyphal apex and the nearest nucleus operate? In multicellular organisms, nuclear spacing is accomplished by cellularization, which does not occur in coenocytes like *Phytophthora*. Being coenocytic comes with advantages, as discussed above, but there is a price to pay. Coenocytes need to respond quickly when wounded to prevent major damage to the organism. It is known that some oomycetes do this by rapid jellification of the cytoplasm that surrounds the wounding site (Chitcholtan et al 2012, Muralidhar et al 2016). Upon fragmentation of the organisms that consist of a large hyphal network, individual fragments can recover, but only so if they contain at least one nucleus. In addition, local transcriptional regulation and local production of transcripts may be considered as advantages of regulated spacing of nuclei. In multinucleate *Drosophila* embryos, nuclei are embedded in an orderly matrix of actin and MTs, ensuring a regular arrangement of nuclei in the *Drosophila* syncytium (Lv et al 2021). The fixed distance between apex and the first nucleus is observed in tip-growing cells of organisms in diverse evolutionary lineages including plants (Ashraf & Facette 2020, Ketelaar et al 2002, Yi & Goshima 2020) and fungi (Gibeaux et al 2017, Gladfelter & Berman 2009). This spacing may represent an optimum between being close to respond to cues and provide transcripts and being away so that there is no interference with the tip growth process itself (Xiang 2018).

The physical characteristics of the MTs cytoskeleton make it highly suitable to control nuclear spacing. MTs are the stiffest cytoskeletal structures and in oomycetes, they originate from MTOCs that are conveniently localized to the envelope of each nucleus. Once MTs encounter a surface, they can generate piconewton forces (Dogterom & Yurke 1997), which are sufficient to position the fission yeast nucleus (Tran et al 2001). In a recent paper from Teapal et al (2021), they created imitation coenocytic yeast, containing multiple nuclei per cell, and they showed that also in this system MTs are key to the positioning of nuclei. Forces required for nuclear positioning in *Phytophthora* hyphae are likely to be similar. The interaction between MTs originating from adjacent nuclei suggests that a conserved spacing module is in place: overlap formation by the conserved antiparallel MTs bundler PRC1/ASE1/MAP65. These overlaps are known to recruit motor proteins that push both polymerizing MTs backwards while limiting the overlap length (Tang et al 2019), thus increasing the distance between MTOCs and nuclei.

The MT and actin cytoskeleton are known to interact in a variety of organisms. Some of these interactions are essential for proper organization and dynamics (Goode et al 2000, Sampathkumar et al 2011). In this work we show that the prolonged lifetimes and cortical localization of actin plaques is not restricted to *P. infestans* but also conserved in *P. palmivora*, even though the lifetime is significantly shorter than in *P. infestans* (Meijer et al 2014). The lifetime of the dot like actin structures has not been studied in other oomycetes, but it is likely that our findings of long plaque lifetime and immobility are representative for plaques in general and that this behaviour is conserved throughout oomycetes. The difference in lifetime may reflect the faster hyphal growth velocity of *P. palmivora* than that of *P. infestans* (Meijer et al 2014). However, since the MTs neither have the density nor the cortical localization for prolonged, direct interaction with actin plaques, it is unlikely that a direct interaction causes the reduced plaque lifetime. The microtubules between nuclei are likely to function as scaffolds that control nuclear positioning and may be involved more broadly in cytoplasmic organization, the reduced lifetimes of plaques may reflect a less organized cytoplasm.

Taken together, our results show that the MT cytoskeleton in *Phytophthora* has conserved features, but also features that may be oomycete specific that are worth further investigation. In future work these oomycete specific features may serve as the basis for a *Phytophthora* control strategy.

5.6 Supplemental files

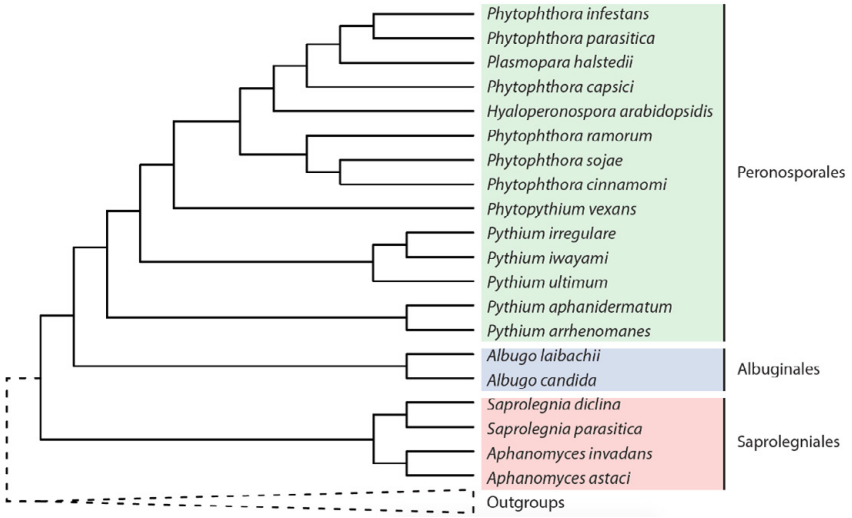

FIGURE S5.1 | Simplified phylogeny of oomycetes and related organisms based on the tree as presented by McCarthy and Fitzpatrick (2017).

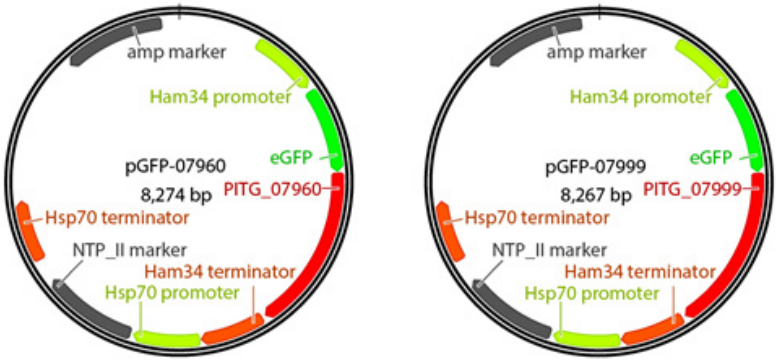

FIGURE S5.2 | Constructs encoding N-terminally GFP-tagged *P. infestans* α-tubulins PITG_07960 (pGFP-07960) and PITG_07999 (pGFP-07999).

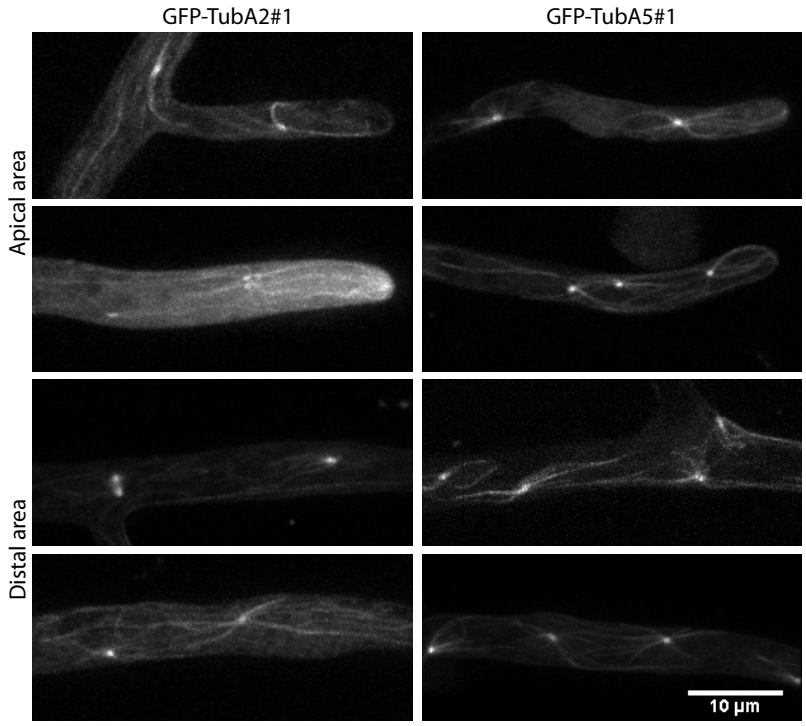

FIGURE S5.3 | Both GFP-PiTubA2 and GFP-PiTubA5 label the same MT population. In all lines, MTOCs, spindles and internuclear MTs were observed in all areas of the hyphae.

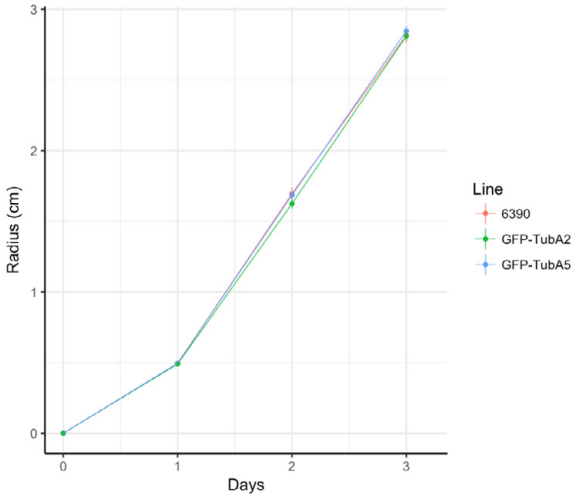

FIGURE S5.4 | Radial growth rate of *P. palmivora* recipient strain P6390 (6390) and two GFP-tubulin strains (GFP-TubA2#1 and GFP-TubA5#1). The graph is representative for three independent growth rate assays that each included five replicates per line. Error bars represent standard deviations.

TABLE S5.1 | Details of oomycete α-tubulin genes.

Gene ID	Product description	Organism	Notes	Seq length (aa)
evm.TU.AC2VRR_s00248g27	unspecified product	*Albugo candida*		449
evm.TU.AC2VRR_s00248g139	unspecified product	*Albugo candida*		453
ALNC14_062890	unspecified product	*Albugo laibachii*		449
CCA24429	splicing factor putative	*Albugo laibachii*	corrected, truncated	436
H257_08698	tubulin alpha chain	*Aphanomyces astaci*		453
H257_15887	tubulin alpha chain	*Aphanomyces astaci*		453
H257_08697	tubulin alpha chain	*Aphanomyces astaci*	corrected	454
H310_12120	tubulin alpha chain	*Aphanomyces invadans*	truncated	362
H310_08859	tubulin alpha chain	*Aphanomyces invadans*		453
HpaG803637	unspecified product	*Hyaloperonospora arabidopsidis*		451
HpaG803651	unspecified product	*Hyaloperonospora arabidopsidis*		452
PHYCA_511272	alpha tubulin 1	*Phytophthora capsici*		452
PHYCA_530856	tubulin alpha-2 chain-like	*Phytophthora capsici*	gap in gene model	429
PHYCA_107024	tubulin alpha-4 chain-like	*Phytophthora capsici*		452
PHYCA_511275	tubulin alpha-3 chain	*Phytophthora capsici*	truncated	410
PHYCA_575859	tubulin alpha-5 chain	*Phytophthora capsici*		450
PHYCI_89449	Alpha tubulin	*Phytophthora cinnamomi*		452
PHYCI_111102	unspecified product	*Phytophthora cinnamomi*	truncated	340
PHYCI_233998	unspecified product	*Phytophthora cinnamomi*		453
PITG_07960	alpha-tubulin, putative	*Phytophthora infestans*		453
PITG_07999	alpha-tubulin, putative	*Phytophthora infestans*		453
PITG_07949	alpha-tubulin, putative	*Phytophthora infestans*		454
PITG_07996	alpha-tubulin	*Phytophthora infestans*		453
PITG_07961	cleavage induced tubulin alpha chain	*Phytophthora infestans*	corrected	453
PPTG_08465	tubulin alpha chain	*Phytophthora parasitica*		452
PPTG_08466	tubulin alpha chain	*Phytophthora parasitica*		452
PPTG_08498	tubulin alpha chain	*Phytophthora parasitica*		453
PPTG_08506	tubulin alpha chain	*Phytophthora parasitica*		453
PPTG_08453	tubulin alpha chain	*Phytophthora parasitica*		454
PSURA_72478	Alpha tubulin	*Phytophthora ramorum*	truncated	322
PSURA_51050	Alpha tubulin	*Phytophthora ramorum*		450
PSURA_72335	Alpha tubulin	*Phytophthora ramorum*		450
PSURA_71889	Alpha tubulin	*Phytophthora ramorum*		452
PSURA_71894	Alpha tubulin	*Phytophthora ramorum*		453
PSURA_51154	unspecified product	*Phytophthora ramorum*		446
PSURA_71890	unspecified product	*Phytophthora ramorum*		452
PHYSODRAFT_338144	hypothetical protein	*Phytophthora sojae*	gap in gene model	438
PHYSODRAFT_288901	hypothetical protein	*Phytophthora sojae*		441
PHYSODRAFT_288898	hypothetical protein	*Phytophthora sojae*		452

Gene ID	Product description	Organism	Notes	Seq length (aa)
PHYSODRAFT_565438	hypothetical protein	*Phytophthora sojae*		452
PHYSODRAFT_356026	hypothetical protein	*Phytophthora sojae*		453
PHYSODRAFT_528260	hypothetical protein	*Phytophthora sojae*		453
Phal02670	tubulin alpha chain	*Plasmopara halstedii*	corrected	296
Phal02671	tubulin alpha chain	*Plasmopara halstedii*	corrected	303
Phal08353	tubulin alpha chain	*Plasmopara halstedii*		453
Phal13640	tubulin alpha chain	*Plasmopara halstedii*	corrected, truncated	136
PAG1_G000452	Alpha-tubulin	*Pythium aphanidermatum*		434
PAG1_G000713	Protein F44F4.11	*Pythium aphanidermatum*	truncated	83
PAR_G009305	Alpha-tubulin	*Pythium arrhenomanes*	truncated	50
PIR_G008598	Alpha-tubulin	*Pythium irregulare*	corrected, truncated	413
PIW_G013767	Alpha-tubulin	*Pythium iwayamai*	truncated	41
PIW_G003138	Alpha-tubulin	*Pythium iwayamai*	truncated	56
PIW_G012562	Alpha-tubulin	*Pythium iwayamai*	truncated	153
PIW_G014282	Alpha-tubulin	*Pythium iwayamai*	truncated	178
PYU1_G011143	unspecified product	*Pythium ultimum*		451
PYU1_G011167	unspecified product	*Pythium ultimum*		452
PYU1_G011535	unspecified product	*Pythium ultimum*		453
PVE_G008283	Alpha tubulin	*Pythium vexans*	gap in gene model	426
PVE_G010441	Alpha-tubulin	*Pythium vexans*	truncated	73
PVE_G010138	Alpha-tubulin	*Pythium vexans*	truncated	140
PVE_G010242	Alpha-tubulin	*Pythium vexans*	truncated	150
PVE_G010239	Alpha-tubulin	*Pythium vexans*	gap in gene model	334
SDRG_17410	tubulin alpha	*Saprolegnia diclina*	truncated	273
SDRG_02711	tubulin alpha	*Saprolegnia diclina*	truncated	299
SDRG_11427	tubulin alpha chain	*Saprolegnia diclina*		449
SDRG_11949	tubulin alpha chain	*Saprolegnia diclina*		451
SDRG_11948	tubulin alpha chain	*Saprolegnia diclina*		453
SPRG_09506	hypothetical protein	*Saprolegnia parasitica*	truncated	186
SPRG_07894	tubulin alpha-1 chain	*Saprolegnia parasitica*		450
SPRG_04481	tubulin alpha chain	*Saprolegnia parasitica*		451
SPRG_04482	tubulin alpha chain	*Saprolegnia parasitica*		453
SPRG_09503	tubulin alpha chain	*Saprolegnia parasitica*		453

TABLE S5.2 | Details of oomycete β-tubulin genes.

Gene ID	Product description	Species	Notes	Seq length (aa)
evm.TU.AC2VRR_s00054g80	unspecified product	*Albugo candida*		446
CCA17899	Tubulin beta chain putative	*Albugo laibachii*	Fragment	381
H257_01711	tubulin beta chain	*Aphanomyces astaci*		446
H310_03943	tubulin beta chain	*Aphanomyces invadans*		446
HpaP814031	Beta-tubulin	*Hyaloperonospora arabidopsidis*		446
PHYCA_576734	beta-tubulin	*Phytophthora capsici*		446
PHYCI_418545	unspecified product	*Phytophthora cinnamomi*		446
PITG_00156	beta-tubulin	*Phytophthora infestans*		446
PPTG_15113	tubulin beta chain	*Phytophthora parasitica*		446
PSURA_72114	Beta tubulin	*Phytophthora ramorum*		446
PHYSODRAFT_507388	hypothetical protein	*Phytophthora sojae*		446
Phalo3888	beta- partial	*Plasmopara halstedii*	Corrected	447
PAG1_G000598	Beta-tubulin	*Pythium aphanidermatum*		446
PAR_G000681	Beta-tubulin	*Pythium arrhenomanes*		446
PIR_G007881	Beta-tubulin	*Pythium irregulare*		446
PIW_G014483	Beta-tubulin	*Pythium iwayamai*	Fragment	127
PIW_G007163	Beta-tubulin	*Pythium iwayamai*	Fragment, corrected	133
PIW_G006543	Beta-tubulin	*Pythium iwayamai*	Fragment, corrected	154
PUG3_G000817	Beta-tubulin	*Pythium ultimum*		446
PVE_G004943	Beta-tubulin	*Pythium vexans*		446
SDRG_08123	tubulin beta chain	*Saprolegnia diclina*		446
SPRG_09415	tubulin beta chain	*Saprolegnia parasitica*		446

TABLE S5.3 | Details of microtubule-associated proteins (MAPs) in *P. infestans*. All MAPs are clustered according to predicted function and/or subcellular localization (grey rows). Expression profiles are based on RNAseq data of *P. infestans* strain 88069 (Schoina et al 2021). Abbreviations: myc mycelium, spor sporangia, zsp zoospores, gc germinating cysts.

Family	Subfamily	Proposed name	Proposed product description
Tubulin subunits			
Alpha tubulin		PiTubA1	Alpha-tubulin-1
		PiTubA2	Alpha-tubulin-2
		PiTubA3	Alpha-tubulin-3
		PiTubA4	Alpha-tubulin-4
		PiTubA5	Alpha-tubulin-5
Beta tubulin		PiTubB1	Beta-tubulin
MTOCs / nucleation factors			
Gamma tubulin		PiTubG1	Gamma-tubulin-1
		PiTubG2	Gamma-tubulin-2
		PiTubG3	Gamma-tubulin-3
		PiTubG4	Gamma-tubulin-4
		PiTubG5	Gamma-tubulin-5
		PiTubG6	Gamma-tubulin-6
TPX2		PiTPX2	TPX2
Other filaments			
FtsZ/cryptic tubulin		PiFtsZ1	FtsZ1
		PiFtsZ2	FtsZ2
		PiFtsZ3	FtsZ3
striated MT-associated fibers		PiSFA1	SF-assemblin
MT+ end binding proteins			
EB1		PiEB1	microtubule -associated protein EB1
CLASP		PiCLASP	CLIP-associating protein
MOR1/MAP215		PiMOR1	microtubule organization 1
Katanin		PiKatp60-1	katanin p60 subunit
		PiKatp60-2	katanin p60 subunit
		PiKatp60-3	katanin p60 subunit
		PiKatp80	katanin p80 subunit
Motor proteins			
Kinesin	KIF 1	PiKIF1A	Kinesin Family Protein 1
	KIF 1	PiKIF1B	Kinesin Family Protein 1
	KIF 1	PiKIF1C	Kinesin Family Protein 1
	KIF 2	PiKIF2A	Kinesin Family Protein 2
	KIF 2	PiKIF2B	Kinesin Family Protein 2
	KIF 2	PiKIF2C	Kinesin Family Protein 2
	KIF 2	PiKIF2D	Kinesin Family Protein 2
	KIF 2	PiKIF2E	Kinesin Family Protein 2
	KIF 3	PiKIF3A	Kinesin Family Protein 3
	KIF 3	PiKIF3B	Kinesin Family Protein 3
	KIF 3	PiKIF3C	Kinesin Family Protein 3
	KIF 3	PiKIF3D	Kinesin Family Protein 3
	KIF 4/10	PiKIF4/10A	Kinesin Family Protein 4/10
	KIF 4/10	PiKIF4/10B	Kinesin Family Protein 4/10
	KIF 4/10	PiKIF4/10C	Kinesin Family Protein 4/10
	KIF 4/10	PiKIF4/10D	Kinesin Family Protein 4/10

Gene ID	Product description	Expression profile	Notes
PITG_07949	alpha-tubulin, putative	up in zsp	
PITG_07960	alpha-tubulin, putative	down in spor	
PITG_07961	cleavage induced tubulin alpha chain	up in zsp	
PITG_07996	alpha-tubulin	up in spor	
PITG_07999	alpha-tubulin, putative	up in spor	
PITG_00156	beta-tubulin	up in spor	
PITG_14807	tubulin gamma chain	up in myc	
PITG_01154	gamma-tubulin complex component, putative	down in spor	
PITG_11106	gamma-tubulin complex component, putative	down in spor	
PITG_00634	gamma-tubulin complex component 4, putative	down in spor/zsp	
PITG_18463	hypothetical protein	down in spor	
PITG_14022	conserved hypothetical protein	down in spor	
PITG_08093	conserved hypothetical protein	down in spor	
PITG_18788	tubulin/FtsZ family	up in myc	
PITG_19212	tubulin/FtsZ family protein, putative	down in spor	
PITG_00509	Putative uncharacterized protein; DELTA TUBULIN	up in myc	
PITG_01027	SF-assemblin, putative	up in zsp	
PITG_14584	microtubule -associated protein EB1	up in myc	
PITG_05233	CLIP-associating protein, putative	down in spor	
PITG_14441	cytoskeleton-associated protein, putative	up in gc	
PITG_12195	katanin p60 ATPase-containing subunit, putative	up in myc	
PITG_21068	katanin p60 ATPase-containing subunit A	up in spor	
PITG_23128	katanin p80 subunit	down in spor	
PITG_06132	katanin p60 ATPase-containing subunit, putative	up in zsp	
PITG_00204	kinesin heavy chain, putative	down in spor	ZZ-type Zinc finger
PITG_06859	kinesin-like protein	up in spor	
PITG_10881	kinesin-like protein	up in myc	
PITG_00111	kinesin-like protein	down in zsp	
PITG_03858	kinesin-like protein	down in spor	
PITG_08423	kinesin-like protein	up in zsp	
PITG_08458	kinesin-like protein	up in spor	
PITG_12987	kinesin-like protein	up in gc	
PITG_02343	kinesin-like protein	down in zsp	
PITG_02538	conserved hypothetical protein	up in zsp	
PITG_12262	kinesin-like protein	up in zsp	
PITG_12263	kinesin-like protein	up in zsp	
PITG_00152	kinesin-like protein	down in spor/zsp	
PITG_03064	kinesin-like protein	down in zsp	
PITG_20348	kinesin-like protein	up in gc	
PITG_20349	kinesin-like protein	down in spor	

Family	Subfamily	Proposed name	Proposed product description
	KIF 5	PiKIF5	Kinesin Family Protein 5
	KIF 6	PiKIF6A	Kinesin Family Protein 6
	KIF 6	PiKIF6B	Kinesin Family Protein 6
	KIF 7	PiKIF7A	Kinesin Family Protein 7
	KIF 7	PiKIF7B	Kinesin Family Protein 7
	KIF 7	PiKIF7C	Kinesin Family Protein 7
	KIF 8	PiKIF8	Kinesin Family Protein 8
	KIF 9	PiKIF9A	Kinesin Family Protein 9
	KIF 9	PiKIF9B	Kinesin Family Protein 9
	KIF 9	PiKIF9C	Kinesin Family Protein 9
	KIF 9	PiKIF9D	Kinesin Family Protein 9
	KIF 9	PiKIF9E	Kinesin Family Protein 9
	KIF 13	PiKIF13A	Kinesin Family Protein 13
	KIF 13	PiKIF13B	Kinesin Family Protein 13
	KIF 13	PiKIF13C	Kinesin Family Protein 13
	KIF 13	PiKIF13D	Kinesin Family Protein 13
	KIF 14	PiKIF14A	Kinesin Family Protein 14
	KIF 14	PiKIF14B	Kinesin Family Protein 14
	KIF 14	PiKIF14C	Kinesin Family Protein 14
	KIF 14	PiKIF14D	Kinesin Family Protein 14
	KIF 14	PiKIF14E	Kinesin Family Protein 14
	KIF 14	PiKIF14F	Kinesin Family Protein 14
	KIF 14	PiKIF14G	Kinesin Family Protein 14
	KIF 14	PiKIF14H	Kinesin Family Protein 14
	KIF 14	PiKIF14I	Kinesin Family Protein 14
	KIF 15	PiKIF15A	Kinesin Family Protein 15
	KIF 15	PiKIF15B	Kinesin Family Protein 15
	KIF 16	PiKIF16A	Kinesin Family Protein 16
	KIF 16	PiKIF16C	Kinesin Family Protein 16
	KIF 16	PiKIF16D	Kinesin Family Protein 16
	KIF 17	PiKIF17	Kinesin Family Protein 17
	KIF 19	PiKIF19	Kinesin Family Protein 19
	KIF 20	PiKIF20A	Kinesin Family Protein 20
	KIF 20	PiKIF20B	Kinesin Family Protein 20
	KIF 20	PiKIF20C	Kinesin Family Protein 20
	KIF 20	PiKIF20D	Kinesin Family Protein 20
	KIF X5	PiKIFX5A	Kinesin Family Protein X5
	KIF X5	PiKIFX5B	Kinesin Family Protein X5
	KIF X8	PiKIFX8	Kinesin Family Protein X8
	KIF X11	PiKIFX11	Kinesin Family Protein X11
	Kinesin Family Protein; ungrouped/orphan	PiKIForph1	Kinesin Family Protein
	Kinesin Family Protein; ungrouped/orphan	PiKIForph2	Kinesin Family Protein
Dynein	Light chain	PiDLC1	Dynein light chain
	Light chain	PiDLC2	Dynein light chain
	Light chain	PiDLC3	Dynein light chain
	Light chain	PiDLC4	Dynein light chain

Gene ID	Product description	Expression profile	Notes
PITG_00226	kinesin-like protein	down in spor	MFS domain
PITG_19553	conserved hypothetical protein	down in spor	
PITG_20287	kinesin-like protein	up in gc	Transmembrane domains
PITG_07125	kinesin-like protein	down in spor	Transmembrane domains
PITG_10520	kinesin-like protein	up in gc	
PITG_18579	kinesin-like protein	up in gc	
PITG_00860	kinesin-like protein	down in spor/zsp	
PITG_08424	kinesin-like protein	up in spor	
PITG_13923	kinesin-like protein	up in zsp	
PITG_14188	kinesin-like protein KIF6	up in spor	
PITG_15530	kinesin-like protein KIF9	up in zsp	
PITG_21476	conserved hypothetical protein		
PITG_03756	kinesin-like protein	up in myc	
PITG_06856	kinesin-like protein	up in myc	
PITG_15042	sporangia-induced kinesin-like protein	up in zsp	
PITG_16513	conserved hypothetical protein	up in spor	
PITG_00188	kinesin-like protein	down in spor	
PITG_00620	kinesin-like protein	up in zsp	
PITG_00666	kinesin-like protein	up in zsp	
PITG_03872	kinesin-like protein	down in spor	
PITG_08046	kinesin-like protein	up in spor	
PITG_09344	kinesin-like protein	up in zsp	
PITG_10514	kinesin-like protein	up in myc	
PITG_18624	kinesin-like protein	up in gc	
PITG_19351	kinesin-like protein	up in gc	
PITG_00078	kinesin-like protein	up in gc	
PITG_10859	kinesin-like protein	down in spor	
PITG_03657	kinesin-like protein	up in zsp	
PITG_19554	kinesin-like protein		
PITG_20283	kinesin-like protein	down in zsp	
PITG_02421	kinesin-like protein	up in spor	
PITG_08916	kinesin-like protein	up in spor	
PITG_01850	kinesin-like protein	down in spor	
PITG_03701	kinesin-like protein	up in myc	
PITG_04888	kinesin-like protein	down in spor	
PITG_06666	kinesin-like protein	up in zsp	
PITG_10474	hypothetical protein	up in zsp	
PITG_10475	kinesin-like protein	up in zsp	
PITG_05224	conserved hypothetical protein	up in gc	
PITG_12579	kinesin-like protein	down in spor/zsp	
PITG_11652	conserved hypothetical protein	up in gc	Oomcyete specific
PITG_03859	conserved hypothetical protein	up in zsp	Chromalveolate/Excavate specific
PITG_04721	Dynein light chain/pantothenate kinase	up in spor	
PITG_09030	dynein light chain, putative	up in spor	
PITG_16973	dynein light chain	up in spor	
PITG_04706	unspecified product		

Family	Subfamily	Proposed name	Proposed product description
	Light chain	PiDLC5	Dynein light chain
	Light chain, Tctex-1	PiTcTex-1-1	Dynein light chain Tctex-type
	Light chain, Tctex-1	PiTcTex-1-2	Dynein light chain Tctex-type
	Light chain, Tctex-1	PiTcTex-1-3	Dynein light chain Tctex-type
	Light chain, Tctex-1	PiTcTex-1-4	Dynein light chain Tctex-type
	Light chain, Tctex-1	PiTcTex-1-5	Dynein light chain Tctex-type
	Light chain, roadblock/LC7	PiLC7-1	Dynein light chain roadblock/LC7
	Light chain, roadblock/LC7	PiLC7-2	Dynein light chain roadblock/LC7
	Light chain, roadblock/LC7	PiLC7-3	Dynein light chain roadblock/LC7
	Light chain, roadblock/LC7	PiLC7-4	Dynein light chain roadblock/LC7
	Light chain, roadblock/LC7	PiLC7-5	Dynein light chain roadblock/LC7
	Intermediate chain	PiDIC1	Dynein intermediate chain
	Intermediate chain	PiDIC2	Dynein intermediate chain
	Intermediate chain	PiDIC3	Dynein intermediate chain
	Intermediate chain	PiDIC4	Dynein intermediate chain
	Heavy chain - DHC1	PiDHC1	Dynein heavy chain 1
	Heavy chain - DHC2	PiDHC2	Dynein heavy chain 2
	Heavy chain - DHC3	PiDHC3A	Dynein heavy chain 3A
	Heavy chain - DHC3	PiDHC3B	Dynein heavy chain 3B
	Heavy chain - DHC4	PiDHC4A	Dynein heavy chain 4A
	Heavy chain - DHC4	PiDHC4B	Dynein heavy chain 4B
	Heavy chain - DHC4	PiDHC4C	Dynein heavy chain 4C
	Heavy chain - DHC4	PiDHC4D	Dynein heavy chain 4D
	Heavy chain - DHC5	PiDHC5	Dynein heavy chain 5
	Heavy chain - DHC7	PiDHC6	Dynein heavy chain 6
	Heavy chain - DHC7	PiDHC7A	Dynein heavy chain 7A
	Heavy chain - DHC7	PiDHC7B	Dynein heavy chain 7B
	Heavy chain - DHC8	PiDHC8A	Dynein heavy chain 8A
	Heavy chain - DHC8	PiDHC8B	Dynein heavy chain 8B
	Heavy chain - DHC9	PiDHC9A	Dynein heavy chain 9A
	Heavy chain - DHC9	PiDHC9B	Dynein heavy chain 9B
	Heavy chain - DHC9	PiDHC9C	Dynein heavy chain 9C
	Heavy chain - DHC14	PiDHC14	Dynein heavy chain 14
	Heavy chain - DHC15	PiDHC15	Dynein heavy chain 15
	Heavy chain - DHC16	PiDHC16	Dynein heavy chain 16
Dynein regulatory complex protein			Sporangia Induced Dynein Regulatory Complex Protein
			Sporangia Induced Dynein Regulatory Complex Protein
Protein kinases			
			Cell division protein kinase 2
			Cell division protein kinase, putative
			Protein kinase
			Serine/threonine protein kinase
	Aurora kinase	PiAur-1	Aurora kinase 1
		PiAur-2	Aurora kinase 2
		PiAur-3	Aurora kinase 3
		PiAur-4	Aurora kinase 4

Gene ID	Product description	Expression profile	Notes
PITG_05682	Putative uncharacterized protein	up in spor	Truncated gene model
PITG_02342	conserved hypothetical protein	up in spor	
PITG_02108	dynein light chain-like protein	up in spor	
PITG_09704	dynein light chain Tctex-type, putative	down in zsp	
PITG_05518	hypothetical protein	down in zsp	
PITG_07793	Outer Dynein Arm Light Chain 2	up in spor	
PITG_08352	conserved hypothetical protein	up in spor	
PITG_16429	conserved hypothetical protein	up in spor	
PITG_18659	conserved hypothetical protein	up in spor	
PITG_09567	conserved hypothetical protein	up in spor	
PITG_12754	Dynein light chain 2B	up in spor	
PITG_01997	Dynein 1 light intermediate chain, putative	up in myc	
PITG_16492	conserved hypothetical protein	up in myc	
PITG_22517	dynein heavy chain	up in zsp	
PITG_19149	Putative uncharacterized protein	down in spor	
PITG_02526	dynein heavy chain	up in myc	
PITG_13968	dynein heavy chain	up in gc	
PITG_15967	dynein heavy chain, outer arm	up in myc	
PITG_05922	dynein heavy chain	down in zsp	
PITG_03423	dynein heavy chain	up in spor	
PITG_12577	sporangia induced dynein heavy chain	down in spor	
PITG_01852	dynein heavy chain	up in myc	
PITG_15625	dynein heavy chain	down in spor/zsp	
PITG_01717	dynein heavy chain	up in myc	
PITG_03180	dynein heavy chain	up in myc	
PITG_11437	axonemal dynein heavy chain	up in gc	
PITG_03488	dynein heavy chain	up in zsp	
PITG_03018	sporangia induced dynein heavy chain	down in spor	
PITG_01088	sporangia induced dynein heavy chain	down in spor	
PITG_01326	dynein heavy chain	up in myc	
PITG_08295	dynein heavy chain	down in spor	
PITG_00998	dynein heavy chain	up in myc	
PITG_03444	dynein heavy chain	up in zsp	Oomycete-specific
PITG_08507	Dynein heavy chain-like protein	up in myc	Oomycete-specific, corrected
PITG_17408	dynein heavy chain	up in myc	Oomycete-specific
PITG_17342	Sporangia Induced Dynein Regulatory Complex Protein	up in spor	
PITG_04697	Putative uncharacterized protein	up in zsp	
PITG_19450	Cell division protein kinase 2	up in myc	
PITG_18073	Cell division protein kinase, putative	down in spor	
PITG_19459	Protein kinase	down in spor	
PITG_11253	Serine/threonine protein kinase	up in spor	
PITG_05364	Putative uncharacterized protein	up in gc	
PITG_16977	Aurora-like protein kinase	down in spor	
PITG_05483	Protein kinase, putative	down in spor	
PITG_19456	Protein kinase, putative	down in spor	
PITG_00115	Protein kinase, putative	down in spor	

Family	Subfamily	Proposed name	Proposed product description
Tubulin assembly			
Chaperones		PiChap1	Tubulin-specific chaperone C, putative
		PiChap2	Tubulin-specific chaperone D, putative
		PiChap3	Putative uncharacterized protein
Polyglutamylases		PiPGS1	tubulin polyglutamylase, putative
		PiPGS2	tubulin polyglutamylase, putative
Tyrosine ligase		PiTTL1	tubulin-tyrosine ligase family
Interflagellar transport proteins			
		PiIFT20	Intraflagellar Transport Protein 20
		PiIFT22	Intraflagellar Transport Protein 22
		PiIFT25	Intraflagellar Transport Protein 25
		PiIFT27	Intraflagellar Transport Protein 27
		PiIFT43	Intraflagellar Transport Protein 43
		PiIFT46	Intraflagellar Transport Protein 46
		PiIFT52	Intraflagellar Transport Protein 52
		PiIFT57	Intraflagellar Transport Protein 57
		PiIFT72/74	Intraflagellar Transport Protein 72/74
		PiIFT80	Intraflagellar Transport protein 80
		PiIFT81	Intraflagellar Transport Protein 81
		PiIFT88	Intraflagellar Transport Protein 88
		PiIFT121	Intraflagellar Transport Protein 121
		PiIFT122	Intraflagellar Transport Protein 122
		PiIFT139	Intraflagellar Transport Protein 139
		PiIFT140	Intraflagellar Transport Protein 140
		PiIFT144	Intraflagellar Transport Protein 144
		PiIFT172	Intraflagellar transport protein 172
Kinetochore			
			centromere/kinetochore protein, putative
			conserved hypothetical protein
			kinetochore protein NUF2-like protein
			Kinetochore protein NDC80
			conserved hypothetical protein
			Voltage-gated Ion Channel (VIC) Superfamily
			Putative uncharacterized protein
			Mitotic checkpoint protein, putative
			Putative uncharacterized protein
			Putative uncharacterized protein
Centromere			
			conserved hypothetical protein
			conserved hypothetical protein
			conserved hypothetical protein
			conserved hypothetical protein
			conserved hypothetical protein

Gene ID	Product description	Expression profile	Notes
PITG_14614	Tubulin-specific chaperone C, putative	down in spor/zsp	
PITG_16797	Tubulin-specific chaperone D, putative	up in myc	
PITG_16735	Putative uncharacterized protein	up in spor	
PITG_02721	tubulin polyglutamylase, putative	up in zsp	
PITG_03077	tubulin polyglutamylase, putative	up in zsp	
PITG_08756	tubulin-tyrosine ligase family	up in spor	
PITG_06949	Intraflagellar Transport Protein 20	up in spor	
PITG_09137	Putative uncharacterized protein	up in spor	
PITG_04711	Putative uncharacterized protein	up in spor	
PITG_20749	Putative uncharacterized protein	up in spor	
PITG_11983	Putative uncharacterized protein	up in spor	
PITG_14226	Putative uncharacterized protein	up in spor	
PITG_20745	Intraflagellar Transport Protein 52	down in zsp	
PITG_16112	Intraflagellar Transport Protein 57	up in spor	
PITG_11472	Intraflagellar Transport Protein 72/74	up in spor	
PITG_18714	Intraflagellar Transport protein 80	up in spor	
PITG_06106	Intraflagellar Transport Protein 81	down in zsp	
PITG_10094	Intraflagellar Transport Protein 88	up in gc	
PITG_13766	WD repeat protein 35	up in spor	
PITG_10664	Intraflagellar Transport Protein 122	up in zsp	
PITG_10096	Putative uncharacterized protein	up in gc	
PITG_03309	Intraflagellar Transport Protein 140	up in spor	
PITG_18065	Putative uncharacterized protein	up in spor	
PITG_20212	Intraflagellar transport protein 172	up in spor	
PITG_00651	centromere/kinetochore protein, putative	up in myc	
PITG_03918	conserved hypothetical protein	up in gc	
PITG_05311	kinetochore protein NUF2-like protein	down in spor/zsp	
PITG_05567	Kinetochore protein NDC80	up in gc	
PITG_06914	conserved hypothetical protein	up in gc	
PITG_17081	Voltage-gated Ion Channel (VIC) Superfamily	up in myc	
PITG_15240	Putative uncharacterized protein	up in gc	
PITG_09827	Mitotic checkpoint protein, putative	down in spor/zsp	
PITG_10233	Putative uncharacterized protein	up in gc	
PITG_01293	Putative uncharacterized protein	down in spor	
PITG_06277	conserved hypothetical protein	up in gc	
PITG_09614	conserved hypothetical protein	up in gc	
PITG_11136	conserved hypothetical protein	down in zsp	
PITG_12723	conserved hypothetical protein	up in spor	
PITG_12840	conserved hypothetical protein	up in myc	

Family	Subfamily	Proposed name	Proposed product description
			conserved hypothetical protein
			conserved hypothetical protein
			conserved hypothetical protein
			Putative uncharacterized protein
Other MT-associated proteins			
MAP65			
RIB43a			
TRAF3IP			
WD-repeat			
Dynamin			

Table S5.4 | Details of augmin subunit encoding genes in oomycetes.

Gene ID	Product description	Organism	Length (aa)
ALNC14_022390	unspecified product	*Albugo laibachii*	285
H257_11484	hypothetical protein	*Aphanomyces astaci*	315
H310_06484	hypothetical protein	*Aphanomyces invadans*	303
PAG1_G011123	hypothetical protein	*Pythium aphanidermatum*	173
PIR_G010251	unspecified product	*Pythium irregulare*	309
PIW_G008869	unspecified product	*Pythium iwayamai*	120
PVE_G008681	unspecified product	*Pythium vexans*	273
PYU1_G003699	unspecified product	*Pythium ultimum*	120
SDRG_08716	hypothetical protein	*Saprolegnia diclina*	293
SPRG_19876	hypothetical protein	*Saprolegnia parasitica*	293

TABLE S5.5 | Primers used in this study.

Name	Target gene	Sequence (5' - 3')
PITG_07960_NotI_F	PITG_07960	GTGCGGCCGCAGGCGCGCCTCGTGAAATTCTCTCCATTCACCTCGGC
PITG_07960_AscI_R	PITG_07960	ACGATGGCGCGCCCAGCACGCAAAATGCTTAGTACTCCTC
PITG_07999_NotI_F	PITG_07999	GTGCGGCCGCAGGCGCGCCTCGTGAGGTCATCTCCATCCACC
PITG_07999_AscI_R	PITG_07999	ACGATGGCGCGCCGAGTCTGCCTAGTACTCCTCGC

Gene ID	Product description	Expression profile	Notes
PITG_12841	conserved hypothetical protein	up in zsp	
PITG_15175	conserved hypothetical protein	up in myc	
PITG_17861	conserved hypothetical protein	up in spor	
PITG_14021	Putative uncharacterized protein	up in spor	
PITG_01921	conserved hypothetical protein	down in spor	
PITG_02163	RIB43a flagellar protofilament ribbon protein	up in spor	
PITG_19387	TRAF3-interacting protein, putative	up in myc	
PITG_10084	Putative uncharacterized protein	up in spor	
PITG_12594	TRAF3-interacting protein, putative	down in spor/zsp	
PITG_11403	WD domain-containing protein	up in myc	
PITG_00797	WD domain-containing protein	down in zsp	
PITG_13618	WD repeat protein pop3	down in spor/zsp	
PITG_11454	Dynamin	up in spor	
PITG_00183	Dynamin-2	down in spor	
PITG_08837	Interferon-induced GTP-binding protein Mx	up in zsp	

Chapter 6

General discussion

The overall aim of this thesis was to explore and identify unique features in the cytoskeleton of *Phytophthora* spp., with the long-term goal to identify potential targets for disease control. For studying the actin cytoskeleton, we have mainly focussed on *Phytophthora infestans* and for studying the microtubule cytoskeleton we used both *P. infestans* and *Phytophthora palmivora*. The research presented in this thesis shows the strength of live cell imaging and the added value of fluorescent tags to label the cytoskeleton. In this chapter, the main results are discussed. I frame my work by discussing related studies and provide a comprehensive overview of studies that have assessed the effect of cytoskeleton interacting drugs on oomycetes. Finally, I discuss recent developments and prospects for disease control based on the results presented in this thesis.

6.1 The oomycete actin cytoskeleton

The actin cytoskeleton is conserved in all eukaryotic kingdoms and plays a role in various cellular processes. In oomycetes it has been shown that the actin cytoskeleton is essential for cell growth and viability (Bachewich & Heath 1998, Deora et al 2008a, Ketelaar et al 2012, Yu et al 2004), but as yet, there are many unknows about its precise functions and configurations in these organisms. Besides actin, a subset of actin binding proteins (ABPs) is conserved in oomycetes (Meijer et al 2014), but this does not necessarily mean that upstream and downstream pathways and associated networks are conserved. This is exemplified by the unique higher-order actin configurations that we identified in *Phytophthora* spp. as presented in this thesis (**chapters 2**, **3** and **4**) and summarized below in 6.1.2. Although the precise functions of these unique configurations and the regulatory pathways that control their formation remain largely elusive, I will integrate our findings and suggest potential functions of the actin cytoskeleton in *Phytophthora* spp., including potential regulatory pathways.

Drugs that affect the oomycete actin cytoskeleton

Several classes of drugs that interfere with the actin cytoskeleton have been reported and are commonly used in research for functional studies (Kustermans et al 2008). Using these drugs to discover the function and activity of the actin cytoskeleton in oomycetes can provide us with valuable information and shine a light on the fundamental functioning of these organisms. As stated above actin is a protein that is highly conserved across kingdoms and therefore targeting the actin cytoskeleton with general broad spectrum actin interacting drugs, makes the interpretation in plant-pathogen interaction studies challenging. After all, the drug will affect the actin cytoskeleton in both, the host and the pathogen. In the host the actin cytoskeleton plays a crucial role in cellular defence processes by targeting delivery of defence-related compounds and cell wall reinforcements to the site of attempted penetration (Hardham 2007, Schmidt & Panstruga 2007). To distinguish between the effects

of actin interacting drugs on pathogen growth and viability and defence responses of the host, one would need drugs that specifically target either the pathogen or the host. However, to date no drugs have been identified that specifically target actin or ABPs in oomycetes. Nevertheless, actin interacting drugs are suitable tools to study the functions of the actin cytoskeleton in *in vitro* cultured oomycetes as shown in studies performed in different oomycete species (**table 6.1**).

TABLE 6.1 | Actin interacting drugs studied in oomycetes.

Group	Compound	Tested on oomycetes	Concentration used	References
Cytochalasins	Cytochalasin D	*Phytophthora* spp.	20 - 200 µM	Evidente et al 1997
	Cytochalasin D	*Phytophthora cinnamomi*	10 - 100 µM	Hyde & Hardham 1993
	Cytochalasin D	*Saprolegnia ferax*	5 - 20 µg/ml	Harold & Harold 1992
	Cytochalasin E	*Saprolegnia ferax*	5 - 10 µg/ml	Harold & Harold 1992
	Cytochalasin B	*Saprolegnia ferax*	5 - 25 µg/ml	Harold & Harold 1992
Latrunculins	Latrunculin B	*Aphanomyces cochlioides*	0.005 - 10 µg/ml	Deora et al 2008a, Deora et al 2010, Islam 2008, Islam & Fukushi 2010
	Latrunculin B	*Phytophthora infestans*	0.1 - 10 µM	Bronkhorst et al 2021, Ketelaar et al 2012, Meijer et al 2014
	Latrunculin B	*Plasmopara viticola*	1-1000 nM	Riemann et al 2002
	Latrunculin B	*Pythium aphanidermatum*	0-5 ug/6mm disc	Deora et al 2008b, Deora et al 2010
	Latrunculin B	*Saprolegnia ferax*	0.5 - 1.3 µM	Bachewich & Heath 1998, Gupta & Heath 1997, Heath et al 2000
Other	Phalloidin	Actin immunolabelling		**See table 1.2**
	Jasplakinolide	None known		

Broadly used actin interacting drugs that have been applied in oomycetes are latrunculin B and cytochalasin D (**table 6.1**). Several isoforms of both drugs are available, differing slightly from each other in attached side groups. Effectiveness of cytochalasin B, D and E was tested on the oomycetes *Saprolegnia ferax* and *Achlya bisexualis* but apart from variations in effective concentrations no substantial differences were found (Heath & Harold 1992). Both cytochalasins and latrunculins are potent polymerization inhibitors and application leads to actin depolymerization. However, their mode of action differs. Latrunculins bind to actin monomers and prevent their incorporation into F-actin (Spector et al 1989) and cytochalasins prevent actin polymerization by binding to the barbed-ends of actin filaments to inhibit incorporation of actin monomers (Miller et al 1999). Both drugs have a similar, concentration dependent effect on hyphae in oomycetes; normal hyphal growth is interrupted, the hyphal morphology is abnormal, cell wall deposition is disturbed and there is a delocalization of actin-linked organelles (Bachewich & Heath 1998, Deora et al 2008a, Deora et al 2010, Ketelaar et al 2012).

Unlike the polymerization inhibitors latrunculin and cytochalasin, jasplakinolide and phalloidin are drugs that prevent depolymerization and stabilize actin filaments (Inman & Crews 1989). Yet, there are no publications describing the effects of actin stabilizing drugs in oomycetes. However, as part of his MSc thesis project Maarten Walraven obtained preliminary data showing the effects of jasplakinolide on the actin cytoskeleton in *P. infestans* over time. We have applied this drug to a Lifeact-GFP expressing *P. infestans* and monitored the consequences on actin organization and dynamics. **Movie S6.1** shows that during jasplakinolide treatment actin cables obtain a more prominent appearance compared to mock treated hyphae. Over a time frame of at least 24 h after application of 100 nM jasplakinolide, hyphae continued to grow, and the formation of new actin cables in the subapical part of the hypha suggested that actin polymerization continued indicating the sustained availability of G-actin for polymerization (M. Walraven and K. Kots, unpublished data). Remarkably, actin cables were more prominent during jasplakinolide treatment while actin plaques were absent from the whole tip region and less numerous in the distal areas (**movie S6.1**), suggesting that actin stabilization leads to a preferential polymerization of actin cables. Treatments with the actin depolymerizing drug latrunculin B, resulted in the opposite response: an increased prominence of actin plaques and less actin cables when compared to untreated hyphae (**chapter 4**, **figure 4.2**). In contrast to the latrunculin treatment, where hyphal top morphology becomes irregular, the jasplakinolide treated hyphae continued to grow normally. This supports the hypothesis that actin cables play a role in supporting hyphal growth. Although the findings solely rely on drug treatments without further experimental validation and quantification of intensities of the indirect actin probe Lifeact are notoriously complicated, they suggest that interference with actin turnover can alter the preference for polymerization of plaques or cables pointing to a possible feedback loop between both actin configurations. Like jasplakinolide, phalloidin is an actin interacting drug that stabilizes filamentous actin. In oomycete research phalloidin is so far only used as a marker for F-actin by linking it to a fluorophore (**table 1.2**), thereby enabling visualization of the actin cytoskeleton in previously fixed cells. Since these studies depend on fixation, they only provide a static image of the actin cytoskeleton and do not provide information about actin dynamics. In **chapter 1** I have presented the findings of studies in oomycetes using rhodamine-phalloidin immunolabelling.

Another drug that was thought to target the *Phytophthora* actin cytoskeleton is flumorph, a compound that is used as an agrochemical to control oomycetes (Zhu et al 2007). In our experiments however, live cell imaging of a Lifeact-GFP expressing *P. infestans* line treated with flumorph did not show any disturbance of the actin configurations in hyphae, even at effective concentrations (**chapter 4**). Hence, despite being a potent anti-oomycete drug, flumorph should not be classified as an actin interacting drug.

Unique actin configurations in *Phytophthora* spp.

Live cell imaging using Lifeact-GFP expressing *P. infestans* lines revealed several oomycete specific configurations of the *Phytophthora* actin cytoskeleton not observed before (**chapter 2** and **3**, Bronkhorst et al 2021, Bronkhorst et al 2022, Meijer et al 2014).

The first actin configuration that was recognized as being oomycete specific is the actin plaque. Cortical actin dots were first observed in static images of oomycete hyphae published in the 1990's (Harold & Harold 1992, Kaminskyj & Heath 1994, Temperli 1990) and were initially thought to have a function in facilitating endocytosis, similar to the function of actin patches in fungi. However, live cell imaging revealed major differences in lifetime and dynamics between plaques and patches, making it unlikely for these structures both fulfil a function in endocytosis (Meijer et al 2014). Almost 10 years after stating that oomycete actin plaques are unique structures with unknown function, we are still in the dark about their exact function. Recent findings however, including those described in this thesis, do favour certain hypotheses over others. In Meijer et al (2014), we hypothesized that actin plaques could function as actin organizing centres by scaffolding actin cables. In certain instances, we observed multiple surrounding cables connected to plaques, forming an interlinked network (figure S7 in Meijer et al 2014). In this thesis I found a putative link between actin plaques and the plasma membrane cell wall continuum that supports this scaffolding hypothesis. In protoplasts that lack a cell wall, the actin plaques display more cortical movement and appear less stable than those in hyphae that do have a cell wall. It would be of immense value to know the proteins involved in the recruitment and maintenance of these actin structures. Many APBs, proteins forming an indispensable part of the actin cytoskeleton, have proven to be kingdom or even species specific, tailoring the actin cytoskeleton to specific lifestyle dependent functions. Examples are proteins in the Networked (NET) superfamily in higher plants (Deeks et al 2012) and spectrins that evolved with the metazoans (Baines 2009). Since many ABPs are indispensable and vital for the correct functioning of the actin cytoskeleton, they are interesting targets for further study. The actin binding Arp2/3 complex is a known actin nucleator involved in actin branching, and based on the punctate structure of plaques, it would be a logical candidate to be involved in actin plaque formation. As part of his MSc thesis project, Joram Westera studied the Arp2/3 complex in *P. infestans*. Genome and transcriptome mining showed that the genes encoding the subunits are present and expressed in *P. infestans*. We attempted to silence the single copy *ARP3* gene but were unsuccessful in establishing transient silencing or obtaining stably silenced transformants. As alternative, we attempted to target the Arp2/3 complex with CK-666, which is a known Arp2/3 specific drug successfully used in animals and yeast (Nolen et al 2009). This drug was also shown to interfere indirectly with a kinase partner protein (KPP) potentially interacting with Arp2/3 in pollen tubes of tomato (*Solanum lycopersicum*) (Liu et al 2020) and to disturb the movement of the amoeba *Naegleria* (Velle and Fritz-Laylin, 2020) suggesting that CK-666 also targets Arp2/3 in these organisms. Whether this drug has any effect on *P. infestans* Arp2/3 is unknown, but in our experiments, we did not observe any growth defects upon

treatment with CK-666. Moreover, the drug did not appear to significantly affect the actin organization in Lifeact–GFP expressing *P. infestans* (J. Westera and K. Kots, unpublished results). It is important to realize that there are no actin plaques present in the growing tip of a healthy hypha. It is therefore unlikely that actin plaques are directly involved in tip growth, and this is supported by the finding that upon treatment with jasplakinolide hyphae lacking plaques were still able to grow (M. Walraven and K. Kots, unpublished data). Potentially, a role of plaques in scaffolding actin cables could optimize the efficiency of long distance transport processes by aligning actin cables. It is worth though to further investigate this because of the presumed role of long-distance transport in sporangia production and energy management within the hypha.

The second actin configuration that we encountered in *P. infestans* is associated with cell wall plugs in germ tubes. When germ tubes emerging from cysts of *P. infestans* were followed over time, we observed the formation of so-called cell wall plugs (**chapter 2**; Kots et al 2017). These plugs are not formed in germ tubes emerging from multi-nuclear sporangia, but only in those emerging from single-nuclear cysts. The cell wall plugs in *Phytophthora* differ from septa in fungi, as they completely seal the distal part of the hypha after retraction of the cytoplasm to the proximal part of the hypha. We hypothesized that these cell wall plugs extend the growth range of the tip in nutrient depleted environments, as it does only have to maintain the growing tip and no longer the cytoplasm depleted cyst and base of the hypha. During the formation of the cell wall plug, we found actin to be associated with the extending edge of the cell wall plug. Some germ tubes can even make several of these cell wall plugs, keeping the apical part cytoplasm-rich, while the more basal compartments appear devoid of cytoplasm. Close observation showed a small amount of cytoplasm being left behind in the largely empty compartment adjacent to the cell wall plug. As there is no nucleus in this compartment, it can be assumed that this small leftover will degrade over time and is therefore sacrificed in order to complete the cell wall plug formation, cutting off the distal compartment. Because of this expensive sacrifice of cytoplasm, it is safe to assume that the formation of the cell wall plug is very important for the germinating cyst. It would be interesting to find out more about this process and the proteins involved. Also, what would be the effect on infection if this process cannot take place.

The third unique actin configuration described in this thesis is the actin aster. The apical actin aster that we observed in hyphal tips spatially correlates with a site of attempted penetration either on glass cover slips or on plant tissue (**chapter 2**). Spotting actin asters during plant infection is challenging and it is even more challenging to capture the events in micrographs because of plant tissues being auto fluorescent or too voluminous. Our study was also limited by the fact that the cover slips used in our experimental set up (**box 1.1**; **chapter 1**) are inaccessible for the hyphae; they cannot penetrate the surface of the cover slips. Bronkhorst et al (2021) followed up on this observation by using polydimethylsiloxane (PDMS) substrates as a model surface. PDMS is transparent, hydrophobic and has elastic moduli that match leaf stiffnesses (Gibson 2012, Onoda et al 2015). When cysts were germinated on a thin

layer of PDMS, the hyphal tips were able to successfully penetrate the surface. As such, PDMS microlayers are ideal cell wall mimics for microscopic analysis of penetration events. The elegant work of Bronkhorst et al (2021) showed that *Phytophthora* spp. use a different penetration strategy than that previously reported for the rice blast fungus *Magnaporthe oryzae* (Rocha et al 2020, Wilson & Talbot 2009). *M. oryzae* uses a brute force approach: it forms a fortified appressorium to build up turgor pressures up to 8 mPa (Howard et al 1991, Wilson & Talbot 2009). While adhering to the host surface (Rocha et al 2020), at the centre of the appressorium a penetration peg is formed, perpendicular to the plant cell wall, piercing the host surface (Ryder et al 2019). In **chapter 2**, we already mentioned that key components driving this infection mechanism such as septins and melanin are missing in *Phytophthora*; their genomes do not contain genes encoding either septins or enzymes for melanin biosynthesis (Chumley & Valent 1990, Wang et al 2020, Wheeler & Bell 1988). Rather than forming an appressorium and penetration peg, *Phytophthora* hyphae consistently indent and invade their host at a distinct oblique angle, of around 45 degrees (Bronkhorst et al 2021). Oblique indentation, also referred to as slicing in fracture mechanics, can facilitate surface fracture by localizing stresses at the surface and generating substantial tensile stresses (Reyssat et al 2012). This penetration mechanism is referred to as 'naifu' invasion, after the Japanese kitchen knives that exploit a similar slicing strategy. Thus, even though the oomycete *Phytophthora* species and true fungi have convergently evolved to penetrate their host surface, they use different strategies to do so.

We hypothesized previously that the actin aster may be involved in targeting and delivering exocytotic vesicles to the site of penetration (**chapter 2**). Recently, a new role of the actin aster was demonstrated. Contact mechanics dictate that pressing a hypha into a surface of equal or larger stiffness under large indentation forces leads to tip flattening (Geitmann & Dumais 2009). This tip flattening is not compatible with the naifu invasion mechanism since a sharp hyphal tip is required to localize stresses to the intended entry point and prevents the loss of mechanical energy to the deformation of the pathogen itself. A sharp hyphal tip is essential for efficient naifu invasion just as a blunt knife cannot be used to create cuts. Bronkhorst et al (2022) reported an actin-based mechanostat that resolves this mechanical conflict. When a hypha is mechanically stimulated, actin rapidly accumulates at the site of mechanical contact. Results presented in **chapter 3** of this thesis, including the effects of laser ablation in hyphae and the local perturbation of hyphae with a microinjection needle and our observations of a penetration attempt on a dead cell, support this hypothesis. Using PDMS cell wall mimics, the appearance of the actin aster, could be spatiotemporally linked to penetration events. When combined with local force measurements, Bronkhorst et al (2022) were able to demonstrate a local and quantitative feedback between actin remodelling and mechanical stress. Using a mechanical modelling approach, they were able to show that the adaptive mechanical actin scaffold is of sufficient stiffness to match the level of stress during indentation and penetration to prevent tip deformation. The actin mechanostat feedback mechanism allows the hyphal tip to remain malleable and at the same time localize force to achieve host penetration.

6.2 The oomycete microtubule cytoskeleton

Microtubules are, like actin filaments conserved throughout eukaryotic kingdoms. Phylogenetic analyses of eukaryotic microbes that diverged early in the evolution revealed a conserved and complete set of microtubule cytoskeleton components (Gottschalk & Hefti 2022). In addition, the role of microtubules in some cellular processes is conserved throughout eukaryotes such as positioning the chromosomes during mitosis and facilitating the motility of flagella and cilia (Mitchell 2007). In addition to these conserved functions, microtubules perform kingdom-specific functions. In plants for example, they control the growth direction of intercalary growing cells by guiding the deposition of cellulose microfibrils, the load bearing structures of plant cell walls (Ehrhardt & Shaw 2006, Lindeboom et al 2013, Wasteneys 2002), while in *Toxoplasma gondii* microtubules, present as cortical arrays along the cell parameters are, together with actin filaments, involved in the intrinsic movement of this protozoan pathogen (Stadler et al 2017). The microtubule cytoskeleton in Stramenopiles has received little attention; so far, the studies are limited to the microtubule organization in a few diverse photosynthetic Stramenopiles and some oomycete species (De Martino et al 2009, Katsaros et al 2006, Tesson & Hildebrand 2010, Tsirigoti et al 2013). In diatoms there is some evidence that microtubules are involved in the positioning of the silica deposition vesicles and are therefore important for correct cell wall deposition (Tesson & Hildebrand 2010). In brown algae, microtubules are reported to radiate from microtubule organizing centres (MTOCs) and there is some evidence that in these organisms, microtubules are important for maintaining intracellular polarity cell (Katsaros et al 2006). Like actin that has dynamic interactions with ABPs, microtubule dynamics and organization are under control of a plethora of proteins, collectively referred to as Microtubule Associated Proteins (MAPs). Using a bioinformatics approach, we identified conserved MAPs in *Phytophthora* as a first step to gain insight in the cellular networks that potentially control microtubule organization in oomycetes (**chapter 5**).

Drugs that affect the oomycete microtubule cytoskeleton

Just like the actin cytoskeleton, most information about the oomycete microtubule cytoskeleton has been obtained by visualization using immunocytochemistry (see **table 1.2)**, and by studying the effects of inhibitors (**table 6.2**). As with the actin interacting drugs one can divide the microtubule interacting drugs in two classes, one class promoting polymerization and stabilization of the microtubule cytoskeleton and the other promoting depolymerization and instability of the microtubule cytoskeleton.

The taxanes, among which taxol, belong to the first class. Studies in oomycetes using taxanes (Hansen et al 2000, Koo et al 2009, Mu et al 1999, Wagner & Flores 1994, Young et al 1992) mainly looked at the growth reduction caused by taxol, with a focus on disease

control and without studying the direct effect on the microtubule cytoskeleton. Young et al (1992) observed that the number of nuclei present per cell decreased with increasing taxol concentrations, showing an inhibition of mitosis caused by taxol. While taxol has little or no effect on the fungi *Pestalotiopsis microspora*, *Aspergillus* sp. and *Fusarium* sp., most oomycetes tested did show sensitiveness to the drug (Mu et al 1999, Wagner & Flores 1994). An exception is *Phytophthora lateralis,* which is a natural pathogen on pacific yew (*Taxus brevifolia*; Hansen et al 2000).

Drugs in the class that causes depolymerization of the microtubule cytoskeleton have successfully been used as pesticides and formed an interesting target for research. Examples that have been tested in oomycetes (**table 6.2**) are quinoline (Lamberth et al 2014), oryzalin (Wilcox 1996), and the benzamides zarilamide (Young 1991) and zoxamide (Young & Slawecki 2001). They all cause severe growth defects in the oomycetes tested and can be considered potent oomicides. Moreover, as observed in *Phytophthora cinnamomi,* oryzalin treatment can prevent segregation of vesicles within the sporangial cortex leading to an abnormal polarization and disturbed zoosporogenesis (Hyde & Hardham 1993). In hyphae of *Saprolegnia ferax*, microtubule depolymerization does slow down growth, however it does not lead to obvious growth abnormalities, and it was therefore hypothesized that microtubules have an indirect role in tip morphogenesis and polarity (Heath et al 2000, Hyde & Heath 1995). Since microtubule depolymerisation blocks nuclear division, and hence the hypha cannot increase the number of nuclei to sustain a growth, it is obvious that application of microtubule depolymerizing drugs slows down hyphal growth.

Since most known microtubule inhibiting drugs will also affect the host plant, their use as agrochemical for disease control in crops is out of the question. Notably oryzalin is commonly used as herbicide, killing off plants without affecting humans and nearby animals (Strachan & Hess 1983). In a search for oomycete specific microtubule interacting compounds, Lee et al (2019) used a phage display method to identify inhibitory peptides with high affinity against *P. capsici* tubulins. This led to the identification of a peptide with a strong growth inhibitory effect at concentrations much lower than that of benomyl, another microtubule interacting drug that is often used as a fungicide. Also, the peptide showed higher specificity for oomycete tubulin in comparison to human tubulin, a feature that seems promising for the development of more species-specific inhibitory drugs.

TABLE 6.2 | Microtubule interacting drugs studied in oomycetes.

Group	Compound	Tested on oomycetes	Concentration used	References
Benzimidazole carbamates	Benomyl	*Phytophthora capsici*	50 - 1000 µM	Koo et al 2009
	Benomyl	*Phytophthora* spp.	-	Kato et al 2013, Vatchev & Maneva 2012
	Benomyl	*Pythium* spp.	-	Kato et al 2013, Vatchev & Maneva 2012
	Benomyl	*Phytophthora infestans*	-	Abdel-Fattah & Baka 2000, Groves & Ristaino 2000, Temperli et al 1991
	Benomyl	*Phytophthora cactorum*	-	Lederer et al 1992
	Carbendazim	*Phytophthora capsici*	MIC value of 7.81 µg/mL	Tian et al 2017
	Methyl benzimidazole-2-yl carbamate (MBC)	*Saprolegnia ferax*	5.2 µM (1 µg/ml)	Heath et al 2000
	Thiabendazole (TBZ)	*Pythium ultimum*	IC50 270±350 µM	Mu et al 1999
Benzamide	Zarilamide	*Phytophthora capsici*	25 µM	Young 1991
	Zoxamide	*Phytophthora capsici*	0.5 ppm	Young & Slawecki 2001
Taxanes	Cephalomannine	*Phytophthora* spp.	10 µM	Wagner & Flores 1994
	Cephalomannine	*Pythium* spp.	10 µM	Wagner & Flores 1994
	Taxol (Paclitaxel)	*Aphanomyces cochlioides*	0.4 - 10 µM	Young et al 1992
	Taxol (Paclitaxel)	*Phytophthora lateralis*	*	Hansen et al 2000
	Taxol (Paclitaxel)	*Phytophthora capsici*	0.4 - 100 µM	Koo et al 2009, Young 1991
	Taxol (Paclitaxel)	*Pythium ultimum*	0.1 - 10 µM	Mu et al 1999
Other	Colchicine	*Phytophthora capsici*	10 - 100 µM	Koo et al 2009
	Colchicine	*Phytophthora infestans*	0.01%	Ritch & Daggett 1995
	Cryptophycin	*Phytophthora cambivora*	**	Biondi et al 2004
	Cryptophycin	*Phytophthora cinnamomi*	**	Biondi et al 2004
	Oryzalin	*Phytophthora cactorum*	0.0625 - 4.0 µg/ml	Wilcox 1996
	Oryzalin	*Phytophthora cambivora*	0.0625 - 4.0 µg/ml	Wilcox 1996
	Oryzalin	*Phytophthora cryptogea*	0.0625 - 4.0 µg/ml	Wilcox 1996
	Oryzalin	*Phytophthora megasperma*	0.0625 - 4.0 µg/ml	Wilcox 1996
	Oryzalin	*Phytophthora cinnamomi*	0.1-1 µM	Hyde & Hardham 1993
	Nocodazole	*Saprolegnia ferax*	3.3 µM (1 µg/ml)	Heath et al 2000, Hyde & Heath 1995
	Nocodazole	*Phytophthora infestans*	10^{-4} M	Temperli et al 1991
	Quinolin-6-yloxyacetamides (QA's)	*Phytophthora infestans*	60 ppm	Lamberth et al 2014
	Ethyl-N-phenyl-carbamate (EPC)	*Plasmopara viticola*	1-200 µM	Riemann et al 2002

* *Phytophthora lateralis* is able to grow on pacific yew; concentration of taxol is not mentioned in the reference

** Strains grown in presence of *Nostoc* sp. which produces cryptophycin; concentration not mentioned in the reference

Microtubule configurations in *Phytophthora* spp.

As described in the introduction (**chapter 1**) all studies that have been performed on the oomycete tubulin cytoskeleton prior to this thesis are based on immunolabeling using fixed, dead material. By generating *P. palmivora* lines expressing fluorescently tagged tubulin, we could visualize the tubulin cytoskeleton by live cell imaging and were able to time mitosis and to link microtubule organization to putative functions. In line with earlier work on *Phytophthora* species using microtubule immunocytochemistry on fixed cells (Hardham 1987, Hyde & Hardham 1993, Ketelaar et al 2012, Temperli et al 1991, Temperli 1990), we demonstrated how microtubules are organized in the spindle (**chapter 5**). Since mitosis in *Phytophthora* species is of the closed type, i.e., the nuclear envelope does not break down during mitosis (Heath 1980), and mitosis does not occur simultaneously in all nuclei, one might speculate that the nuclear membrane plays a role in sequestering the cell cycle regulating machinery in individual nuclei. After completion of the mitotic process, the two daughter nuclei remain connected via microtubules while the internuclear distance rapidly increases. Since the microtubules originate from centrioles based on the nuclear membranes, it is likely that their minus ends are associated with the centrioles and their plus ends extend away from the nuclei (Tran et al 2001; **chapter 5**). Plus ends from microtubules that emerge from two daughter nuclei after segregation remain associated to each other during their segregation (**chapter 5**). In other organisms from diverse evolutionary kingdoms, it has been shown that the conserved microtubule bundling protein Ase1/PRC1/MAP65 is recruited specifically to antiparallel overlaps (Loïodice et al 2005). In our inventory of MAPs in *P. infestans* we identified a single copy gene encoding this protein (**chapter 5**). The antiparallel overlaps decorated with the Ase1/PRC1/MAP65 protein allow kinesin-based microtubule sliding to occur as observed in yeast (Janson et al 2007) and mammalian mitosis (Harper & Brooks 2005). In the moss *Physcomitrium patens*, it was shown that these overlaps are essential for scaffolding cell plate formation and recruitment of a vesicle fusion machinery (de Keijzer et al 2017, Tang et al 2019). Thus, the observed microtubule connections between nuclei in *Phytophthora* are likely to represent antiparallel microtubules that control internuclear spacing. To test this hypothesis, fluorescent tagging of Ase1/PRC1/MAP65 and silencing or knocking out the encoding gene would be key experiments.

These observations raise the question of whether microtubules can generate sufficient force to space nuclei. Firstly, microtubules exposed to compressive, lateral forces respond by buckling when forces are in the piconewton range (Dogterom & Yurke 1997). We observed microtubule buckling, suggesting that lateral compressive forces are exerted on the microtubules in *Phytophthora* hyphae. Interestingly, we did not only observe buckling of internuclear microtubules, but also of microtubules that reach into the hyphal tip from the most apical nucleus, suggesting that microtubules may also function in retaining nuclei from the tip. Using a combined imaging and modelling approach, Janson et al (2007) showed that in the fission yeast *Schizosaccharomyces pombe*, force generation by microtubule polymerization is sufficient to position the nucleus to the centre of the cell. Since the

nucleus positions the cytokinetic machinery in this organism, nuclear positioning is essential for producing equally sized daughter cells. By using cells expressing heat sensitive CDC11, Teapal et al (2021) were able to generate multinucleated *S. pombe* cells that resemble the multicellular hyphae of *Phytophthora*. In these cells, nuclei were equidistantly spaced by microtubule generated forces, suggesting that microtubule-based mechanisms could be sufficient to position nuclei in *Phytophthora*. By studying nuclear spacing in hyphae with disrupted microtubule cytoskeleton, this hypothesis can be tested.

6.3 Conclusions and prospects

In this thesis, we demonstrate the value of live cell imaging in understanding the cytoskeleton of *Phytophthora* pathogens. We describe previously unknown configurations including features that appear to be unique for oomycetes. Our work on the microtubule cytoskeleton allowed us to generate new hypotheses on nuclear positioning in oomycetes that should be tested. Disruption of nuclear positioning in hyphae may have limited consequences on the viability of oomycetes, but during zoosporogenesis this disruption would have major impact. Detailed knowledge about the players that control microtubule organization may open new avenues for identifying novel potential oomicide targets.

Our studies on the actin cytoskeleton lay the foundation for a novel way of regarding oomycete plant infection as demonstrated by the recently published follow-up studies mentioned above (Bronkhorst et al 2021, Bronkhorst et al 2022). Besides being able to uncover a role for the actin aster, these follow-up studies nicely demonstrate the strength of interdisciplinary research to address long standing questions in the phytopathology field. As a next step, it would be immensely fascinating to identify the molecular mechanisms that underly force sensing and the subsequent machinery that transduces this signal to activate the actin polymerization machinery. Two different approaches seem to be the way forward here. Firstly, mutate or delete genes encoding known ABPs that may be involved in actin aster assembly using recently developed CRISPR/Cas strategies (Ah-Fong et al 2021, Fang & Tyler 2016). This strategy could be combined with searches for interactors, for example by proximity labelling, pull-downs of protein complexes or yeast two hybrid screening. Alternatively, a bioinformatics-based screening strategy to identify candidate mechanoreceptors could be employed, followed by functional characterization e.g., via disruption or mutation of the encoded genes, complementation studies or biomechanical assays. Since the actin mechanostat is at the heart of the naifu invasion mechanism and has not been identified in organisms other than *Phytophthora*, it may be an ideal target to consider when designing novel strategies for controlling oomycete plant pathogens. Altogether, such studies would increase our understanding of the infection biology of oomycete pathogens and support the development of sustainable strategies to control oomycete plant diseases. The multidisciplinary environment at Wageningen University and Research is an ideal setting for future research in this direction.

6.4 Supplemental material

MOVIE S6.1 | shows confocal fluorescence time series of hypha treated with 100 nM jasplakinolide visualized in the Lifeact-GFP-expressing *P. infestans* strain. The time interval per frame is 15 seconds. Scale bar is 10 µm.

References

Abdel-Fattah GM, Baka ZAM. 2000. The effect of benomyl on growth and ultrastructure of two isolates of *Phytophthora infestans* from Egypt. Microbiological Research 155: 243-48

Aghamohammadzadeh S, Ayscough KR. 2010. The yeast actin cytoskeleton and its function in endocytosis. Fungal Biology Reviews 24: 37-46

Ah-Fong AMV, Judelson HS. 2011. Vectors for fluorescent protein tagging in *Phytophthora*: tools for functional genomics and cell biology. Fungal Biology 115: 882-90

Ah-Fong AMV, Boyd AM, Matson MEH, Judelson HS. 2021. A Cas12a-based gene editing system for *Phytophthora infestans* reveals monoallelic expression of an elicitor. Molecular Plant Pathology 22: 737-52

Akhmanova A, Steinmetz MO. 2015. Control of microtubule organization and dynamics: two ends in the limelight. Nature Reviews Molecular Cell Biology 16: 711-26

Ali I, Yang WC. 2020. The functions of kinesin and kinesin-related proteins in eukaryotes. Cell Adhesion & Migration 14: 139-52

Anthony RG, Waldin TR, Ray JA, Bright SW, Hussey PJ. 1998. Herbicide resistance caused by spontaneous mutation of the cytoskeletal protein tubulin. Nature 393: 260-3

Ashraf MA, Facette M. 2020. Plant biology: BASL gives the plant nucleus a sense of direction. Current Biology 30: 1375-R77

Bachewich C, Heath IB. 1998. Radial F-actin arrays precede new hypha formation in *Saprolegnia*: implications for establishing polar growth and regulating tip morphogenesis. Journal of Cell Science. 111: 2005-16

Badreddine I, Lafitte C, Heux L, Skandalis N, Spanou Z, et al. 2008. Cell wall chitosaccharides are essential components and exposed patterns of the phytopathogenic oomycete *Aphanomyces euteiches*. Eukaryotic Cell 7: 1980-93

Baines AJ. 2009. Evolution of spectrin function in cytoskeletal and membrane networks. Biochemical Society Transactions 37: 796-803

Bakthavatsalam D, Meijer HJG, Noegel AA, Govers F. 2006. Novel phosphatidylinositol phosphate kinases with a G-protein coupled receptor signature are shared by *Dictyostelium* and *Phytophthora*. Trends in Microbiology 14: 378-82

Baldauf SL. 2003. The deep roots of eukaryotes. Science 300: 1703-06

Balint EE, Petres J, Szabo M, Orban CK, Szilagyi L, Abraham B. 2013. Fluorescence of a histidine-modified enhanced green fluorescent protein (EGFP) effectively quenched by copper(II) ions. Journal of Fluorescence 23: 273-81

Berepiki A, Lichius A, Read ND. 2011. Actin organization and dynamics in filamentous fungi. Nature Reviews Microbiology 9: 876-87

Bibikova TN, Blancaflor EB, Gilroy S. 1999. Microtubules regulate tip growth and orientation in root hairs of *Arabidopsis thaliana*. Plant Journal 17: 657-65

Biondi N, Piccardi R, Margheri MC, Rodolfi L, Smith GD, Tredici MR. 2004. Evaluation of *Nostoc* strain ATCC 53789 as a potential source of natural pesticides. Applied and Environmental Microbiology 70: 3313-20

Blum M, Boehler M, Randall EVA, Young V, Csukai M, et al. 2010. Mandipropamid targets the cellulose synthase-like PiCesA3 to inhibit cell wall biosynthesis in the oomycete plant pathogen, *Phytophthora infestan*s. Molecular Plant Pathology 11: 227-43

Bodakuntla S, Jijumon AS, Villablanca C, Gonzalez-Billault C, Janke C. 2019. Microtubule-associated proteins: Structuring the cytoskeleton. Trends in Cell Biology 29: 804-19

Boddy L. 2016. Chapter 8 - Pathogens of autotrophs. In: Watkinson SC, Boddy L, Money NP (eds) The Fungi (Third Edition): 245-92. Boston: Academic Press

Bouwmeester K, van Poppel PMJA, Govers F. 2009. Genome biology cracks enigmas of oomycete plant pathogens In Annual plant reviews: Molecular aspects of plant disease resistance, ed. J Parker, 102-34. New Jersey, US: Wiley-Blackwell

Bouwmeester K. 2010. The interplay between a *Phytophthora* RXLR effector and an *Arabidopsis* lectin receptor kinase. (Doctoral thesis, Wageningen University, Wageningen, the Netherlands). ISBN 978-90-8585-647-4

Bronkhorst J, Kasteel M, van Veen S, Clough JM, Kots K, et al. 2021. A slicing mechanism facilitates host entry by plant-pathogenic *Phytophthora*. Nature Microbiology 6: 1000-06

Bronkhorst J, Kots K, De Jong D, Kasteel M, Van Boxmeer T, et al. 2022. An actin mechanostat ensures hyphal tip sharpness in *Phytophthora infestans* to achieve host penetration. Science Advances 8(23), eab00875.

Burki F, Roger AJ, Brown MW, Simpson AGB. 2020. The new tree of eukaryotes. Trends in Ecology & Evolution 35: 43-55

Butler EE, Erwin DC, Bartnicki-Garcia S, Tsao PH. 1983. *Phytophthora*: its biology, taxonomy, ecology, and pathology. Mycologia 76(2):380

Cai M, Lin D, Chen L, Bi Y, Xiao L, Liu X-l. 2015. M233I Mutation in the β-tubulin of *Botrytis cinerea* confers resistance to zoxamide. Scientific Reports 5: 16881-81

Capella-Gutierrez S, Silla-Martinez JM, Gabaldon T. 2009. trimAl: a tool for automated alignment trimming in large-scale phylogenetic analyses. Bioinformatics 25: 1972-3

Caten CE, Jinks JL. 1968. Spontaneous variability of single isolates of *Phytophthora infestans*. Cultural Variation. Canadian Journal of Botany 46: 329-48

Chen L, Zhu S, Lu X, Pang Z, Cai M, Liu X. 2012. Assessing the risk that *Phytophthora melonis* can develop a point mutation (V1109L) in CesA3 conferring resistance to carboxylic acid amide fungicides. PLOS One 7: e42069

Chitcholtan K, Garrill A. 2005. A beta 4 integrin-like protein co-localises with a phosphotyrosine containing protein in the oomycete *Achlya bisexualis*: Inhibition of tyrosine phosphorylation slows tip growth. Fungal Genetics and Biology 42: 534-45

Chitcholtan K, Harris E, Yu YP, Harland C, Garrill A. 2012. An investigation into plasmolysis in the oomycete *Achlya bisexualis* reveals that membrane-wall attachment points are sensitive to peptides containing the sequence RGD and that cell wall deposition can occur despite retraction of the protoplast. Canadian Journal of Microbiology 58: 1212-20

Chumley FG, Valent B. 1990. Genetic analysis of melanin-deficient, nonpathogenic mutants of *Magnaporthe grisea*. Molecular Plant-microbe Interactions 3: 135-43

Cohen Y, Coffey MD. 1986. Systemic fungicides and the control of oomycetes. Annual Review of Phytopathology 24: 311-38

Dagdas YF, Yoshino K, Dagdas G, Ryder LS, Bielska E, et al. 2012. Septin-mediated plant cell invasion by the rice blast fungus, *Magnaporthe oryzae*. Science 336: 1590-95

De Keijzer J, Kieft H, Ketelaar T, Goshima G, Janson ME. 2017. Shortening of microtubule overlap regions defines membrane delivery sites during plant cytokinesis. Current Biology 27: 514-20

De Martino A, Amato A, Bowler C. 2009. Mitosis in diatoms: rediscovering an old model for cell division. BioEssays 31: 874-84

De Souza CP, Osmani SA. 2007. Mitosis, not just open or closed. Eukaryotic Cell 6: 1521-7

Deeks MJ, Calcutt JR, Ingle EK, Hawkins TJ, Chapman S, et al. 2012. A superfamily of actin-binding proteins at the actin-membrane nexus of higher plants. Current Biology 22: 1595-600

Delgado-Alvarez DL, Callejas-Negrete OA, Gomez N, Freitag M, Roberson RW, et al. 2010. Visualization of F-actin localization and dynamics with live cell markers in *Neurospora crassa*. Fungal Genetics and Biology 47: 573-86

Deora A, Hashidoko Y, Tahara S. 2008a. Actin filaments predominate in morphogenic cell stages, whereas plaques predominate in non-morphogenic cell stages in Peronosporomycetes. Mycological Research 112: 868-82

Deora A, Hashidoko Y, Tahara S. 2008b. Antagonistic effects of *Pseudomonas jessenii* against *Pythium aphanidermatum*: morphological, ultrastructural and cytochemical aspects. Journal of Basic Microbiology 48: 71-81

Deora A, Hatano E, Tahara S, Hashidoko Y. 2010. Inhibitory effects of furanone metabolites of a rhizobacterium, *Pseudomonas jessenii*, on phytopathogenic *Aphanomyces cochlioides* and *Pythium aphanidermatum*. Plant Pathology 59: 84-99

Desai A, Mitchison TJ. 1997. Microtubule polymerization dynamics. Annual Review of Cell and Developmental Biology 13: 83-117

Dogterom M, Yurke B. 1997. Measurement of the force-velocity relation for growing microtubules. Science 278: 856-60

Doonan JH, Cove DJ, Lloyd CW. 1988. Microtubules and microfilaments in tip growth: evidence that microtubules impose polarity on protonemal growth in *Physcomitrella patens*. J. Cell Sci. 89: 533-40

Dumas C, Knox RB. 1983. Callose and determination of pistil viability and incompatibility. Theoretical and Applied Genetics 67: 1-10

Edgar LA, Zavortink M. 1983. The mechanism of diatom locomotion. II. Identification of actin. Proceedings of the Royal Society Series B-Biological Sciences 218: 345-48

Edzuka T, Yamada L, Kanamaru K, Sawada H, Goshima G. 2014. Identification of the augmin complex in the filamentous fungus *Aspergillus nidulans*. PLOS One 9: e101471

Ehrhardt DW, Shaw SL. 2006. Microtubule dynamics and organization in the plant cortical array. Annual Review Plant Biology 57: 859-75

Engelbrecht J, Van den Berg N. (2013). Expression of defence-related genes against *Phytophthora cinnamomi* in five avocado rootstocks. South African Journal of Science 109(11-12).

Erickson HP. 2007. Evolution of the cytoskeleton. BioEssays 29: 668-77

Esseling-Ozdoba A, Houtman D, Lammeren AAM, Eiser E, Emons AMC. 2008. Hydrodynamic flow in the cytoplasm of plant cells. Journal of Microscopy 231: 274-83

Evans NA, Hoyne PA, Stone BA. 1984. Characteristics and specificity of the interaction of a fluorochrome from aniline blue (sirofluor) with polysaccharides. Carbohydrate Polymers 4: 215-30

Evidente A, Cristinzio G, Capasso R, Andolfi A. 1997. Fungitoxic activity of some cytochalasins and their derivatives on *Phytophthora* species. Natural Toxins 5: 228-33

Fang YF, Tyler BM. 2016. Efficient disruption and replacement of an effector gene in the oomycete *Phytophthora sojae* using CRISPR/Cas9. Molecular Plant Pathology 17: 127-39

Fischer R, Zekert N, Takeshita N. 2008. Polarized growth in fungi - interplay between the cytoskeleton, positional markers and membrane domains. Molecular Microbiology 68: 813-26

Freitag J, Lanver D, Boehmer C, Schink KO, Boelker M, Sandrock B. 2011. Septation of infectious hyphae is critical for appressoria formation and virulence in the smut fungus *Ustilago Maydis*. PLOS Pathogens (5): e1002044

Fry W. 2008. *Phytophthora infestans*: the plant (and R gene) destroyer. Molecular Plant Pathology 9: 385-402

Gardiner J. 2013. The evolution and diversification of plant microtubule-associated proteins. Plant Journal 75: 219-29

Geitmann A, Dumais J. 2009. Not-so-tip-growth. Plant Signal & Behavior 4: 136-38

Gibbon BC, Kovar DR, Staiger CJ. 1999. Latrunculin B has different effects on pollen germination and tube growth. Plant Cell 11: 2349-63

Gibeaux R, Politi AZ, Philippsen P, Nedelec F. 2017. Mechanism of nuclear movements in a multinucleated cell. Molecular Biology of the Cell 28: 645-60

Gibson LJ. 2012. The hierarchical structure and mechanics of plant materials. Journal of The Royal Society Interface 9: 2749-66

Gladfelter A, Berman J. 2009. Dancing genomes: fungal nuclear positioning. Nature Reviews Microbiology 7: 875-86

Goode BL, Drubin DG, Barnes G. 2000. Functional cooperation between the microtubule and actin cytoskeletons. Current Opinion Cell Biology 12: 63-71

Goodson HV, Dzurisin JS, Wadsworth P. 2010. Methods for expressing and analyzing GFP-tubulin and GFP-microtubule-associated proteins. Cold Spring Harbor Protocols 2010(9): pdb.top85

Gottschalk AC, Hefti MM. 2022. The evolution of microtubule associated proteins – a reference proteomic perspective. BMC Genomics 23: 266

Govers F, Gijzen M. 2006. *Phytophthora* genomics: The plant destroyers' genome decoded. Molecular Plant-Microbe Interactions 19: 1295-301

Govers F. 2001. Misclassification of pest as 'fungus' puts vital research on wrong track. Nature 411: 633-33

Grenville-Briggs LJ, Anderson VL, Fugelstad J, Avrova AO, Bouzenzana J, et al. 2008. Cellulose synthesis in *Phytophthora infestans* is required for normal appressorium formation and successful infection of potato. Plant Cell 20: 720-38

Grenville-Briggs LJ, Avrova AO, Bruce CR, Williams A, Whisson SC, et al. 2005. Elevated amino acid biosynthesis in *Phytophthora infestans* during appressorium formation and potato infection. Fungal Genetics and Biology 42: 244-56

Grenville-Briggs LJ, Avrova AO, Hay RJ, Bruce CR, Whisson SC, van West P. 2010. Identification of appressorial and mycelial cell wall proteins and a survey of the membrane proteome of *Phytophthora infestans*. Fungal Biology 114: 702-23

Groves CT, Ristaino JB. 2000. Commercial fungicide formulations induce in vitro oospore formation and phenotypic change in mating type in *Phytophthora infestans*. Phytopathology 90: 1201-08

Gupta GD, Heath IB. 1997. Actin disruption by latrunculin B causes turgor-related changes in tip growth of *Saprolegnia ferax* hyphae. Fungal Genetics and Biology 21: 64-75

Haas BJ, Kamoun S, Zody MC, Jiang RH, Handsaker RE, et al. 2009. Genome sequence and analysis of the Irish potato famine pathogen *Phytophthora infestans*. Nature 461: 393-8

Hansen EM, Goheen DJ, Jules ES, Ullian B. 2000. Managing Port-Orford-cedar and the introduced pathogen *Phytophthora lateralis*. Plant Disease 84(1): 4-14

Hardham AR, Takemoto D, White RG. 2008. Rapid and dynamic subcellular reorganization following mechanical stimulation of Arabidopsis epidermal cells mimics responses to fungal and oomycete attack. BMC Plant Biology 8(63)

Hardham AR. 1987. Microtubules and the flagellar apparatus in zoospores and cysts of the fungus *Phytophthora cinnamomi*. Protoplasma 137: 109-24

Hardham AR. 2007. Cell biology of plant-oomycete interactions. Cellular Microbiology 9: 31-39

Hardham AR. 2009. The asexual life cycle in oomycete genetics and genomics: diversity, interactions and research tools, ed. K Lamour, S Kamoun, 93-119. Oxford: Wiley-Blackwell

Harold RL, Harold FM. 1992. Configuration of actin microfilaments during sporangium development in *Achlya bisexualis* - comparison of two staining protocols. Protoplasma 171: 110-16

Harper JV, Brooks G. 2005. The mammalian cell cycle in cell cycle control: mechanisms and protocols, ed. T Humphrey, G Brooks, 113-53. Totowa, NJ: Humana Press

Harrington BJ, Hageage GJ. 2003. Calcofluor white: a review of its uses and applications in clinical mycology and parasitology. Laboratory Medicine 34: 361-67

Haverkort AJ, Boonekamp PM, Hutten R, Jacobsen E, Lotz LAP, et al. 2008. Societal costs of late blight in potato and prospects of durable resistance through cisgenic modification. Potato Research 51: 47-57

Heath IB, Greenwood AD. 1968. Electron microscopic observations of dividing somatic nuclei in *Saprolegnia*. Journal of General Microbiology 53: 287-89

Heath IB, Greenwood AD. 1970. Centriole replication and nuclear division in *Saprolegnia*. Journal of General Microbiology 62: 139-48

Heath IB, Gupta G, Bai S. 2000. Plasma membrane-adjacent actin filaments, but not microtubules, are essential for both polarization and hyphal tip morphogenesis in *Saprolegnia ferax* and *Neurospora crassa*. Fungal Genetics and Biology 30: 45-62

Heath IB, Harold RL. 1992. Actin has multiple roles in the formation and architecture of zoospores of the oomycetes, *Saprolegnia ferax* and *Achlya bisexualis*. Journal of Cell Science 102: 611-27

Heath IB, Kaminskyj SGW. 1989. The organization of tip-growth-related organelles and microtubules revealed by quantitative-analysis of freeze-substituted oomycete hyphae. Journal of Cell Science 93: 41-52

Heath IB, Rethoret K, Moens PB. 1984. The ultrastructure of mitotic spindles from conventionally fixed and freeze-substituted nuclei of the fungus *Saprolegnia*. European Journal of Cell Biology 35: 284-95

Heath IB. 1980. Variant mitosis in lower eukaryotes - indicators of the evolution of mitosis. International Review of Cytology-a Survey of Cell Biology 64: 1-80

Heikal AA, Hess ST, Webb WW. 2001. Multiphoton molecular spectroscopy and excited-state dynamics of enhanced green fluorescent protein (EGFP): acid–base specificity. Chemical Physics 274: 37-55

Hijmans RJ, Forbes GA, Walker TS. 2000. Estimating the global severity of potato late blight with GIS-linked disease forecast models. Plant Pathology 49: 697-705

Horio T, Murata T. 2014. The role of dynamic instability in microtubule organization. Frontiers in Plant Science 5: 511-11

Howard RJ, Ferrari MA, Roach DH, Money NP. 1991. Penetration of hard substrates by a fungus employing enormous turgor pressures. PNAS 88: 11281-84

Hu JY, Liu C, Yan H. 2008. Degradation of flumorph in soils, aqueous buffer solutions, and natural waters. Journal of Agricultural and Food Chemistry 56: 8574-79

Hua C, Kots K, Ketelaar T, Govers F, Meijer HJG. 2015. Effect of flumorph on F-Actin dynamics in the potato late blight pathogen *Phytophthora infestans*. Phytopathology 105: 419-23

Hua C, Meijer HJG, de Keijzer J, Zhao W, Wang Y, Govers F. 2013. GK4, a G-protein-coupled receptor with a phosphatidylinositol phosphate kinase domain in *Phytophthora infestans*, is involved in sporangia development and virulence. Molecular Microbiology 88: 352-70

Hugdahl JD, Morejohn LC. 1993. Rapid and reversible high-affinity binding of the dinitroaniline herbicide oryzalin to tubulin from *Zea mays* L. Plant Physiology 102: 725-40

Hussey PJ, Ketelaar T, Deeks MJ. 2006. Control of the actin cytoskeleton in plant cell growth. Annual Review of Plant Biology 57: 109-25

Hyde GJ, Hardham AR. 1992. Confocal microscopy of microtubule arrays in cryosectioned sporangia of *Phytophthora cinnamomi*. Experimental Mycology 16: 207-18

Hyde GJ, Hardham AR. 1993. Microtubules regulate the generation of polarity in zoospores *of Phytophthora cinnamomi*. European Journal of Cell Biology 62: 75-85

Hyde GJ, Heath IB. 1995. Ca^{2+}-dependent polarization axis establishment in the tip-growing organism, *Saprolegnia ferax*, by gradients of the ionophore a23187. European Journal of Cell Biology 67: 356-62

Inman W, Crews P. 1989. Novel marine sponge-derived amino acids. 8. Conformational analysis of jasplakinolide. Journal of the American Chemical Society 111: 2822-29

Ishikawa-Ankerhold HC, Muller-Taubenberger A. 2019. Actin assembly states in *Dictyostelium discoideum* at different stages of development and during cellular stress. The International Journal of Developmental Biology 63: 417-27

Islam MT, Fukushi Y. 2010. Growth inhibition and excessive branching in *Aphanomyces cochlioides* induced by 2,4-diacetylphloroglucinol is linked to disruption of filamentous actin cytoskeleton in the hyphae. World Journal of Microbiology & Biotechnology 26: 1163-70

Islam MT. 2008. Dynamic rearrangement of F-actin organization triggered by host-specific plant signal is linked to morphogenesis of *Aphanomyces cochlioides* zoospores. Cell Motility and the Cytoskeleton 65: 553-62

Jackson SL, Hardham AR. 1998. Dynamic rearrangement of the filamentous actin network occurs during zoosporogenesis and encystment in the oomycete *Phytophthora cinnamomi*. Fungal Genetics and Biology 24: 24-33

Janson ME, Loughlin R, Loïodice I, Fu C, Brunner D, et al. 2007. Crosslinkers and motors organize dynamic microtubules to form stable bipolar arrays in fission yeast. Cell 128: 357-68

Jones P, Binns D, Chang HY, Fraser M, Li W, et al. 2014. InterProScan 5: genome-scale protein function classification. Bioinformatics 30: 1236-40

Judelson HS, Blanco FA. 2005. The spores of *Phytophthora*: weapons of the plant destroyer. Nature Reviews Microbiology 3: 47-58

Judelson HS, Shrivastava J, Manson J. 2012. Decay of genes encoding the oomycete flagellar proteome in the downy mildew *Hyaloperonospora arabidopsidis*. PLOS ONE 7(10): e47624

Kaksonen M, Sun Y, Drubin DG. 2003. A pathway for association of receptors, adaptors, and actin during endocytic internalization. Cell 115: 475-87

Kaminskyj SGW, Heath IB. 1994. A comparison of techniques for localizing actin and tubulin in hyphae of *Saprolegnia ferax*. Journal of Histochemistry & Cytochemistry. 42: 523-30

Kamoun S, Furzer O, Jones JDG, Judelson HS, Ali GS, et al. 2015. The top 10 oomycete pathogens in molecular plant pathology. Molecular Plant Pathology 16: 413-34

Kara M, Oztas E, Ramazanoğulları R, Kouretas D, Nepka C, et al. 2020. Benomyl, a benzimidazole fungicide, induces oxidative stress and apoptosis in neural cells. Toxicology Reports 7: 501-09

Kato M, Minamida K, Tojo M, Kokuryu T, Hamaguchi H, Shimada S. 2013. Association of *Pythium* and *Phytophthora* with pre-emergence seedling damping-off of soybean grown in a field converted from a paddy field in Japan. Plant Production Science 16: 95-104

Katoh K, Standley DM. 2013. MAFFT multiple sequence alignment software version 7: improvements in performance and usability. Molecular Biology and Evolution 30: 772-80

Katsaros C, Karyophyllis D, Galatis B. 2003. F-actin cytoskeleton and cell wall morphogenesis in brown algae. Cell Biology International 27: 209-10

Katsaros C, Karyophyllis D, Galatis B. 2006. Cytoskeleton and morphogenesis in brown algae. Annals of Botany 97: 679-93

Keeling PJ, Burki F. 2019. Progress towards the tree of eukaryotes. Current Biology 29: R808-r17

Ketelaar T, Faivre-Moskalenko C, Esseling JJ, de Ruijter NCA, Grierson CS, et al. 2002. Positioning of nuclei in *Arabidopsis* root hairs: An actin-regulated process of tip growth. Plant Cell 14: 2941-55

Ketelaar T, Meijer HJG, Spiekerman M, Weide R, Govers F. 2012. Effects of latrunculin B on the actin cytoskeleton and hyphal growth in *Phytophthora infestans*. Fungal Genetics and Biology 49: 1014-22

Ketelaar T. 2013. The actin cytoskeleton in root hairs: all is fine at the tip. Current Opinion in Plant Biology 16: 749-56

Koestler SA, Rottner K, Lai F, Block J, Vinzenz M, Small V. 2009. F- and G-Actin concentrations in lamellipodia of moving cells. PLOS ONE 4(3): e4810

Kollmar M. 2016. Fine-tuning motile cilia and flagella: evolution of the dynein motor proteins from plants to humans at high resolution. Molecular Biology and Evolution 33: 3249-67

Konam JK, Guest DI. 2004. Role of beetles (Coleoptera: Scolytidae and Nitidulidae) in the spread of *Phytophthora palmivora* pod rot of cocoa in Papua New Guinea. Australasian Plant Pathology 33: 55-59

Koo B-S, Park H, Kalme S, Park H-Y, Han JW, et al. 2009. Alpha- and beta-tubulin from *Phytophthora capsici* KACC 40483: molecular cloning, biochemical characterization, and antimicrotubule screening. Applied Microbiology and Biotechnology 82: 513-24

Koonin EV. 2010. The incredible expanding ancestor of eukaryotes. Cell 140: 606-08

Koornneef M, Hanhart CJ, Martinelli L. 1987. A genetic-analysis of cell-culture traits in tomato. Theoretical and Applied Genetics 74: 633-41

Kortekamp A. 2005. Growth, occurrence and development of septa in *Plasmopara viticola* and other members of the Peronosporaceae using light- and epifluorescence-microscopy. Mycological Research 109: 640-48

Kots K, Meijer HJG, Bouwmeester K, Govers F, Ketelaar T. 2017. Filamentous actin accumulates during plant cell penetration and cell wall plug formation in *Phytophthora infestans*. Cellular and Molecular Life Sciences 74: 909-20

Kramer R, Freytag S, Schmelzer E. 1997. In vitro formation of infection structures of *Phytophthora infestans* is associated with synthesis of stage specific polypeptides. European Journal of Plant Pathology 103: 43-53

Kroon L, Brouwer H, de Cock A, Govers F. 2012. The genus *Phytophthora* anno 2012. Phytopathology 102: 348-64

Krtková J, Benáková M, Schwarzerová K. 2016. Multifunctional microtubule-associated proteins in plants. Frontiers in plant science 7: 474-74

Kustermans G, Piette J, Legrand-Poels S. 2008. Actin-targeting natural compounds as tools to study the role of actin cytoskeleton in signal transduction. Biochemical Pharmacology 76: 1310-22

Lamberth C, Kessabi FM, Beaudegnies R, Quaranta L, Trah S, et al. 2014. Synthesis and fungicidal activity of quinolin-6-yloxyacetamides, a novel class of tubulin polymerization inhibitors. Bioorganic & Medicinal Chemistry 22: 3922-30

Laporte D, Courtout F, Pinson B, Dompierre J, Salin B, et al. 2015. A stable microtubule array drives fission yeast polarity reestablishment upon quiescence exit. Journal of Cell Biology 210: 99-113

Latijnhouwers M, de Wit PJGM, Govers F. 2003. Oomycetes and fungi: similar weaponry to attack plants. Trends in Microbiology 11: 462-69

Lederer W, Lorenz KH, Seemuller E. 1992. Studies on antagonistic effects of *Trichoderma* isolates against *Phytophthora cactorum*. Journal of Phytopathology 136: 154-64

Lee SC, Kim SH, Hoffmeister RA, Yoon MY, Kim SK. 2019. Novel peptide-based inhibitors for microtubule polymerization in *Phytophthora capsici*. International Journal of Molecular Sciences 20: 11

Lee SC, Ristaino JB, Heitman J. 2012. Parallels in intercellular communication in oomycete and fungal pathogens of plants and humans. PLOS Pathogens 8: e1003028

Letunic I, Doerks T, Bork P. 2015. SMART: recent updates, new developments and status in 2015. Nucleic Acids Research 43: D257-60

Levesque CA. 2011. Fifty years of oomycetes-from consolidation to evolutionary and genomic exploration. Fungal Diversity 50: 35-46

Levina NN, Heath IB, Lew RR. 2000. Rapid wound responses of *Saprolegnia ferax* hyphae depend upon actin and Ca^{2+}-involving deposition of callose plugs. Protoplasma 214: 199-209

Lichius A, Berepiki A, Read ND. 2011. Form follows function - The versatile fungal cytoskeleton. Fungal Biology 115: 518-40

Lindeboom JJ, Nakamura M, Hibbel A, Shundyak K, Gutierrez R, et al. 2013. A mechanism for reorientation of cortical microtubule arrays driven by microtubule severing. Science 342: 1245533

Liu H-K, Li Y-J, Wang S-J, Yuan T-L, Huang W-J, et al. 2020. Kinase partner protein plays a key role in controlling the speed and shape of pollen tube growth in tomato. Plant Physiology 184: 1853-69

Liu W, Li Z, Zhang Z, Liu C. 2000. Antifungal activity and prospect of flumorph and its mixtures. Zhejiang Chemical Industry 31: 87-8

Liu ZY, Persson S, Sanchez-Rodriguez C. 2015. At the border: the plasma membrane-cell wall continuum. Journal of Experimental Botany 66: 1553-63

Loïodice I, Staub J, Setty TG, Nguyen N-PT, Paoletti A, Tran PT. 2005. Ase1p organizes antiparallel microtubule arrays during interphase and mitosis in fission yeast. Molecular Biology of the Cell 16: 1756-68

Lord EM, Holdaway-Clarke T, Roy SJ, Jauh GY, Hepler PK. 2000. Arabinogalactan-proteins in pollen tube growth. In: Nothnagel E.A., Bacic A., Clarke A.E. (eds) Cell and Developmental Biology of Arabinogalactan-Proteins: 152-67. Springer, Boston, MA.

Lu R, Drubin DG, Sun Y. 2016. Clathrin-mediated endocytosis in budding yeast at a glance. Journal of Cell Science 129: 1531-36

Lucas JR, Courtney S, Hassfurder M, Dhingra S, Bryant A, Shaw SL. 2011. Microtubule-associated proteins MAP65-1 and MAP65-2 positively regulate axial cell growth in etiolated *Arabidopsis* hypocotyls. The Plant Cell 23: 1889-903

Lv Z, de-Carvalho J, Telley IA, Großhans J. 2021. Cytoskeletal mechanics and dynamics in the *Drosophila* syncytial embryo. Journal of Cell Science 134

Matuszak JM, Fernandez-Elquezabal J, Gu WK, Villarreal-Gonzalez M, Fry WE. 1994. Sensitivity of *Phytophthora infestans* populations to metalaxyl in Mexico: distribution and dynamics. Plant Disease 78: 911-16

McCarthy CGP, Fitzpatrick DA. 2017. Phylogenomic reconstruction of the oomycete phylogeny derived from 37 genomes. mSphere 2(2): e00095-17

McHau GRA, Coffey MD. 1994. Isozyme diversity in *Phytophthora palmivora*: evidence for a southeast Asian centre of origin. Mycological Research 98: 1035-43

Meijer HJG, Govers F. 2006. Genomewide analysis of phospholipid signaling genes in *Phytophthora* spp.: novelties and a missing link. Molecular Plant Microbe Interactions 19: 1337-47

Meijer HJG, Hua C, Kots K, Ketelaar T, Govers F. 2014. Actin dynamics in *Phytophthora infestans*; rapidly reorganizing cables and immobile, long-lived plaques. Cellular Microbiology 16: 948-61

Meijer HJG, van de Vondervoort PJ, Yin QY, de Koster CG, Klis FM, et al. 2006. Identification of cell wall-associated proteins from *Phytophthora ramorum*. Molecular Plant-Microbe Interactions 19: 1348-58

Melida H, Sandoval-Sierra JV, Dieguez-Uribeondo J, Bulone V. 2013. Analyses of extracellular carbohydrates in Oomycetes unveil the existence of three different cell wall types. Eukaryotic Cell 12: 194-203

Miller DD, de Ruijter NCA, Bisseling T, Emons AMC. 1999. The role of actin in root hair morphogenesis: studies with lipochito-oligosaccharide as a growth stimulator and cytochalasin as an actin perturbing drug. Plant Journal 17: 141-54

Miller MA, Pfeiffer W, Schwartz T. 2010. Creating the CIPRES Science Gateway for inference of large phylogenetic trees. Gateway Computing Environments Workshop 2010: 1-8

Mitchell DR. 2007. The evolution of eukaryotic cilia and flagella as motile and sensory organelles. Advances in Experimental Medicine and Biology 607: 130-40

Mitchison TJ, Salmon ED. 2001. Mitosis: a history of division. Nature Cell Biology 3: E17-E21

Moseley JB, Goode BL. 2006. The yeast actin cytoskeleton: from cellular function to biochemical mechanism. Microbiology and Molecular Biology Reviews 70: 605-45

Mu JH, Bollon AP, Sidhu RS. 1999. Analysis of beta-tubulin cDNAs from taxol-resistant *Pestalotiopsis microspora* and taxol-sensitive *Pythium ultimum* and comparison of the taxol-binding properties of their products. Molecular and General Genetics 262: 857-68

Muralidhar A, Swadel E, Spiekerman M, Suei S, Fraser M, et al. 2016. A pressure gradient facilitates mass flow in the oomycete Achlya bisexualis. Microbiology 162: 206-13

Nagata T, Nemoto Y, Hasezawa S. 1992. Tobacco BY-2 cell line as the "HeLa" cell in the cell biology of higher plants. International Review of Cytology-a Survey of Cell Biology 132: 1-30

Nolen BJ, Tomasevic N, Russell A, Pierce DW, Jia Z, et al. 2009. Characterization of two classes of small molecule inhibitors of Arp2/3 complex. Nature 460: 1031-U121

Nowicki M, Lichocka M, Nowakowska M, Kłosińska U, Kozik EU. 2012. A simple dual stain for detailed investigations of plant-fungal pathogen interactions. Vegetable Crops Research Bulletin: 61-74

Ochoa JC, Herrera M, Navia M, Romero HM. 2019. Visualization of *Phytophthora palmivora* infection in oil palm leaflets with fluorescent proteins and cell viability markers. Plant Pathology Journal 35: 19-31

Odronitz F, Kollmar M. 2006. Pfarao: a web application for protein family analysis customized for cytoskeletal and motor proteins (CyMoBase). BMC Genomics 7: 300

Onoda Y, Schieving F, Anten NPR. 2015. A novel method of measuring leaf epidermis and mesophyll stiffness shows the ubiquitous nature of the sandwich structure of leaf laminas in broad-leaved angiosperm species. Journal of Experimental Botany 66: 2487-99

Overdijk EJR, De Keijzer J, De Groot D, Schoina C, Bouwmeester K, et al. 2016. Interaction between the moss *Physcomitrella patens* and *Phytophthora*: a novel pathosystem for live-cell imaging of subcellular defence. Journal of Microscopy 263: 171-80

Paquin B, Roewer I, Wang Z, Lang BF. 1995. A robust fungal phylogeny using the mitochondrially encoded NAD5 protein-sequence. Canadian Journal of Botany 73: S180-S85

Paredez AR, Persson S, Ehrhardt DW, Somerville CR. 2008. Genetic evidence that cellulose synthase activity influences microtubule cortical array organization. Plant Physiology 147: 1723-34

Pelham RJ, Chang F. 2001. Role of actin polymerization and actin cables in actin-patch movement in *Schizosaccharomyces pombe*. Nature Cell Biology 3: 235-44

Perrine-Walker F. 2020. *Phytophthora palmivora*-cocoa interaction. Journal of Fungi 6: 167

Pollard TD, Borisy GG. 2003. Cellular motility driven by assembly and disassembly of actin filaments. Cell 112: 453-65

Pollard TD, Cooper JA. 2009. Actin, a central player in cell shape and movement. Science 326: 1208-12

Pollard TD. 2016. Actin and actin-binding proteins. Cold Spring Harbor Perspectives in Biology 8: a018226

Porschewski P, Specht V, Stubner S, Kindl H. 2001. A novel tetratricopeptide repeat-containing J-protein localized in a plasma membrane-bound protein complex of the phytopathogenic oomycete *Phytophthora megasperma*. European Journal of Cell Biology 80: 527-38

Preble AM, Giddings TM, Dutcher SK. 1999. Basal bodies and centrioles: Their function and structure. Current Topics in Developmental Biology 49: 207-33

Qiang L, Yu W, Andreadis A, Luo M, Baas PW. 2006. Tau protects microtubules in the axon from severing by katanin. Journal of Neuroscience 26: 3120-29

Qin Y, Yang Z. 2011. Rapid tip growth: insights from pollen tubes. Seminars in Cell & Developmental Biology 22: 816-24

Raudaskoski M, Astrom H, Laitiainen E. 2001. Pollen tube cytoskeleton: structure and function. Journal of Plant Growth Regulation 20: 113 -30

Reyssat E, Tallinen T, Le Merrer M, Mahadevan L. 2012. Slicing softly with shear. Physical Review Letters 109: 244301

Richards TA, Cavalier-Smith T. 2005. Myosin domain evolution and the primary divergence of eukaryotes. Nature 436: 1113-18

Richards TA, Soanes DM, Jones MDM, Vasieva O, Leonard G, et al. 2011. Horizontal gene transfer facilitated the evolution of plant parasitic mechanisms in the oomycetes. Proceedings of the National Academy of Sciences 108: 15258-63

Richardson DN, Simmons MP, Reddy ASN. 2006. Comprehensive comparative analysis of kinesins in photosynthetic eukaryotes. BMC Genomics 7(18)

Riedl J, Flynn KC, Raducanu A, Gaertner F, Beck G, et al. 2010. Lifeact mice for studying F-actin dynamics. Nature Methods 7: 168-69

Riemann M, Buche C, Kassemeyer HH, Nick P. 2002. Cytoskeletal responses during early development of the downy mildew of grapevine (*Plasmopara viticola*). Protoplasma 219: 13-22

Riquelme M, Reynaga-Pena CG, Gierz G, Bartnicki-Garcia S. 1998. What determines growth direction in fungal hyphae? Fungal Genetics and Biology 24: 101-09

Ritch DL, Daggett SS. 1995. Nuclear-DNA content and chromosome-number in German isolates of *Phytophthora infestans*. Mycologia 87: 579-81

Rocha RO, Elowsky C, Pham NTT, Wilson RA. 2020. Spermine-mediated tight sealing of the *Magnaporthe oryzae* appressorial pore–rice leaf surface interface. Nature Microbiology 5: 1472-80

Roman HN, Zitouni NB, Kachmar L, Ijpma G, Hilbert L, et al. 2013. Unphosphorylated calponin enhances the binding force of unphosphorylated myosin to actin. Biochimica Et Biophysica Acta - General Subjects 1830: 4634-41

Ryder LS, Dagdas YF, Kershaw MJ, Venkataraman C, Madzvamuse A, et al. 2019. A sensor kinase controls turgor-driven plant infection by the rice blast fungus. Nature 574: 423-27

Sampathkumar A, Lindeboom JJ, Debolt S, Gutierrez R, Ehrhardt DW, et al. 2011. Live cell imaging reveals structural associations between the actin and microtubule cytoskeleton in *Arabidopsis*. The Plant Cell 23: 2302-13

Sassmann S, Rodrigues C, Milne SW, Nenninger A, Allwood E, et al. 2018. An immune-responsive cytoskeletal-plasma membrane feedback loop in plants. Current Biology 28: 2136-44.e7

Schmidt A, Hall MN. 1998. Signaling to the actin cytoskeleton. Annual Review of Cell and Developmental Biology 14: 305-38

Schmidt SM, Panstruga R. 2007. Cytoskeleton functions in plant-microbe interactions. Physiological and Molecular Plant Pathology 71: 135-48

Schmiedel G, Schnepf E. 1980. Polarity and growth of caulonema tip cells of the moss *Funaria hygrometrica*. Planta 147: 405-13

Schoina C, Bouwmeester K, Govers F. 2017. Infection of a tomato cell culture by *Phytophthora infestans*; a versatile tool to study *Phytophthora*-host interactions. Plant Methods 13

Schoina C, Govers F. 2015. The oomycete *Phytophthora infestans*, the Irish potato famine pathogen. In: Principles of Plant-Microbe Interactions; Microbes for sustainable agriculture, 371-78: Springer International Publishing Switzerland

Schoina C, Rodenburg SYA, Meijer, HJG, Seidl MF, Lacambra LT, Bouwmeester K, Govers F (2021) Mining oomycete proteomes for metalloproteases leads to identification of candidate virulence factors in *Phytophthora infestans*. Molecular Plant Pathology 22: 551–63.

Seidl MF, Van den Ackerveken G, Govers F, Snel B. 2011. A domain-centric analysis of oomycete plant pathogen genomes reveals unique protein organization. Plant Physiology 155: 628-44

She Z-Y, Wei Y-L, Lin Y, Li Y-L, Lu M-H. 2019. Mechanisms of the Ase1/PRC1/MAP65 family in central spindle assembly. Biological Reviews 94: 2033-48

Sirotkin V, Berro J, Macmillan K, Zhao L, Pollard TD. 2010. Quantitative analysis of the mechanism of endocytic actin patch assembly and disassembly in fission yeast. Molecular Biology of the Cell 21: 2894-904

Snow AA, Spira TP. 1991. Differential pollen-tube growth-rates and nonrandom fertilization in *Hibiscus moscheutos* (Malvaceae). American Journal of Botany 78: 1419-26

Spector I, Shochet NR, Blasberger D, Kashman Y. 1989. Latrunculins—novel marine macrolides that disrupt microfilament organization and affect cell growth: I. Comparison with cytochalasin D. Cell Motility 13: 127-44

Stadler RV, White LA, Hu K, Helmke BP, Guilford WH. 2017. Direct measurement of cortical force generation and polarization in a living parasite. Molecular Biology of the Cell 28: 1912-23

Stajich JE, Harris T, Brunk BP, Brestelli J, Fischer S, et al. 2012. FungiDB: an integrated functional genomics database for fungi. Nucleic Acids Research 40: D675-81

Stamatakis A. 2014. RAxML version 8: a tool for phylogenetic analysis and post-analysis of large phylogenies. Bioinformatics 30: 1312-3

Steinberg G, Schliwa M, Lehmler C, Bolker M, Kahmann R, McIntosh JR. 1998. Kinesin from the plant pathogenic fungus *Ustilago maydis* is involved in vacuole formation and cytoplasmic migration. Journal of Cell Science 111: 2235-46

Strachan SD, Hess FD. 1983. The biochemical-mechanism of action of the dinitroaniline herbicide oryzalin. Pesticide Biochemistry and Physiology 20: 141-50

Taheri-Talesh N, Horio T, Araujo-Bazan L, Dou XW, Espeso EA, et al. 2008. The tip growth apparatus of *Aspergillus nidulans*. Molecular Biology of the Cell 19: 1439-49

Tanabe S, Kamada T. 1994. The role of astral microtubules in conjugate division in the dikaryon of *Coprinus cinereus*. Experimental Mycology 18: 338-48

Tang H, de Keijzer J, Overdijk EJR, Sweep E, Steentjes M, et al. 2019. Exocyst subunit Sec6 is positioned by microtubule overlaps in the moss phragmoplast prior to cell plate membrane arrival. Journal of Cell Science 132: jcs222430

Teapal J, Schuitman LJ, Mulder BM, Janson ME. 2021. Forced apart: a microtubule-based mechanism for equidistant positioning of multiple nuclei in single cells. The European Physical Journal Plus 136: 858

Temperli E, Roos U-P, Hohl HR. 1991. Germ tube growth and the microtubule cytoskeleton in *Phytophthora infestans*: effects of antagonists of hyphal growth, microtubule inhibitors, and ionophores. Mycological Research 95: 611-17

Temperli E, Roos, U. P., and Hohl, H. R. 1990. Actin and tubulin cytoskeletons in germlings of the oomycete fungus *Phytophthora infestans*. European Journal of Cell Biology 78: 75-88

Tesson B, Hildebrand M. 2010. Extensive and intimate association of the cytoskeleton with forming silica in diatoms: control over patterning on the meso- and micro-scale. PLOS ONE 5(12): e14300

Thines M, Kamoun S. 2010. Oomycete-plant coevolution: recent advances and future prospects. Current Opinion in Plant Biology 13: 427-33

Tian H, Shafi J, Ji MS, Bi YH, Yu ZG. 2017. Antimicrobial metabolites from *Streptomyces* sp SN0280. Journal of Natural Products 80: 1015-19

Tolmie F, Poulet A, McKenna J, Sassmann S, Graumann K, et al. 2017. The cell wall of *Arabidopsis thaliana* influences actin network dynamics. Journal of Experimental Botany 68: 4517-27

Torres GA, Sarria GA, Martinez G, Varon F, Drenth A, Guest DI. 2016. Bud rot caused by *Phytophthora palmivora*: a destructive emerging disease of oil palm. Phytopathology 106: 320-29

Tovey CA, Conduit PT. 2018. Microtubule nucleation by gamma-tubulin complexes and beyond. Essays in Biochemistry 62: 765-80

Tran PT, Marsh L, Doye V, Inoué S, Chang F. 2001. A mechanism for nuclear positioning in fission yeast based on microtubule pushing. Journal of Cell Biology 153: 397-412

Tsirigoti A, Küpper FC, Gachon CMM, Katsaros C. 2013. Cytoskeleton organisation during the infection of three brown algal species, *Ectocarpus siliculosus*, *Ectocarpus crouaniorum* and *Pylaiella littoralis*, by the intracellular marine oomycete *Eurychasma dicksonii*. Plant Biology 16(1); 272-81

Upadhyay S, Shaw BD. 2008. The role of actin, fimbrin and endocytosis in growth of hyphae in *Aspergillus nidulans*. Molecular Microbiology 68: 690-705

Van den Berg AH, McLaggan D, Dieguez-Uribeond J, van West P. 2013. The impact of the water moulds *Saprolegnia diclina* and *Saprolegnia parasitica* on natural ecosystems and the aquaculture industry. Fungal Biology Reviews 27: 33-42

Van der Honing HS, Emons AMC, Ketelaar T. 2007. Actin based processes that could determine the cytoplasmic architecture of plant cells. Biochimica Et Biophysica Acta-Molecular Cell Research 1773: 604-14

Van West P, Reid B, Campbell TA, Sandrock RW, Fry WE, et al. 1999. Green fluorescent protein (GFP) as a reporter gene for the plant pathogenic oomycete *Phytophthora palmivora*. FEMS Microbiology Letters 178: 71-80

Vatchev T, Maneva S. 2012. Chemical control of root rot complex and stem rot of greenhouse cucumber in straw-bale culture. Crop Protection 42: 16-23

Vicente JJ, Wordeman L. 2015. Mitosis, microtubule dynamics and the evolution of kinesins. Experimental Cell Research 334: 61-69

Vidali L, Rounds CM, Hepler PK, Bezanilla M. 2009. Lifeact-mEGFP reveals a dynamic apical F-actin network in tip growing plant cells. PLOS ONE 4(5): e5744

Wade RH. 2009. On and around microtubules: an overview. Molecular Biotechnology. 43: 177-91

Wagner LJ, Flores HE. 1994. Effect of taxol and related-compounds on growth of plant-pathogenic fungi. Phytopathology 84: 1173-78

Walker SK, Chitcholtan K, Yu YP, Christenhusz GM, Garrill A. 2006. Invasive hyphal growth: an F-actin depleted zone is associated with invasive hyphae of the oomycetes *Achlya bisexualis* and *Phytophthora cinnamomi*. Fungal Genetics and Biology 43: 357-65

Wang CL, Shaw BD. 2016. F-actin localization dynamics during appressorium formation in *Colletotrichum graminicola*. Mycologia 108: 506-14

Wang T, Ren D, Guo H, Chen X, Zhu P, et al. 2020. CgSCD1 is essential for melanin biosynthesis and pathogenicity of *Colletotrichum gloeosporioides*. Pathogens 9(2):141

Wasteneys GO. 2002. Microtubule organization in the green kingdom: chaos or self-order? Journal of Cell Science 115(Pt 7): 1345-54

Wheeler MH, Bell AA. 1988. Melanins and their importance in pathogenic fungi. In: McGinnis MR (ed) Current Topics in Medical Mycology, 338-87. New York, NY: Springer New York

Wickstead B, Gull K, Richards TA. 2010. Patterns of kinesin evolution reveal a complex ancestral eukaryote with a multifunctional cytoskeleton. BMC evolutionary biology 10: 110

Wickstead B, Gull K. 2011. The evolution of the cytoskeleton. Journal of Cell Biology 194: 513-25

Wilcox WF. 1996. Influence of dinitroanaline herbicides on growth, sporulation, and infectivity of four *Phytophthora* spp pathogenic to deciduous fruit trees. Phytopathology 86: 906-13

Williams JH. 2008. Novelties of the flowering plant pollen tube underlie diversification of a key life history stage. PNAS 105: 11259-63

Wilson RA, Talbot NJ. 2009. Under pressure: investigating the biology of plant infection by *Magnaporthe oryzae*. Nature Reviews Microbiology 7: 185-95

Wu SZ, Bezanilla M. 2018. Actin and microtubule cross talk mediates persistent polarized growth. The Journal of cell biology 217: 3531-44

Xiang X, Plamann M. 2003. Cytoskeleton and motor proteins in filamentous fungi. Current Opinion in Microbiology 6: 628-33

Xiang X. 2018. Nuclear movement in fungi. Seminars in cell & developmental biology 82: 3-16

Yi P, Goshima G. 2020. Rho of plants GTPases and Cytoskeletal elements control nuclear positioning and asymmetric cell division during *Physcomitrella patens* branching. Current Biology 30: 2860-68.e3

Young DH, Michelotti EL, Swindell CS, Krauss NE. 1992. Antifungal properties of taxol and various analogues. Experientia 48: 882-85

Young DH, Slawecki RA. 2001. Mode of action of zoxamide (RH-7281), a new oomycete fungicide. Pesticide Biochemistry and Physiology 69: 100-11

Young DH. 1991. Effects of zarilamide on microtubules and nuclear division in *Phytophthora capsici* and tobacco suspension-cultured cells. Pesticide Biochemistry and Physiology 40: 149-61

Yu YP, Jackson SL, Garrill A. 2004. Two distinct distributions of F-actin are present in the hyphal apex of the oomycete *Achlya bisexualis*. Plant Cell Physiology 45: 275-80

Yuan SK, Liu XL, Si NG, Dong J, Gu BG, Jiang H. 2006. Sensitivity of *Phytophthora infestans* to flumorph: in vitro determination of baseline sensitivity and the risk of resistance. Plant Pathology 55: 258-63

Zhang T, Zhao Q, Zhang Y, Ning J. 2014. Assessment of genotoxic effects of flumorph by the comet assay in mice organs. Human Experimental Toxicology 33: 224-9

Zhu S, Liu P, Liu X, Li J, Yuan S, Si N. 2008. Assessing the risk of resistance in *Pseudoperonospora cubensis* to the fungicide flumorph in vitro. Pest Management Science 64: 255-61

Zhu S, Liu X, Wang Y, Wu X, Liu P, et al. 2007a. Resistance of *Pseudoperonospora cubensis* to flumorph on cucumber in plastic houses. Plant Pathology 56: 967-75

Zhu SS, Liu XL, Liu PF, Li Y, Li JQ, et al. 2007b. Flumorph is a novel fungicide that disrupts microfilament organization in *Phytophthora melonis*. Phytopathology 97: 643-49

Summary

The phylogenetic group of oomycetes harbours many plant pathogens that cause enormous losses in a large variety of crop plants and damage to natural ecosystems. The number of known plant pathogenic oomycetes expands each year as new species and affected host plants are being discovered. A notorious group of plant pathogenic oomycetes is the *Phytophthora* genus. The research described in this thesis is aimed to deepen the fundamental knowledge on the structure and dynamics of the cytoskeleton of *Phytophthora* spp. and its role in different life stages and infection structures. The cytoskeleton is made up of filamentous assemblies of the proteins tubulin or actin. Microtubules and actin filaments form highly dynamic higher order organizations that are vital for all eukaryotic cells and fulfil a myriad of functions.

Previous studies on the actin cytoskeleton in oomycetes were largely based on observations in fixed tissue using phalloidin labelling or occasionally immunolabelling (**chapter 1**) and hence provide a static view of the actin cytoskeleton. The most striking observation in these fixed tissues was the presence of dot-like actin structures in all studied oomycetes and in all life stages, except in zoospores. A subsequent study using life cell imaging revealed that the dynamic behaviour of these dot-like actin structures, now named actin plaques, markedly differs from that of dot-like actin patches in yeast and filamentous fungi, showing that actin plaques are unique and oomycete specific.

In this thesis, we used a Lifeact-GFP expressing *Phytophthora infestans* transformant to gain more insight in the organization, the dynamic behaviour and the role of actin in various life stages and during plant cell infection. Besides actin plaques, we identified two novel actin configurations, one associated with cell wall plugs and the other in hyphal tips attempting to penetrate artificial surfaces. In germinating cysts, the cytoplasm migrates with the growing tip, leaving the cyst and the base of the germ tube empty. A hypha can seal off this depleted area by forming a cell wall plug. During the centripetal formation of this plug, actin is located at the leading edge of the expanding plug and we hypothesize that actin is involved in the delivery and/or deposition of cell wall material (**chapter 2**).

The actin configuration found in hyphae attempting to invade a glass coverslip resembles the shape of an aster. This so-called actin aster is present at the exact spot where the hypha touches the substrate, raising the question whether it is involved in facilitating plant cell penetration. An actin aster as prominent as observed on glass was not found during plant infection; nevertheless, an accumulation of actin at the site where *P. infestans* penetrated the plant cell was detected (**chapter 2**). Although these findings strongly suggest a role for actin during plant cell infection, the actin aster could also be a direct response to physical interaction with a surface. To test this, hyphae were damaged with a needle or by laser ablation. Both types of damaging led to the formation of an actin aster (**chapter 3**). In case of laser ablation, aster assembly took place within seconds after the laser pulse. Based on

these observations, we hypothesize that the actin aster is important for delivery of cell wall components and other components to the site of damage or, in case of contact with a plant cell, the site of penetration.

The oomycete specific actin plaques have a yet unknown function. When followed over time, these cortical actin plaques reveal great stability and longevity, hardly moving along the plasma membrane, showing no inward movement and with an estimated lifetime of several hours. Based on these observations it was previously hypothesized that they could function as a scaffold for organizing actin cables by linking the actin cytoskeleton with the membrane cell wall continuum. To test this, we studied the actin cytoskeleton in protoplasts. The removal of the cell wall led to the loss of immobility and longevity of plaques and frequently also to the formation of a rotating ring consisting of actin cables (**chapter 3**). Our results support the hypothesis that actin plaques function as cell wall anchors that establish the linkage between actin cables and the cell wall.

Lifeact-GFP expressing *Phytophthora* spp. are powerful tools to study the effects of oomicides at the cellular level. To showcase this tool, we re-evaluated the mode of action of the crop protection agent flumorph. This drug was previously suggested to interact with actin cables. However, the application of flumorph does not alter the actin organization in a Lifeact-GFP expressing *P. infestans* transformant in any way (**chapter 4**), thereby disproving the hypothesis. The actual mode of action of flumorph is yet to be discovered.

The microtubule cytoskeleton is a dynamic network of intracellular hollow rods, consisting of a backbone of α and β-tubulin heterodimers. Many proteins, collectively called Microtubule Associated Proteins (MAPs), have been found to interact with the microtubule cytoskeleton. Although the microtubule cytoskeleton is conserved among eukaryotes, it is involved in a variety of processes in different organisms, from providing structural rigidity to cells, to facilitating polarized growth and driving nuclear and cell divisions. We provide an inventory of putative MAPs present in *P. infestans*. The conserved motor proteins dynein and kinesin were identified, albeit with unique domain combinations not found in other eukaryotes (**chapter 5**). For visualizing tubulin in oomycetes, all studies so far made use of immunolabelling in fixed cells (**chapter 1**). Previously, oomycete microtubules were most extensively studied in *Saprolegnia ferax*. Here they found microtubule organizing centres associated with the nuclear membrane from which microtubules radiate into the cytoplasm during interphase and form the spindle during nuclear division. Interestingly, during nuclear division, the nuclear membrane stays intact, classifying oomycete nuclear division as a closed mitosis. To study microtubule organization and dynamics in *Phytophthora* spp., we generated transgenic *Phytophthora palmivora* lines expressing GFP-α-tubulin, enabling live cell imaging of the microtubule cytoskeleton in an oomycete for the first time. In these lines we were able to see the dynamics and instability of microtubules, displayed as growing and shrinking of microtubules in the spindle and in cytoplasmic microtubules (**chapter 5**). Occasionally we observed microtubule buckling, both in spindle microtubules as well as

cytoplasmic microtubules. It was previously hypothesized that microtubules might play a role in nuclear positioning. Buckling or bending of microtubules is a consequence of compressive forces. This observation supports the hypothesis that forces are exerted on internuclear microtubules and microtubules protruding into the cell tip. These forces are likely to play a role in the positioning of nuclei.

Fundamental knowledge on the cytoskeletal components in *Phytophthora* is important for understanding the pathogens' biology. In studying the *Phytophthora* cytoskeleton, we identified several features unique to oomycetes. Such features could be leads for identifying potential targets for novel oomicides. Besides offering potential as potent control agents, drugs targeting the cytoskeleton are valuable tools for experimental research on the cytoskeleton in oomycetes (**chapter 6**). In the general discussion, I elaborate on the results, observations and hypotheses obtained in this thesis and place these in the context of results and hypotheses obtained by others, in particular in studies based on drugs that target the cytoskeleton. Overall, the research described in this thesis demonstrates the power of live cell imaging in identifying unique features of the cytoskeleton that were not observed previously by studying fixed material. We believe that life cell imaging of the *Phytophthora* cytoskeleton may lay the foundation for the discovery of novel insights in the biology of oomycetes and may lead to the discovery of novel strategies to combat this group of notorious plant pathogens.

Acknowledgements

During my PhD I met so many amazing people, way too many to mention here. The road to my defence was a long and bumpy one. At some point I didn't think I was going to make it to the end and without the help of all of you, I am sure I never would have made it! A big thank you to all of you who helped me in and outside the lab!

First and most importantly I would like to thank my supervisors **Francine** and **Tijs**, for their extreme patience and all of their support over the years! **Tijs**; your limitless optimism and fresh opinions on technical problems really made it is pleasure to work with you! **Francine**; thank you so much for always finding time to listen to me and for all the advice you gave over the years, both on professional as well as personal subjects.

The Pinf group; **Rob**, thank you for all the flowers and chocolates, I'll let you know when the next batch of soup is ready! **Natalie**, thank you for all the good discussions and for being a true openminded and openhearted friend. **Klaas**, I miss your informative stories on nature. Thank you for sharing your very broad knowledge with everyone around you! **Chara**, thank you for being a true inspiration to me. **Shuqing**, my baby sister, I miss you so much! I will visit China and maybe then we can go shopping again! **Johan**, pretty boy, it was a real pleasure working alongside you. **Sander**, thank you for making bioinformatics a little less boring. Just kidding! But thank you for making it understandable to me. **Elysa**, no, I still don't want children, but thank you anyway for trying so hard to convince me. **Michiel**, you have been an amazing student and colleague and boy, am I happy I managed to finish my PhD before you will finish yours! Good luck with the last bits and pieces! **Chenlei** and **Harold**; thank you so much for all the help in the lab and on the manuscripts! **Yan**, **Yu**, **Miao,** and all the other **Pinf members** over the years; thank you for making the group such a warm and loving familia!

The phytopathology group; **Ali**, **Anneke**, **Aranka**, **Bart**, **Carolina**, **Ciska**, **David**, **Edgar**, **Einar**, **Ester**, **Gert**, **Gabriel**, **Grardy**, **Giuliana**, **Henriek**, **Hui**, **Jan**, **Jasper**, **Jinbin**, **Jinling**, **Katharina**, **Laurens**, **Lorena**, **Maikel**, **Martin**, **Matthieu, Michael, Michele**, **Mireille**, **Malaika**, **Nelia**, **Nick**, **Petra**, **Sander**, **Sergio**, **Si**, **Yaohua** and **Wen**. Thank you all for everything! The lovely events, nice discussions and all the shared cakes!

The CLB group; **Henk**, thank you for everything you taught me and for listening to me when I was in trouble. **Hannie,** you are an amazing colleague! Thank you for all your support. **Ale,** I always enjoyed our conversations at work and I really miss them! **Otto**, I really enjoyed working together with you, your enthusiasm for the things you work on is really infectious! **Marie-José**, thank you for making all my bureaucratic problems disappear like snow in the sun! You are the best secretary I have ever met! **Bela**, **Marcel**, **Kris**, **Jeroen**, **Elysa**, **André**, **Norbert**, **Han**, **Peter**, **Michiel** and all other CLB members, thank you for creating such a pleasant work atmosphere, I have really enjoyed being your colleague!

I would also like to thank the Plant Developmental Biology cluster as a whole, although I only was part of the group for a short while, I really enjoyed working with you all. Special thanks to **Marijke**, **Carolien**, **Andrea** and **Olga** for all their helpfulness, kindness and sense of humour!

Of course also a very big thank you to all of my students; **Hari**, **JQ**, **Maarten**, **Michiel**, **Rick**, **Tim**, **Juliette**, **Thomas**, **Tanweer** and **Levi**. If you only learned halve as much from me, as I have learned from you, it was well worth it!

During my PhD I was lucky to have a number of collaborations. **Jochem**, when I first met you, I never thought that our collaboration would result in a publication, let alone multiple publications. I am really proud of what you achieved (despite the fact that you have often made my flesh crawl when you would write about *phytophthora* isolates or transformants) and I am really honoured you asked me to help you with start with *Phytophthora* experiments. **Ayelen**, you came across from New Zealand even twice to perform experiments in our lab and we visited a conference together. I spend more time with you than with many other colleagues permanently located in Wageningen! I learned a lot from you and really enjoyed our collaboration!

To my fellow members of the EPS-PhD-counsel; **Amalia**, **Francesca**, **Jarst**, **Jesse**, **Jordi**, **Kim**, **Malaika**, **Peter**, **Sandeep**, **Sara**, **Shanice**, **Tieme** and **Tom**.

En dan mijn paranimfen **Ciska** en **Peter**! Beiden super bedankt voor alle steun en alle fijne gesprekken. **Peter**; soms wel een tikje irritant om 2x per dag de vraag te krijgen of alles wel goed gaat, maar alles went en ik moet bekennen dat ik het zelfs een beetje mis nu! Dat alles in je tuintje maar groen mag blijven en zo hard mag groeien als Chloe! **Ciska**; zo fijn om jou in de laatste jaren van mijn PhD nog tegen te komen en af en toe met je te kunnen praten. Ik hoop dat we dat in de toekomst nog vaak kunnen doen!

Mijn vrienden van de campinggroep; **Arjan**, **Amber**, **Anna**, **Anneke**, **Helen**, **Iris**, **Jelco**, **Jora**, **Jorick**, **Onnika**, **Niels**, **Martijn**, **Yorick** en **Wessel**. Dankjewel voor alle gezellige avonden vol afleiding en discussie! En dat er maar vele mogen volgen!

Iris, Helen en Onnika; jullie natuurlijk ook heel erg bedankt voor alle extra afleiding; het delen van kennis over de moestuin en het leven. Dat we nog maar vele plantjes mogen uitwisselen! **Eefke**; Wageningen is zo stil geworden zonder jou! Ik zag in de winkel dat er veel nieuwe soorten wereldgerechten zijn, dus misschien moeten we dat project maar eens afmaken. **Olya**, you truly are the kindest and most righteous person I know, I am looking forward to our next diner together!

Natuurlijk wil ik ook **mijn ouders** en **mijn oma's** bedanken die me al die tijd zijn blijven steunen. Ik zie mezelf als bevoorrecht dat mijn ouders mij altijd zo veel vrijheid hebben gegeven dat te doen wat ik wilde, dankjewel!

En dan mijn lieve **Maarten**; dankjewel dat je mij het vertrouwen in mezelf hebt teruggegeven. Zonder jou was het boekje er nooit gekomen. Er zijn niet genoeg woorden om uit te drukken hoeveel je voor me betekent en hoeveel ik geniet van ieder moment dat we samen zijn. Ik zou me geen leven meer kunnen voorstellen zonder jou!

About the author

In 2007 I graduated from VWO in Winterswijk and decided to study Biology at Wageningen University. I was fascinated by plants after following several courses on plant biology and choose to specialize in plant health. I looked up every course on plant-pathogen interactions given at Wageningen University and followed as many as possible during the remainder of my BSc and MSc. During my BSc thesis I had learned to use the confocal microscopy, studying plant cell division under supervision of Andre van Lammeren. In search for an MSc project I ran across a subject where a student, able to work independently on the confocal microscope, was asked to study the actin cytoskeleton of *Phytophthora infestans*. I jumped at it and spent a lovely six months in a dark and cosy microscope room, emerging with a wonderful data set and enough material for a publication. A second thesis followed, also on *P. infestans*. After obtaining my MSc degree, I worked for six months in a cosy microscope room on the other side of the world in the laboratory of Adrienne Hardham in Canberra, Australia, also studying *Phytophthora*.

After returning from Australia in the summer of 2015, my MSc thesis supervisors, Francine Govers and Tijs Ketelaar, offered me the opportunity to continue with research on the actin cytoskeleton in *Phytophthora*, but then as a PhD student on a project shared between the Laboratories of Phytopathology and Cell Biology. Next to spending even more time in a cosy microscope room, I also had the privilege to participate in teaching, in particular in plant biology and phytopathology courses. In 2019, when my colleague Henk started working less, I was appointed at the Laboratory of Cell biology to take over many of Henk's tasks in teaching and lab management. More recently, I have taken up a new challenge as researcher phytopathology of fruit crops at Wageningen University and Research in Randwijk

List of publications

Meijer HJG*, Hua C*, **Kots K**, Ketelaar T and Govers F (2014). "Actin dynamics in *Phytophthora infestans*; rapidly reorganizing cables and immobile, long-lived plaques." Cellular Microbiology 16(6): 948-961.

Hua C*, **Kots K***, Ketelaar T, Govers F and Meijer HJG (2015). "Effect of flumorph on F-Actin dynamics in the potato late blight pathogen *Phytophthora infestans*." Phytopathology 105(4): 419-423.

Kots K*, Meijer HJG*, Bouwmeester K, Govers F and Ketelaar T (2017). "Filamentous actin accumulates during plant cell penetration and cell wall plug formation in *Phytophthora infestans*." Cellular and Molecular Life Sciences 74(5): 909-920.

Bronkhorst J, Kasteel M, Van Veen S, Clough JM, **Kots K**, Buijs J, Van der Gucht J, Ketelaar T, Govers F and Sprakel J. (2021). "A slicing mechanism facilitates host entry by plant-pathogenic *Phytophthora*." Nature Microbiology 6(8): 1000-1006.

Bronkhorst J*, **Kots K***, De Jong D, Kasteel M, Van Boxmeer T, Joemmanbaks T, Govers F, Van der Gucht J, Ketelaar T and Sprakel J (2022). "An actin mechanostat ensures hyphal tip sharpness in *Phytophthora infestans* to achieve host penetration." Science Advances 8(23), eab00875

*Equal contributions

Education Statement of the Graduate School Experimental Plant Sciences

Issued to: **Kiki Kots**
Date: **28 October 2022**
Group: **Laboratory of Phytopathology & Laboratory of Cell Biology**
University: **Wageningen University & Research**

1) Start-Up Phase	*date*	*cp*
▶ **First presentation of your project**		
Unravelling the function and molecular composition of oomycete specific plaques	2016, Oct 25	1,5
▶ **Writing or rewriting a project proposal**		
▶ **Writing a review or book chapter**		
▶ **MSc courses**		
Subtotal Start-Up Phase		1,5

2) Scientific Exposure	*date*	*cp*
▶ **EPS PhD student days**		
EPS Get2Gether 2016, Soest, NL	2016, Jan 28-29	0,6
EPS Get2Gether 2017, Soest, NL	2017, Feb 9-10	0,6
EPS Get2Gether 2018, Soest, NL	2018, Feb 15-16	0,6
▶ **EPS theme symposia**		
EPS theme 2 symposium & Willie Commelin Scholten day 'Interactions between plants and biotic agents', Leiden, NL	2016, Jan 22	0,3
EPS theme 2 symposium & Willie Commelin Scholten day 'Interactions between plants and biotic agents', Wageningen, NL	2017, Jan 23	0,3
EPS theme 2 symposium & Willie Commelin Scholten day 'Interactions between plants and biotic agents', Amsterdam, NL	2018, Jan 24	0,3
EPS theme 2 symposium & Willie Commelin Scholten day 'Interactions between plants and biotic agents', Wageningen, NL	2019, Feb 1	0,3
▶ **Lunteren Days and other national platforms**		
Annual Meeting 'Experimental Plant Sciences', Lunteren, NL	2016, Apr 11-12	0,6
Annual Meeting 'Experimental Plant Sciences', Lunteren, NL	2017, Apr 10-11	0,6
Annual Meeting 'Experimental Plant Sciences', Lunteren, NL	2018, Apr 9-10	0,6
Annual Meeting 'Experimental Plant Sciences', Lunteren, NL	2019, Apr 8	0,3
▶ **Seminars (series), workshops and symposia**		
Jane Parker - Plant intracellular immunity: evolutionary and molecular underpinnings	2016, Jan 21	0,1
Laura Grenville-Briggs - Molecular oomycete-host interactions; the good, the bad and the ugly	2016, Feb 19	0,1
Caitlyn Allen - How *Ralstonia solanacearum* succeeds in plant xylem vessels	2016, Feb 19	0,1
Wenbo Ma - Effectors as molecular probes to understand pathogenesis	2016, Jun 20	0,1
Niels Galjart - Quality control systems that regulate microtubule dynamics and behaviour	2016, Oct 28	0,1
Birgit Kemmerling - The Arabidopsis BIR family – negative regulators of BAK1 receptor complexes and more	2016, Nov 25	0,1

	Hans Thordal-Christensen - Membrane trafficking in plant cells attacked by powdery mildew fungi	2016, Dec 12	0,1
	Magalena Bezanilla - Cytoskeletal crosstalk impacts cell shape and development	2017, Nov 6	0,1
	Remco Stam - Breeding durable resistance against *Phytophthora*	2018, Jan 26	0,1
	Stefan Sassmann - An actin nucleating formin that is recruited to sites of pathogen attack in Arabidopsis	2018, Feb 8	0,1
	Mary C. Wildermuth - Salicylic acid and cell cycle control of plant-microbe interactions	2018, Jun 25	0,1
	Melvin Bolton - Increasing sugar beet productivity and sustainability	2018, Sep 7	0,1
	Yan Wang - A leucine-rich repeat receptor-like protein as PAMP receptor recognising XEG1	2018, Sep 10	0,1
	Volker Lipka - Live and Let Die or Live and Let Live - Interactions of Arabidopsis with fungal pathogens	2018, Sep 14	0,1
	Tom Wood - Nanopath: Utilising nanopore sequencing for *Septoria* surveillance	2018, Sep 14	0,1
	David Geiser - A phylogenomic view of *Fusarium oxysporum* taxonomy and evolution	2018, Oct 10	0,1
	Nick Talbot - Investigating the biology of plant infection by rice blast fungus	2019, Apr 2	0,1
	Symposium - Leading women in fungal biology, Utrecht, NL	2017, Aug 30-31	0,6
▶	**Seminar plus**		
	Birgit Kemmerling - The Arabidopsis BIR family – negative regulators of BAK1 receptor complexes and more	2016, Nov 25	0,1
	Hans Thordal-Christensen - Membrane trafficking in plant cells attacked by powdery mildew fungi	2016, Dec 12	0,1
	Magalena Bezanilla - Cytoskeletal crosstalk impacts cell shape and development	2017, Nov 6	0,1
	Nick Talbot - Investigating the biology of plant infection by rice blast fungus	2019, Apr 2	0,1
▶	**International symposia and congresses**		
	Gordon Research Conference 2016 - The Plant and Microbial Cytoskeleton, Andover NH, US	2016, Aug 14-19	1,3
	Oomycete Molecular Genetics Network Annual Meeting, Asilomar, Monterey CA, US	2017, Mar 12-13	0,6
	29th Fungal Genetics Conference, Asilomar, Monterey CA, US	2017, Mar 14-19	1,3
	Oomycete Molecular Genetics Network Annual Meeting, Oban, UK	2019, Jul 10-12	0,9
▶	**Presentations**		
	Oral presentation at EPS theme 2 symposium & Willie Commelin Scholten Day, Leiden, NL	2016, Jan 22	1,0
	Poster presentation at GRC - The Plant and Microbial Cytoskeleton, Andover NH, US	2016, Aug 15	1,0
	Oral & poster presentation at Oomycete Molecular Genetics Network Annual Meeting, Asilomar, Monterey CA, US	2017, Mar 13	1,0
	Oral presentation at 29th Fungal Genetics Conference, Asilomar, Monterey CA, US	2017, Mar 17	1,0
	Oral presentation at Annual Meeting 'Experimental Plant Sciences', Lunteren, NL	2017, Apr 11	1,0
	Poster presentation at Annual Meeting 'Experimental Plant Sciences', Lunteren, NL	2018, Apr 9	1,0
	Oral presentation at Oomycete Molecular Genetics Network Annual Meeting, Oban, UK	2019, Jul 12	1,0
▶	**IAB interview**		
▶	**Excursions**		
	EPS company visit Tomato World, NL	2016, Oct 14	0,2
		Subtotal Scientific Exposure	19,1

3) In-Depth Studies	date	cp
▶ **Advanced scientific courses & workshops**		
Instructions on the use of real-time PCR detection system and software (Biorad), Wageningen, NL	2018, Jun 18	0,1
EPS advanced course Transcription Factors and Transcriptional Regulation, Wageningen, NL	2018, Dec 10-12	1,0
▶ **Journal club**		
Thursday morning literature discussion in *P. infestans* group	2016-2020	1,5
▶ **Individual research training**		
RNA interference in *P. infestans* training in Wageningen by Maja Brus from SLU, Alnarp, SE	2015, Nov	1,0
Lab-on-a-chip training in Wageningen by Ayelen Tayagui from University of Canterbury, Christchurch, NZ	2018, May	1,0
	Subtotal In-Depth Studies	4,6

4) Personal Development	date	cp
▶ **General skill training courses**		
EPS Introduction Course, Wageningen, NL	2016, Feb 11	0,3
WGS course Information literacy PhD including EndNote introduction, Wageningen, NL	2016, Jun 14-15	0,4
WGS course Brain Training, Wageningen, NL	2017, Apr 12	0,3
EPS workshop Transferable Skills, Wageningen, NL	2018, Jun 28	0,2
Workshop Stratego for Women, Wageningen, NL	2018, Okt 2	0,3
Workshop eLabjournal, Wageningen, NL	2018, Dec 6	0,1
WGS PhD Workshop Carousel, Wageningen, NL	2019, May 24	0,3
EPS Writing Support Group, Hertz Training for Scientists, online	2021, Jan-Mar	1,0
▶ **Organisation of meetings, PhD courses or outreach activities**		
Organisation of PhD student days Get2Gether 2017	2017, Feb 9-10	1,5
Organisation of PhD student days Get2Gether 2018	2018, Feb 15-16	1,5
▶ **Membership of EPS PhD Council**		
Member of the EPS PhD council	2016-2018	1,4
	Subtotal Personal Development	7,3

TOTAL NUMBER OF CREDIT POINTS*	**32,5**

Herewith the Graduate School declares that the PhD candidate has complied with the educational requirements set by the Educational Committee of EPS with a minimum total of 30 ECTS credits.

** A credit represents a normative study load of 28 hours of study.*

This research was performed at the Laboratory of Phytopathology and the Laboratory of Cell Biology Group of Wageningen University & Research. This work was financially supported by a private donor (via the University Fund Wageningen) and by Wageningen University & Research.

Cover & layout design: Iliana Boshoven-Gkini | AgileColor.com
Printed by Ridderprint | Ridderprint.nl